# Identifying Operating Conditions of Tires During Highway Driving Maneuvers

Thesis

Presented in Partial Fulfillment of the Requirements for the Degree Master of Science in the Graduate School of The Ohio State University

By

Siddarth Kashyap Attravanam, B.S. M.E.

Graduate Program in Mechanical Engineering

The Ohio State University

2018

Thesis Committee

Levent Guvenc, Advisor

Jeffrey P. Chrstos

Gary J. Heydinger

Copyrighted by

Siddarth Kashyap Attravanam

2018

## Abstract

Tires play a critical role in influencing vehicle behavior. Determining vehicle handling, implementation of active safety systems such as anti-lock braking systems and electronic stability control systems rely on robust understanding of tire behavior. Tire behavior changes with operating conditions such as normal load, camber angle, slip angle and temperature. These operating conditions were identified with on track testing using wheel force transducers, slip angle sensors and an array of data acquisition systems. Data from 20 days of driving on public roads with data acquisition provided guidance to design the on track testing. Data from on track testing was used to design high slip angle and low slip angle tire testing on the FlatTrac III tire test rig at Smithers Rapra in Akron, Ohio. Correlation between wheel force transducer and FlatTrac III was presented. In addition, correlation between the test track surface and FlatTrac III belt surface was also presented by using the same physical tires between track testing and FlatTrac III testing. The on track data can be used to reduce testing time and cost by about 40% by utilizing an asymmetric tire test matrix. Further, Magic Formula 6.1 tire models are fit to the data from FlatTrac III and scaling factors are developed which can further reduce testing time and cost by 50%. The correlation between lateral force predicted by these scaled models to measured lateral force on the FlatTrac III for a combination of normal load, slip angle and camber is provided.

## Acknowledgments

I would like to thank my advisors Dr. Jeff Chrstos and Dr. Levent Guvenc for their guidance and support over the course of graduate studies at The Ohio State University.

I would like to thank Smithers Rapra in Akron, OH for working with me in scheduling and running the tire test on their FlatTrac III machine that was critical for the success of this research.

I would like to thank my company Cooper Tire & Rubber Company for sponsoring my graduate studies, providing time and equipment to test and the time off to finish my research. I would like to especially thank Dr. Patrick Majors, my mentor at Cooper Tire & Rubber Company for his constant support, guidance and motivation across work, school and life.

I would like to thank my family for constantly supporting, motivating and often listening to my rants about the complex nature of vehicle handling and tires. Thank you for your love, support and patience.

# Vita

Begin Typing Here

December 2012……..….University of Texas at Arlington

Jan 2013 – June 2013……...…….FixRim Racing

June 2013 – September 2014…….……OptimumG, LLC

October 2014 – Current ……Cooper Tire & Rubber Company

August 2016 – August 2018 …….Graduate Student, The Ohio State University

# Fields of Study

Major Field: Mechanical Engineering

Table of Contents

Abstract ..... iii
Acknowledgments ..... iv
Vita ..... v
Table of Contents ..... vi
List of Tables ..... viii
List of Figures ..... ix
Chapter 1. Introduction ..... 1
a. Motivation ..... 1
b. Document Structure ..... 3
Chapter 2. Literature Review ..... 6
a. Vehicle Dynamic Simulation ..... 6
b. Vehicle safety systems – Anti Lock Braking (ABS) and Electronic Stability Control (ESC) ..... 8
c. Tire performance metrics as an indicator of vehicle handling ..... 8
d. Tire Modeling ..... 13
e. Tire Testing Rigs ..... 15
f. Tire Force and Moment Testing for lateral handling ..... 16
Chapter 3. Testing Equipment ..... 18
a. Test Vehicle ..... 18
b. VBOX 3i ..... 19
c. MoTeC L180 ..... 21
d. Michigan Scientific Wheel Force Transducers ..... 22
e. Kistler Optical Slip Angle Sensor ..... 24
f. Tire internal temperature ..... 27
g. Tire tread surface temperature sensor ..... 31

h. CAN bus communication ..... 33
i. MTS Flat-Trac III CTTire Test System ..... 34
Chapter 4. On-Vehicle Testing ..... 37
a. Integration of data acquisition systems on the test vehicle ..... 37
b. Daily driving log ..... 41
c. On Track Testing ..... 42
Chapter 5. Tire Testing on FlatTrac III ..... 53
a. sLAT02 ..... 54
b. sLAT12 ..... 56
c. Track Replay ..... 58
d. Data Analysis ..... 60
a. Pre-Processing the data ..... 60
b. Wheel force transducer to MTS FlatTrac III Data Comparison ..... 60
c. Tire F&M Analysis ..... 74
d. Tread Surface temperature and Cornering Stiffness ..... 83
e. Modification of Tire Test Procedure ..... 89
a. Scaling the tire model ..... 91
b. Track replay using tire model ..... 98
Chapter 6. Conclusion and Future Remarks ..... 102
a. Concluding Remarks ..... 102
b. Future Work ..... 103
References ..... 105
Appendix A: Fast Fourier Transforms of Lateral Acceleration, Lateral Force measured by Wheel Force Transducer and Normal Force measured by Wheel Force Transducer ..... 110
Appendix B: Transition between command normal load and command inclination angle for sLAT02 and sLAT12 ..... 113
Appendix C: Total Error, Root Mean Square Error and $R^2$ Calculation ..... 115
a. Total Error ..... 115
b. Root Mean Square Error (RMSE) ..... 115
c. $R^2$ – Coefficient of determination [51] ..... 116
Appendix D: Comparison between Magic Formula 6.1 Tire Model fit and Linear fit between -1 and +1 deg slip angle for sLAT02 and sLAT12 ..... 117

List of Tables

Table 1 – MTS Flat-Trac III CTTire Test System specifications ..... 34
Table 2 – Time shift (in seconds) applied to each run for each tire to synchronize the data ..... 41
Table 3 – Summarize $R^2$ and Root Mean Square Error (RMSE) of linear fits of correlation ..... 73
Table 4 – Summarized $R^2$ and Root Mean Square Error (RMSE) of quadratic fit of correlation for UHP Tire ..... 73
Table 5 – Normal load and camber angle conditions for sLAT12. Notice the symmetry in test conditions ..... 90
Table 6 – Normal load and camber angle conditions for asymmetric sLAT12 after modification ..... 90
Table 7 – Summary of total error between different MF 6.1 tire models and tire test data from sLAT02 for both Broadline and UHP Tires ..... 96
Table 8 – Coefficients and scaling factors of MF 6.1 that were modified for the asymmetric sLAT12 tire model for UHP Tire ..... 97
Table 9 – Coefficients and scaling factors of MF 6.1 that were modified for asymmetric sLAT12 tire model for Broadline Tire ..... 97
Table 10 – Summarized errors between tire model and measured lateral force on FT III from track replay ..... 101

List of Figures

Figure 1 – Lateral Force versus Slip angle plot showing calculation of Cornering stiffness. Cornering stiffness is the slope of the lateral force versus slip angle curve when slip angle is 0. ..... 7
Figure 2 – Four Parameter method to evaluate vehicle transient response [20] [21]. ..... 9
Figure 3 – Cornering stiffness versus Normal Load for a passenger car tire ..... 10
Figure 4 – Cornering stiffness variation due to inflation pressure [5]. Blue curve is baseline ..... 10
Figure 5 – Cornering stiffness variation due to tread wear [5]. Blue curve is baseline .... 11
Figure 6 – Cornering stiffness variation due to bulk/core temperature [5]..... 11
Figure 7 – Comparison of cornering stiffness change with storage modulus over temperature [9]. ..... 12
Figure 8 – Cornering stiffness dependence on tire core temperature [9]..... 13
Figure 9 – Tire Force and Moment testing machine at Calspan Corporation [10]. ..... 16
Figure 10 – 2016 Ford Mustang lent by Cooper Tire & Vehicle Test Center as test vehicle. The vehicle was previously used in a promotional campaign, thus it is covered in decals..... 18
Figure 11 - VBOX 3i by Racelogic data acquisition system ..... 19
Figure 12 – GPS/GLONASS antennae mounted on the roof of the vehicle. The fore 'secondary' antenna is circled blue and the rear 'primary' antenna is circled red. ..... 20
Figure 13 – (Left) IMU in integrated roof mount with rear GPS/GLONASS antenna moutned on the roof of the vehicle. (Right) Exploded view of IMU, roof mount and GPS/GLONASS antenna [33]..... 21
Figure 14 – MoTeC L180 Data acquisition system ..... 21
Figure 15 – Michigan Scientific Wheel Force Transducer LW12.8..... 22
Figure 16 – CT2 Signal conditioning box from Michigan Scientific ..... 23
Figure 17 – Custom made wheel with mounting holes (circled in red) for the LW12.8 wheel force transducer ..... 23
Figure 18 – Slip ring and amplifier package..... 24
Figure 19 – Tire coordinate system according to SAE J2047 [35]..... 25
Figure 20 – Optical slip angle sensor mounted on the wheel force transducer ..... 26
Figure 21 – Kistler signal conditioning box ..... 27
Figure 22 – Texense IRN8-WS4 internal temperature sensor..... 28
Figure 23 – Texense IRN8-WS4 internal tire temperature sensor mounted on a 3D printed housing..... 28

Figure 24 – Schematic of IR sensor mounted inside the wheel to measure the internal tire temperature ..... 29
Figure 25 – Schematic of operation of IR sensor to measure temperature on the inner liner of the tire. ..... 30
Figure 26 – IRN8-WS4 internal tire temperature sensor mounted on the 3D printer housing which is glued on to the wheel. ..... 31
Figure 27 – Texense IR temperature sensor for measuring tread surface temperature. [37] ..... 32
Figure 28 – IRN-RC Texense infrared temperature sensors mounted underneath the fender ..... 32
Figure 29 – Texense IRN-RC temperature sensors measuring the tread surface in three locations – inside, middle and outside. ..... 33
Figure 30 – MTS Flat-Trac III CTTire Test System [26] ..... 35
Figure 31 – Tread surface temperature measurement on the MTS FlatTrac III using three infrared (highlighted in red) sensors (left). Zoomed in view of the sensors (highlighted in red) facing the tire tread (right). ..... 36
Figure 32 – Racelogic VBOX file manager used to control the start/stop of data recording on the VBOX 3i. ..... 38
Figure 33 – Schematic of connection between sensors and data acquisition system ..... 39
Figure 34 – Lateral acceleration logged between the VBOX 3i and L180. The figure shows that the VBOX 3i lateral acceleration is leading the L180 lateral acceleration signal ..... 40
Figure 35 – Lateral acceleration comparison after the time shift applied using the cross correlation between the two signals ..... 40
Figure 36 – Percentage of time spent in different ranges of lateral acceleration during data collected over 20 days of driving ..... 42
Figure 37 – Layout of Cooper Tire & Vehicle Test Center. Testing area of the handling oval highlighted in red (Right). ..... 43
Figure 38 – Lateral Acceleration profile from on track testing ..... 44
Figure 39 – CS5 Ultra Touring Broadline Tire (Left). RS3-G1 UHP Tire (Right) [45] [44] ..... 45
Figure 40 – Measured lateral Acceleration and slip angle profiles from on track testing 46
Figure 41 – Lateral acceleration versus camber showing the range of tire camber for both UHP and Broadline tires ..... 47
Figure 42 – Lateral Acceleration versus Normal Load profiles for left front and left rear tires for Broadline Tire (top) and UHP Tire (bottom). ..... 48
Figure 43 – Lateral acceleration versus front tire tread surface temperature (top) and rear tire tread surface temperature (bottom) for Broadline tire. ..... 49
Figure 44 – Lateral Acceleration versus Tread Surface temperature for front (top) and rear tire (bottom) for UHP Tire ..... 50
Figure 45 – Lateral Acceleration versus Tire Inner liner temperature for Broadline tire (top) and UHP tire (bottom) ..... 51
Figure 46 – One of the test tires from on track testing being fitted with the wheel force transducer to be tested on the MTS FlatTrac III machine at Smithers. ..... 54

Figure 47 – Slip Angle, Inclination angle and Normal Load command profiles for sLAT02. ..... 55
Figure 48 – Lateral force versus Slip Angle at different inclination angles and normal loads from sLAT02 test for the Broadline tire ..... 56
Figure 49 – Slip Angle, inclination angle and normal load command profiles for sLAT12 test procedure. ..... 57
Figure 50 – Lateral force versus slip angle at different inclination angles and normal loads from sLAT02 test for the Broadline tire. ..... 58
Figure 51 – Time history profile of slip angle, normal load and inclination angle from driving on the oval at CTVTC. This time history profile is fed into the MTS FlatTrac III machine to get a direct correlation between the belt surface and CTVTC asphalt surface for both Broadline and UHP tires. ..... 59
Figure 52 – The Michigan Scientific CT2 communications box connected to an analog breakout box (in yellow) providing the analog signals from the WFT into the Smithers data acquisition system. Power to the CT2 is provided by a bench top DC power supply at 12V (in red) ..... 61
Figure 53 – Comparison between FlatTrac III Normal Force and WFT Normal Force for both sLAT02 and sLAT12 test procedures for Broadline Tire. ..... 62
Figure 54 – Comparison between FlatTrac III Lateral Force and WFT Lateral Force for both sLAT02 and sLAT12 test procedures for Broadline Tire. ..... 63
Figure 55 – Lateral force correlation between WFT on the Test Track (CTVTC) and WFT on the FlatTrac III belt surface for Broadline tire for track replay input. The solid red line shows the linear fit to the data and the dashed line shows the linear fit +/- 10% bound ..... 64
Figure 56 – Lateral force comparison between WFT on Track and FlatTrac III Measurement for Broadline Tire for track replay input. The solid red line shows the linear fit to the data and the dashed line shows the linear fit +/- 10% bound ..... 65
Figure 57 – Time history plot of lateral force profiles as measured by WFT on FlatTrack III belt, WFT on test track and lateral force measured by FlatTrac III measurement system ..... 66
Figure 58 – Lateral force comparison between WFT on the Test Track (CTVTC) and WFT on the FlatTrac III belt surface for the UHP Tire for track replay input. The solid red line shows the linear fit to the data and the dashed line shows the linear fit +/- 10% bound ..... 67
Figure 59 – Lateral force comparison between WFT on the Test Track (CTVTC) and WFT on the FlatTrac III belt surface for the UHP Tire for track replay input. The gradient indicates the tire slip angle. ..... 68
Figure 60 – Lateral force comparison between WFT on the Test Track (CTVTC) and WFT on the FlatTrac III belt surface for the UHP Tire for track replay input. The solid green line shows the quadratic fit to the data and the dashed line shows the quadratic fit +/- 10% bound. ..... 69
Figure 61 – Lateral force comparison between WFT on Track and FlatTrac III Measurement for UHP Tire for track replay input (top and bottom). (Top) The solid red line shows the linear fit to the data and the dashed line shows the linear fit +/- 10%

bound. (Bottom) The solid green line shows the quadratic fit to the data and the dashed line shows the quadratic fit +/- 10% bound. ..... 70
Figure 62 – Lateral Force vs Slip Angle for track replay as measured on the FlatTrac III colored by Normal Load for UHP Tire ..... 71
Figure 63 – Lateral Force vs Slip Angle for track replay comparison between WFT on Track and WFT on FlatTrac III for UHP Tire. ..... 72
Figure 64 – Lateral Force versus Slip Angle for track replay comparison between WFT on Track and WFT on FlatTrac III for Broadline Tire. ..... 72
Figure 65 – Lateral force versus Slip Angle plot with test data (dots) and MF 6.1 model (solid line) at different inclination angles and normal loads for Broadline Tire from sLAT02. ..... 75
Figure 66 – Lateral force versus Slip Angle plot with test data (dots) and MF 6.1 model (solid line) at different inclination angles and normal loads for UHP Tire from sLAT02. ..... 76
Figure 67 – Cornering stiffness versus Normal Load for both Broadline and UHP tire calculated using the MF 6.1 tire model fit to the data. ..... 77
Figure 68 – MF 6.1 model fit (solid lines) to test data (dots) from Broadline Tire (top) and UHP Tire (bottom) from sLAT12 test procedure. ..... 78
Figure 69 – Lateral Force versus Slip Angle Magic data for UHP tire from sLAT02 and sLAT12 tests. Note that the tire data from sLAT02 predicts higher cornering stiffness than the sLAT12 with a higher slope. ..... 79
Figure 70 – Cornering stiffness versus Normal load comparison for Broadline tire between tire models fit for sLAT02 and sLAT12 test data. ..... 80
Figure 71 – Cornering stiffness versus Normal Load comparison for UHP tire between tire model fit for sLAT02 and sLAT12 test data. ..... 81
Figure 72 – Tread surface temperatures for sLAT02 and sLAT12 test procedures ..... 82
Figure 73 – Slip Angle profile for sLAT12. Notice that the slip passes through 0 three times for each combination of load and inclination angle (camber). ..... 83
Figure 74 – Slip angle profile and tread surface temperature for sLAT12 ..... 84
Figure 75 – Cornering stiffness versus normal load plots for UHP tire all three inclination angles for each sweep through 0 degree slip angle. Notice that the highest load is first test condition for each inclination angle condition as outlined in section b above. ..... 85
Figure 76 – Tread Surface Center Temperature versus Normal load at all three inclination angles for UHP Tire for each sweep through 0 degree slip angle. Notice that the highest load is first test condition for each inclination angle condition as outlined in section b above ..... 86
Figure 77 – Cornering stiffness versus Normal load for Broadline tire at all three inclination angles for each sweep through 0 degree slip angle. Notice that the highest load is first test condition for each inclination angle condition as outlined in section b above. ..... 87
Figure 78 – Tread surface temperature versus Normal Load for Broadline Tire at all three inclination angles for each sweep through 0 degree slip angle. Notice that the highest load is first test condition for each inclination angle condition as outlined in section b above 88

Figure 79 – Tire normal load versus slip angle colored by tire camber as measured from on track testing ..... 89
Figure 80 – Cornering stiffness versus normal load comparison between tire model from sLAT02 and asymmetric sLAT12 ..... 91
Figure 81 – Cornering stiffness versus normal comparison between tire model from sLAT02 and asymmetric sLAT12 after scaling the model for UHP tire ..... 92
Figure 82 – Lateral force versus slip angle at 0 deg inclination angle (camber) for scaled, unscaled MF 6.1 tire models from asymmetric sLAT12 and MF 6.1 from sLAT02 for UHP tire ..... 93
Figure 83 – Lateral force versus slip angle at 1.5 deg inclination angle (camber) for scaled, unscaled MF 6.1 tire models from asymmetric sLAT12 and MF 6.1 from sLAT02 for UHP tire. ..... 94
Figure 84 – Lateral force versus slip angle at 3 deg inclination angle (camber) for scaled, unscaled MF 6.1 tire models from asymmetric sLAT12 and MF 6.1 from sLAT02 for UHP tire. ..... 95
Figure 85 – UHP Tire: Scatter plot of Lateral force predicted by MF 6.1 model from sLAT02 model (top) and measured by FT III for the track replay. Similarly, scatter plot of Lateral Force predicted by scaled MF 6.1 model from asymmetric sLAT12 (bottom) and measured by FT III for track replay input. Also presented is the linear fit, coefficients and ±10% error bounds ..... 99
Figure 86 - Broadline Tire: Scatter plot of Lateral force predicted by MF 6.1 model from sLAT02 model (top) and measured by FT III for the track replay. Similarly, scatter plot of Lateral Force predicted by scaled MF 6.1 model from asymmetric sLAT12 (bottom) and measured by FT III for track replay input. Also presented is the linear fit, coefficients and ±10% error bounds ..... 100

# Chapter 1. Introduction

## a. Motivation

The topic of vehicle handling has been studied for several decades. Vehicle handling is primarily controlled by the forces and moments at the tire contact patch [1] [2]and research has been done to investigate the influence of tire properties on vehicle handling [3] [4]. It has also been established that conditions such as normal load, slip angle, temperature and camber affect the tire force and moment properties [5] [6]. Extensive work has been done to capture tire behavior due to changes in normal load, camber, and slip angle. One of the most popular tire models used in vehicle dynamic simulation called the 'Magic Formula', captures this tire behavior by empirically fitting a model [7] [8]. While it can characterize the tire based on normal load, slip angle, camber and more recently inflation pressure, it does not have any temperature effects. Tire temperature and tire wear have been shown to have a strong influence on tire properties [5] [9] [10] [11]. Several research attempts to modify the Magic Formula tire model by incorporating tire surface and tire bulk temperature [5] [11]. In addition to simulation, this is also important from a safety standpoint since all vehicle active stability systems such as electronic stability control (ESC) systems are based on a tire model [5] [12].

Tire data is needed to fit the empirical Magic Formula model and bulk of the research has been performed on an indoor tire testing machine. Consequently current guidelines for tire testing are designed for an indoor tire testing machine which include all possible combinations of operating conditions (normal load, slip angle and camber) [13]. This could potentially test the tire at conditions that are not relevant and cause excessive wear and modify the temperature of the tire to what the tire actually experiences on the road. Since studies have shown the influence of tire wear and temperature on tire performance [5], it is important to test the tire in the most relevant operating conditions. Testing at relevant conditions can reduce testing time, cost and unnecessary wear on the tire. The Magic Formula model can also be fit to this relevant tire data to give higher quality tire models in the relevant region of operation.

This research will focus on identifying the most relevant operating conditions of a tire by instrumenting the test vehicle with wheel force transducers (to measure loads) and slip sensors (to measure slip angle and camber angle) during highway (on-center) type driving maneuvers. Temperature probes to measure the temperature of the internal rubber of the tire and the surface of the tire will also be installed on the vehicle. Testing will be performed on a test track which is designed for vehicles to travel at highway speeds. This data will be used to modify the indoor tire test procedure to measure tire force and moment properties under realistic highway conditions.

In addition to identifying the relevant operating conditions, the tires will also be tested at a low slip angle and high slip angle to investigate if the data shows that the tire behaves differently. As mentioned previously, typical Magic Formula testing requires testing the

tire across the entire load and slip angle range. The findings from this test data will be used to determine any scaling factors or correlations as necessary to adjust the Magic Formula to predict vehicle response under both low slip and high slip tire conditions.

b. Document Structure

The rest of the document is organized as follows:

Chapter 2. Literature Review

This chapter summarizes the historical and current research and technology in understanding tire performance. Initially, an overview of vehicle dynamic simulation and the need for understanding tire performance for use in vehicle dynamic simulation is presented. Next, the importance of understanding tire performance from a safety standpoint such as implementing in vehicle active safety systems is presented. Further, influence of various factors such as load, pressure and temperature on tire performance is presented. It then extends into a background into tire modeling – the most basic to the most recent to the most widely used tire models are discussed. Next, a background on tire testing rigs is presented. Historical and current technologies on tire testing rigs are presented with a discussion on drum based and flat surface based tire testing. This section is then concluded with a discussion on designing a tire testing procedure on previously mentioned tire test rigs. Historical and industry recommendations along with more recently invented novel test methods are discussed.

Chapter 3. Testing Equipment

This chapter provides a description of the various testing equipment that were used for this research. Initially the test vehicle, array of sensors along with their data acquisition system is presented. Next, a discussion of the communication protocol used is presented. It is concluded with a discussion on the specific tire test rig used for this research with machine specifications.

Chapter 4. On Vehicle Testing

This chapter discusses the process by which different sensors and the data acquisition system is integrated with the vehicle. An outline of the configuration of the communications protocol to allow for efficient data recording is presented. Next, a summary of data from daily driving to identify the most common driving conditions is presented. It is concluded with a thorough analysis of design of on vehicle testing at the test track based on daily driving data. The various tire and vehicle operating conditions are presented which are used in subsequent chapters.

Chapter 5. Tire Testing on FlatTrac III

This chapter discusses the design and implementation of the tire testing procedures used in this research. Next, a detailed analysis of the tire performance is presented along with tire dependence on various operating conditions such as normal load, camber and slip angle. Correlation between two different measurement systems and surfaces are presented with a correlation equation. Next, tire models fit to different tire test procedures are discussed along with scaling factors and corresponding errors in the quality of the model

fit. The tire models were simulated with one of the tire testing procedures to get a direct correlation between simulated and measured parameters.

Chapter 6. Conclusion and Future Work

The main conclusions from this research are presented along with recommendations to further the work presented here. While a few questions were answered, several more questions remain unanswered, and this section provides guidance for future effort.

# Chapter 2. Literature Review

The tire is the only physical connection between the road surface and the vehicle [1] [2]. All the primary forces necessary for acceleration, braking and cornering are generated by the tire at the tire contact patch [1] [2] [5]. Thus, the tire plays a significant role in determining vehicle performance. From a safety standpoint, modern day electronic stability control systems and anti-lock braking systems rely on having a tire model for their operation. Simulating vehicle dynamic performance heavily relies on having an accurate understanding of tire performance [5] [14] [15].

## a. Vehicle Dynamic Simulation

From a simulation standpoint, a tire model is a critical component to predict vehicle performance. Vehicle dynamic simulation helps reduce cost of development by reducing number of physical prototypes that have to be built and several iterations can be quickly performed on a computer which could take several test sessions to be performed on track [14]. An accurate vehicle dynamic simulation is immune to any weather or logistical hurdles that could be faced while scheduling on track testing to evaluate the tire or vehicle. In addition, potentially dangerous maneuvers to test the limit stability of the vehicle-tire system can also be avoided on the track if done virtually [5] [14]. Thus is it critical to have a thorough understanding the tires and have an accurate mathematical model that can be

used in simulation. In addition, tire model parameters can also be used to correlate with subjective and objective vehicle testing [16].

The most commonly used simple vehicle dynamic simulation model is a bicycle model. A bicycle model is a two degree of freedom vehicle model describing the lateral and yaw dynamics of the vehicle [1] [2]. Other variants of the bicycle model also include roll degree of freedom which also includes weight transfer [16]. Even such simple vehicle dynamic models require a tire model for reliable simulation. Alternatively, the cornering compliance concept has also been proposed to describe vehicle handling behavior [3]. The biggest contributor of cornering compliance is the tire. The tire cornering stiffness plays a significant role in determining the cornering compliance and thus the handling response of the tire [3] [4].

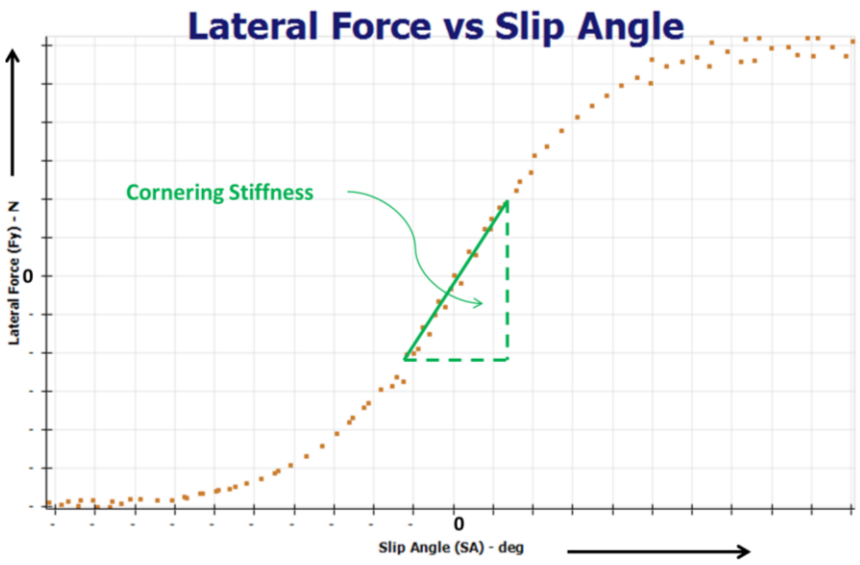


Figure 1 – Lateral Force versus Slip angle plot showing calculation of Cornering stiffness. Cornering stiffness is the slope of the lateral force versus slip angle curve when slip angle is 0.

b. Vehicle safety systems – Anti Lock Braking (ABS) and Electronic Stability Control (ESC)

Anti-lock Braking Systems (ABS) and Electronic Stability Control systems (ESC) are considered among the most critical safety components in a car. ABS systems intervene to prevent tire lock under panic braking to ensure that the tire is near peak slip conditions to ensure stable vehicle response [17]. Several studies have shown that the ABS performance will change if the tire performance changes based on conditions such as operating temperature and inflation pressure [18].

ESC systems use the knowledge of the tire lateral and longitudinal performance envelope to ensure that the vehicle is tracking a reference yaw rate and is within the performance envelope. This reference yaw rate and performance envelope in the ESC system is based on a vehicle model, which uses a tire model [5]. However, the tire will change under different operating conditions and may not adhere to the reference tire model, thus compromising the effectiveness of the stability control system [5] [19].

c. Tire performance metrics as an indicator of vehicle handling

It has been established that the yaw rate gain, yaw rate damping ratio, lateral acceleration phase lag and yaw rate natural frequency are correlated with driver's perception of vehicle handling based on the Four Parameter Evaluation Method [20] [21].

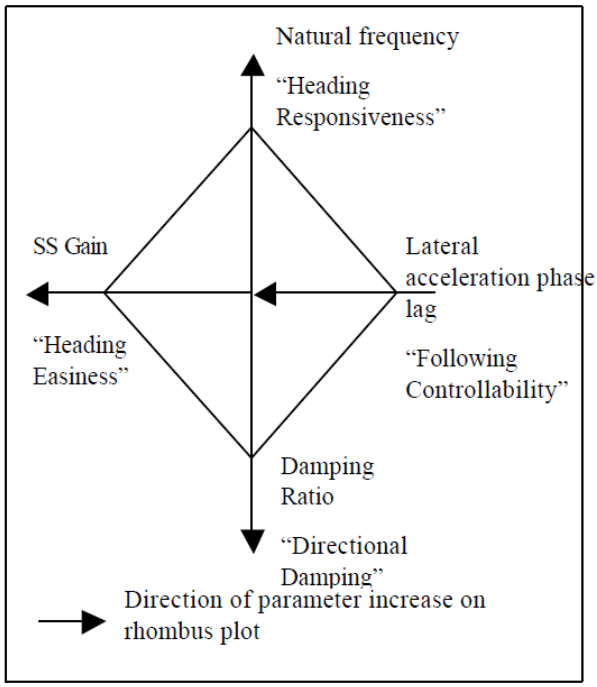


Figure 2 – Four Parameter method to evaluate vehicle transient response [20] [21].

Subsequent research has shown that cornering stiffness and the cornering stiffness load dependency has an influence on lateral transient response of the vehicle [22]. Tire cornering stiffness also directly influences vehicle understeer gradient which has also been shown to be an indicator of subjective handling [9].

Since cornering stiffness is a derived parameter from empirical tire data, cornering stiffness also varies with tire operating conditions. Inflation pressure, normal load, inclination angle, operating temperature, tread depth all influence tire cornering stiffness [5] [6] [9]. Figure 3 shows dependency of cornering stiffness on normal load. Figure 4, Figure 5 and Figure 6 show percent change in cornering stiffness from baseline under inflation pressure, treadwear and temperature.

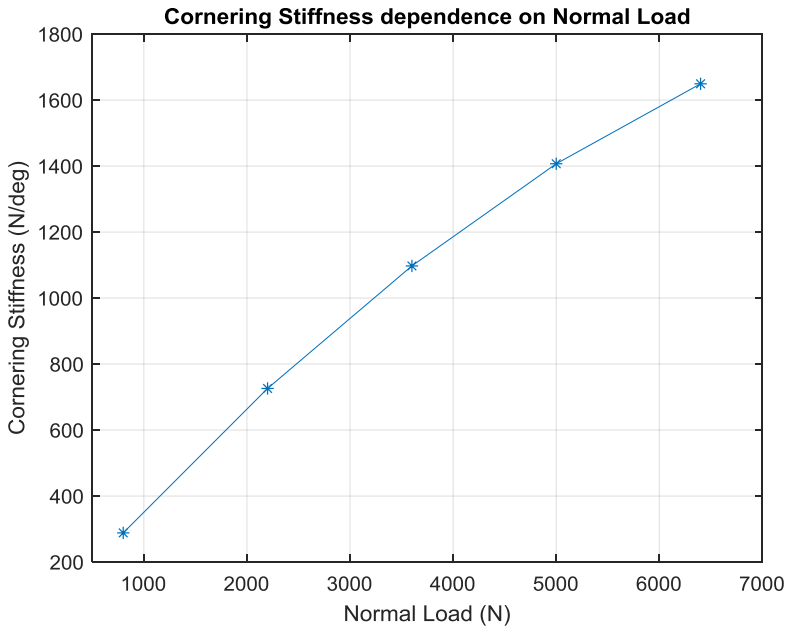


Figure 3 – Cornering stiffness versus Normal Load for a passenger car tire

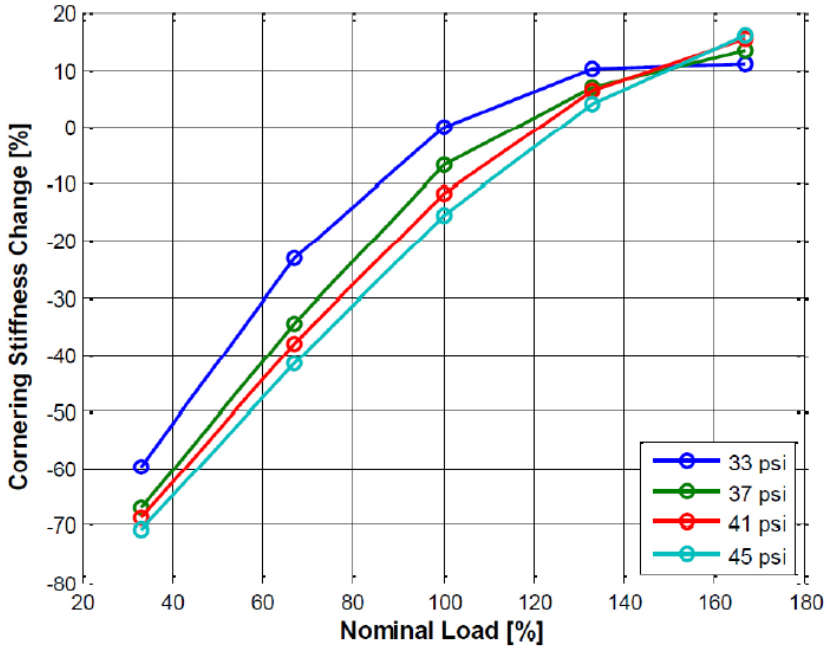


Figure 4 – Cornering stiffness variation due to inflation pressure [5]. Blue curve is baseline

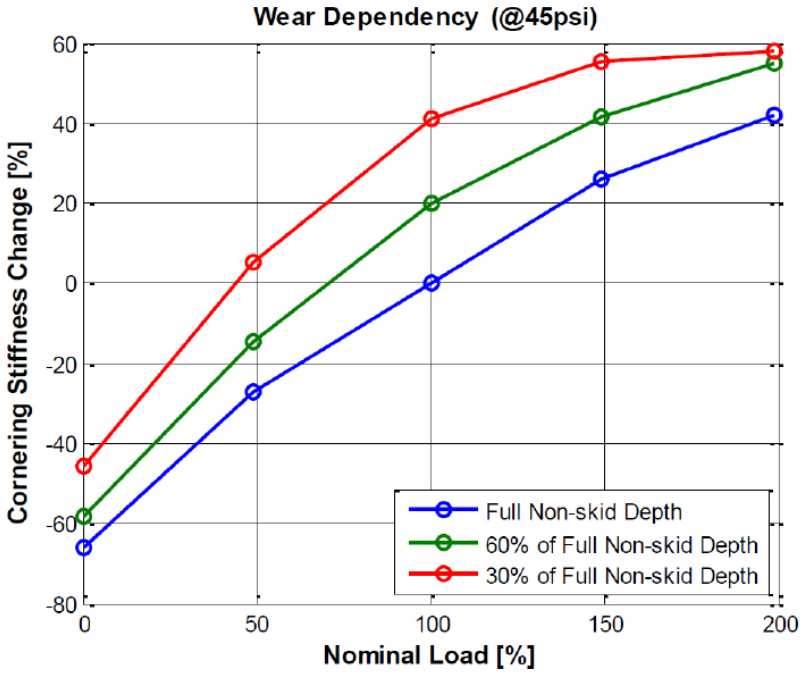


Figure 5 – Cornering stiffness variation due to tread wear [5]. Blue curve is baseline

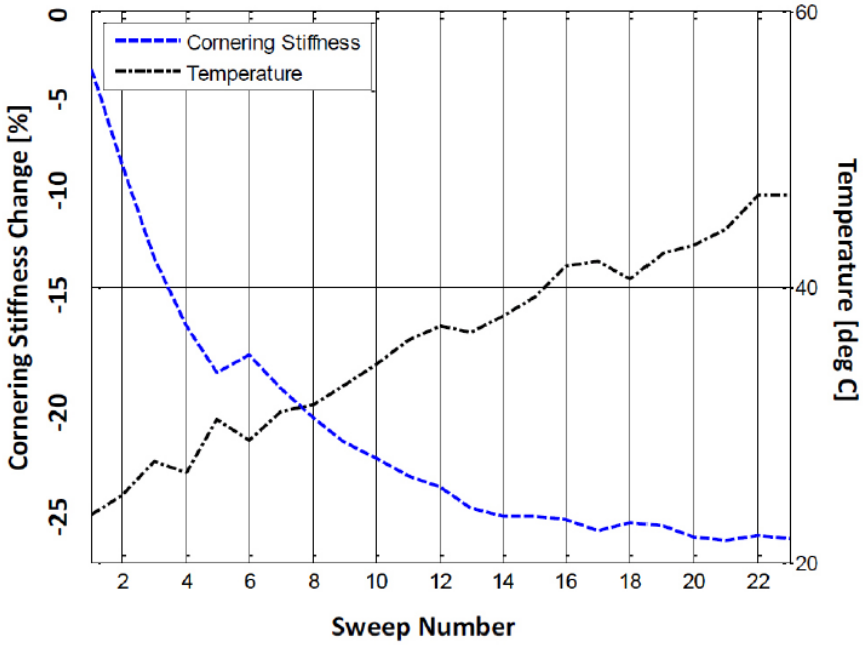


Figure 6 – Cornering stiffness variation due to bulk/core temperature [5]

Tire cornering stiffness is dependent on shear modulus of the tread material [9]. Increase in temperature has shown to decrease shear modulus and thus the storage modulus of the tread material. This leads to a decrease in cornering stiffness with increase tread material temperature. Angrick et al [9] estimates that the cornering stiffness will decrease by about 3-4% per $10^{o}$ C increase in tire temperature.

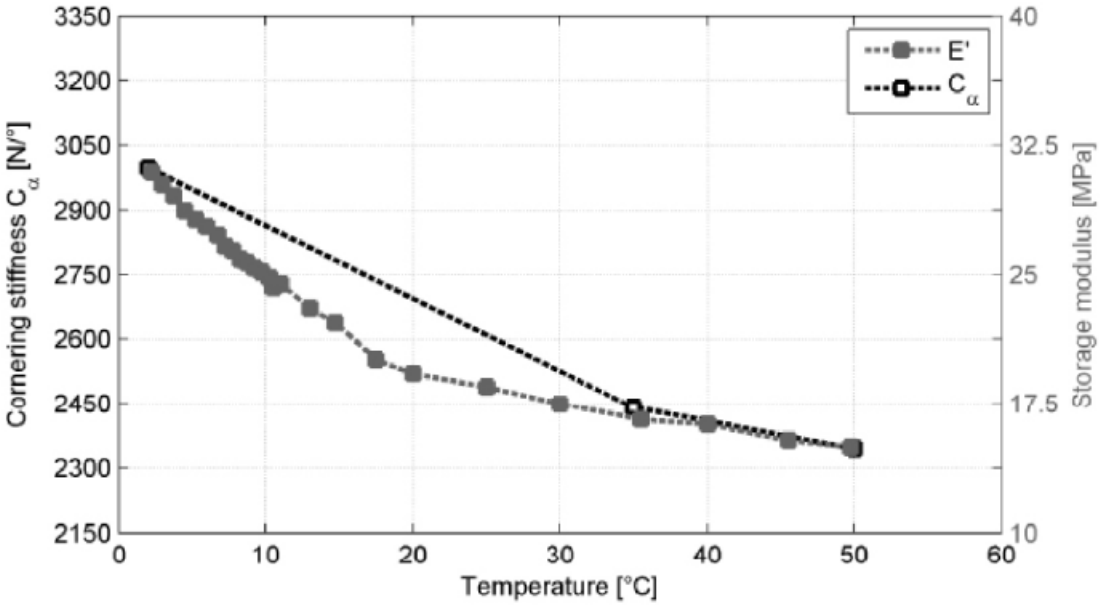


Figure 7 – Comparison of cornering stiffness change with storage modulus over temperature [9].

Figure 8 show cornering stiffness dependency on tire bulk temperature at different normal loads. Thus it is critical to have an understanding of the operating conditions of the tire and to use relevant tire data to determine tire performance metrics.

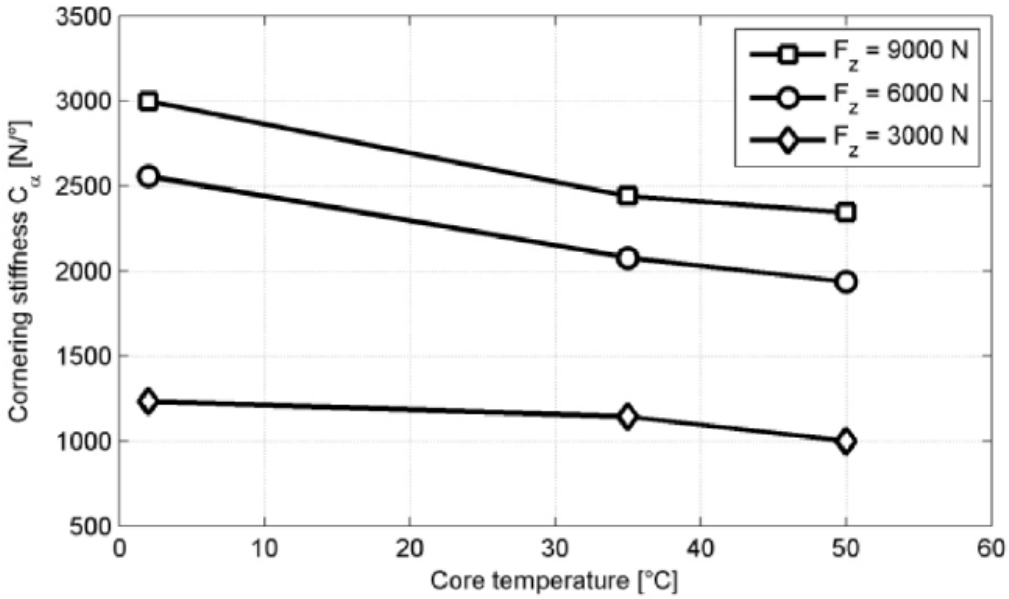

Figure 8 – Cornering stiffness dependence on tire core temperature [9]

d. Tire Modeling

Given that tire models are critical for vehicle dynamic simulation, calculating tire performance metrics and safety systems such as ABS and ESC, considerable work has been devoted to the development of tire models. The appropriate model to be used depends on the desired application [14] [15] [16]. One type of tire models are physical models such as the brush model and the stretched string tire model developed by Fiala in 1954. Such physical models provide qualitative explanation of tires but require more complexity to describe tire-road interaction. Such simulations require extensive computations which make them time consuming for modeling and simulating purposes [23]. Semi empirical models such as FTire [24] and CDTire [25] are often used for ride and handling analysis but also require extensive modeling and characterization [23]. Fully empirical models on the other hand, rely solely on experimental data to generate the model. One of the most

popular tire models is an empirical model called the Magic Formula, first developed in 1984 [7]. Since then several iterations have been developed, each iteration consisting of more fidelity in the model [7] [8].

The Magic Formula tire model, also referred to as 'Pacejka Tire model' or 'MF-Tire' model attempts to capture the response of the tire under different slip angle, inclination angle, normal load and inflation pressure conditions. The model has been extensively used in simple and multi-body vehicle dynamic simulations for vehicle dynamic prediction. It also been extensively used in development of ABS and ESC systems [14]. Several of these active safety systems have an internal tire model which uses MF-Tire model [5]. The popularity of the MF-Tire model is due to relative ease of implementation compared to semi-empirical and physical models described above. Another big benefit of the MF-Tire model is the ability to do sensitivity studies by varying tire coefficients [15].

While the MF-Tire model has been useful for vehicle dynamic analysis, it does not take into account tire operating temperature or tread depth. Given that studies have established that tire performance will vary with these factors, several modifications to the model have been proposed which take into account these parameters. One such model proposed by Mizuno modifies the Magic Formula tire model to include tire surface temperature [11]. A thermodynamic model of the tire surface was defined which analytically describes the heat flux across the tire surface. This heat flux is described by the interaction of the tire on the road surface. Results from this modified MF-Tire model show good correlation with experimental data at different surface temperatures. Different surface temperatures were achieved by modifying the slip angle speed of the tire [11].

Another modification to the MF-Tire model proposed by Singh et al [5] incorporates both variation in tread depth and tire bulk/core temperature. It was determined that cornering stiffness has low dependency on tire surface temperature but high dependency on tire bulk/core temperature and thus the tire model was modified based on bulk/core temperature.

However, the tire data needed for the tire model is dependent on the kind of test the tire is subject to. Modification of the test procedure itself will modify the data. A simple parameter such as slip angle speed had an effect on tire surface temperature which changed the tire data and thus the tire model [11]. Smith et al [14] proposed a modification to the tire test procedure itself to monitor the tire wear and tread surface temperature. Thus it is important to have a thorough understanding of the tire testing process to ensure relevant tire data is acquired and thus a relevant tire model is generated.

e. Tire Testing Rigs

Tire testing to generate data for tire modeling used in vehicle dynamic simulation is typically done on machines called Tire Test Rigs such as the MTS Flat-Trac III CTTire Test System [26] at Smithers Rapra, Calspan Tire Research Facility [2] [10], see Figure 9, and SoVa Motion Tire Testing Services [27]. All these three machines have a flat steel belt that is suspended between two large drums. The steel belt is supported by either an air or water bearing creating a flat level surface to test the tire. The steel belt is covered by sandpaper, the grit can be specified by the user commissioning the test [14].

Figure 9 – Tire Force and Moment testing machine at Calspan Corporation [10].

An alternate to testing the tire on a flat belt testing is testing the tire on a drum. However, Pottinger et al [28] have concluded that the surface curvature tends to reduce slip and camber generated lateral force and aligning torque. In addition, there is no simple flat to curve surface transformation relationship.

f. Tire Force and Moment Testing for lateral handling

Pottinger et al [19] states that tire forces and moments have been extensively studied since the 1930's. The SAE Highway Tire Committee has taken the responsibility to produce updated and comprehensive standards for tire force and moment testing. The SAE [29] recommendation split the test procedure into low-slip angle procedure and full range slip angle procedure. The recommended loads are 20%, 40%, 60%, 80%, 100%, 120%, 140% and 160% of the target normal load at a specified inflation pressure. The slip angle sequence is 0, +1, -1, -2, +2, +4, -4, -6, +6, +8, -8, -10, +10 degrees for full-range slip angle

procedure and 0, +1, -1, -2, +2, +4, -4, -6, +6 degrees for low-slip angle procedure. The forces and moments are meant to be measured at these discrete slip angle values. The test speed is recommended to be 2mph since the goal with this standard is to objectively compared tires for strictly research and development purposes. SAE recommends higher roadway speeds to be used when the intent is to simulate vehicle behavior [29].

Kasprzak et al [30] propose tire force and moment with a slip angle sweep in contrast to the discrete slip angle testing proposed by SAE. This test procedure was designed for Formula SAE tires but can be applied to passenger car tires as well. There is no split between low and full range slip angle testing. The procedure recommends slip angle sweeps to ±12 degrees at all combinations of loads (1557N, 1112N, 667N, 222N and 2002N) and inclination angles (0, 1, 2, 3 and 4 deg).

Both the procedures described above are examples of 'square matrix' testing where every combination of load, camber (inclination angle) and slip angle are tested. In contrast, Smith et al [14] propose GS2MF, a modification to the conventional square matrix testing by eliminating some combinations of normal load and slip angle based on weight transfer calculations. In addition, a variable rate slip angle speed is recommended as it accounted for the least mechanical hysteresis in small-slip angle conditions and lower thermal hysteresis in the large slip angle conditions. The central idea behind GS2MF lateral test is to minimize the tire surface temperature throughout the test with each sweep designed to start at the same baseline temperature by integrating cool down periods.

# Chapter 3. Testing Equipment

A variety of testing equipment was used to collect data for this research. Below is a description of the equipment

a. Test Vehicle

Cooper Tire & Vehicle Test Center lent a 2016 Ford Mustang as the test vehicle for this project. This car was previously used in a promotional campaign and is thus covered in decals.

Figure 10 – 2016 Ford Mustang lent by Cooper Tire & Vehicle Test Center as test vehicle. The vehicle was previously used in a promotional campaign, thus it is covered in decals.

b. VBOX 3i

VBOX 3i is a data acquisition system manufactured by Racelogic Corporation that is capable of logging data at 100Hz via analog, digital and CAN communication. The system has a GPS/GLONASS system integrated with Inertia Measurement Unit (IMU) to measure accelerations and rotation rates along all three axes [31].

Figure 11 - VBOX 3i by Racelogic data acquisition system

The VBOX 3i used here uses a dual antenna system. The GPS/GLONASS antennae and IMU are mounted on the roof of the vehicle to give the GPS/GLONASS direct line of sight with the satellites. This setup in shown in Figure 12 with the fore antenna circled blue and the rear antenna circled red. The rear antenna serves as the 'primary' antenna to measure speed, distance and acceleration. The fore antenna or secondary antenna is used to measure the slip in the chassis by measuring the direction the two antennae are pointing [32].

Figure 12 – GPS/GLONASS antennae mounted on the roof of the vehicle. The fore ‘secondary’ antenna is circled blue and the rear ‘primary’ antenna is circled red.

The IMU is mounted along with the rear antennae using an integrated roof mount as shown in Figure 13. This fixes the distance between the IMU and the rear antenna. The distance between the approximate location of the center of gravity (CG) of the vehicle and IMU are entered. The VBOX 3i uses this information to estimate the acceleration and rotation rates at the CG of the vehicle. Figure 13 shows the rear antenna along with the IMU mounted together on the roof of the vehicle using the roof mount.

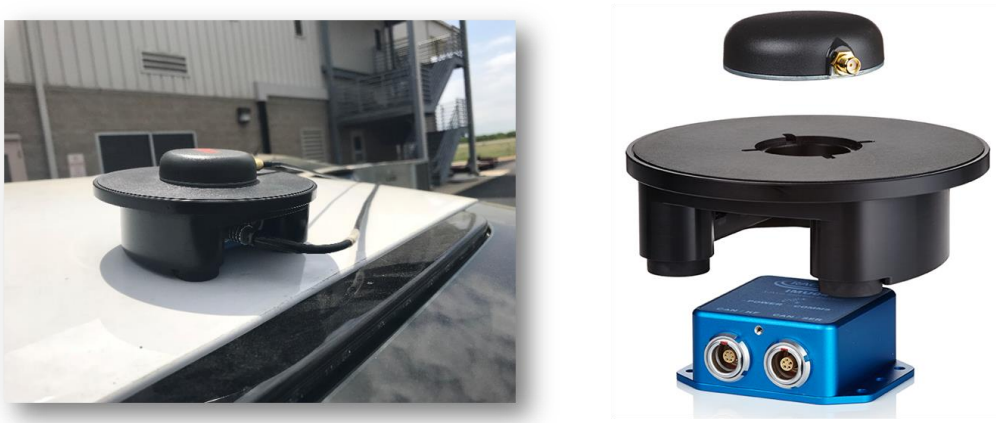

Figure 13 – (Left) IMU in integrated roof mount with rear GPS/GLONASS antenna moutned on the roof of the vehicle. (Right) Exploded view of IMU, roof mount and GPS/GLONASS antenna [33]

c. MoTeC L180

A MoTeC L180 data acquisition system was also used in addition to the VBOX 3i since the VBOX 3i only allows data logging at up to 100Hz. The L180 allows much higher logging frequencies up to 1000Hz per channel. It also has 4 individually programmable CAN buses allowing for channels with different baud rates to communicate with the L180.

Figure 14 – MoTeC L180 Data acquisition system

d. Michigan Scientific Wheel Force Transducers

Wheel Force Transducers (WFT) are used to measure the forces and moments at the directly at the wheel. The WFT used for this research was manufactured by Michigan Scientific Corporation. The LW12.8 WFT, shown in Figure 15, has a maximum normal and longitudinal load capacity of 53.4kN, a maximum lateral load of 26.7kN and 8100 N-m maximum moment capacity. It can also measure accelerations along the normal and longitudinal directions rated at 55g [34].

Figure 15 – Michigan Scientific Wheel Force Transducer LW12.8

The transducer mounts onto a custom-made wheel with mounting holes for the LW12.8 WFT as shown in Figure 17. The system also comes with a signal conditioning box referred to as CT2, shown in Figure 16, which performs real-time coordinate

transformation and cross-talk compensation. It also allows for zero and shunt calibration. The CT2 box is the communication unit via which the data acquisition system can interface with the LW12.8 WFT.

Figure 16 – CT2 Signal conditioning box from Michigan Scientific

Figure 17 – Custom made wheel with mounting holes (circled in red) for the LW12.8 wheel force transducer

The system has a slip ring amplifier package that interfaces the WFT with the signal conditioning box. This slip ring, as shown in Figure 18, has internal accelerometers and stores all zero and calibration data for the WFT. Thus is it essential that the slip ring package and WFT pair always matched to ensure the appropriate signal gains are applied.

Figure 18 – Slip ring and amplifier package

e. Kistler Optical Slip Angle Sensor

The slip angle (α) of a tire is defined as the angle between a rolling wheel's actual direction of travel and the direction towards which it is heading [8]. Figure 19 shows the tire coordinate system in SAE according to SAE J2047 [35].

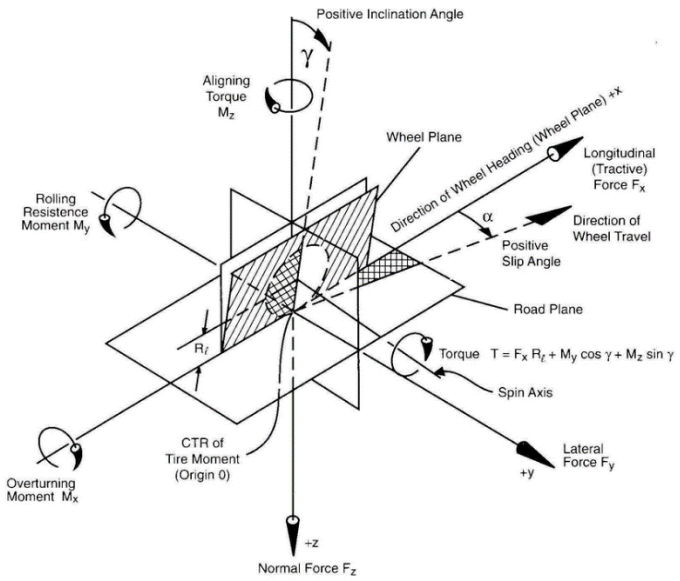


Figure 19 – Tire coordinate system according to SAE J2047 [35]

Optical slip angle sensors were used to get a direct measurement of slip angle at the wheel. The optical slip angle sensor works by measuring the lateral ($V_y$) and longitudinal ($V_x$) speeds of the vehicle. The slip angle of the wheel is given by inverse tangent of the ratio between lateral and longitudinal speeds is the wheel slip angle [8].

$$\alpha = \tan^{-1}\frac{V_y}{V_x} \ldots (1)$$

The slip angle sensor is mounted on the slip ring portion of the wheel force transducer assembly. The system has a GPS antenna and an integrated IMU unit to compensate for any roll or pitch in the system to give true slip angle relative to the road surface. Due to the method of mounting the unit, the measured roll angle is the camber angle the wheel makes with the road surface. However, this measured camber is relative to the horizon. The road surface has a crown to facilitate water drainage. The true camber of the wheel will be the difference between the measured camber and road crown.

Figure 20 – Optical slip angle sensor mounted on the wheel force transducer

The slip angle sensor is then connected to a signal conditioning box which does real time calculation of slip angle and acts as the interface between the slip angle sensor and the data acquisition system. The signal conditioning box is placed inside the vehicle, see Figure 21, and connected to the VBOX 3i data acquisition via CAN bus.

Figure 21 – Kistler signal conditioning box

f. Tire internal temperature

The internal temperature of the tire was measured by using a Texense IRN8-WS4 wireless infrared temperature sensor shown in Figure 22. Figure 24 shows the schematic of the location of the sensor to measure internal tire temperature. The sensor can measure between -20C to +200C with a 260ms response time at full scale. The unit can communicate via CAN bus between 125k to 1Mbps baud rates at 1Hz, 10Hz, 50Hz or 100Hz [36].

Figure 22 – Texense IRN8-WS4 internal temperature sensor

Figure 23 – Texense IRN8-WS4 internal tire temperature sensor mounted on a 3D printed housing

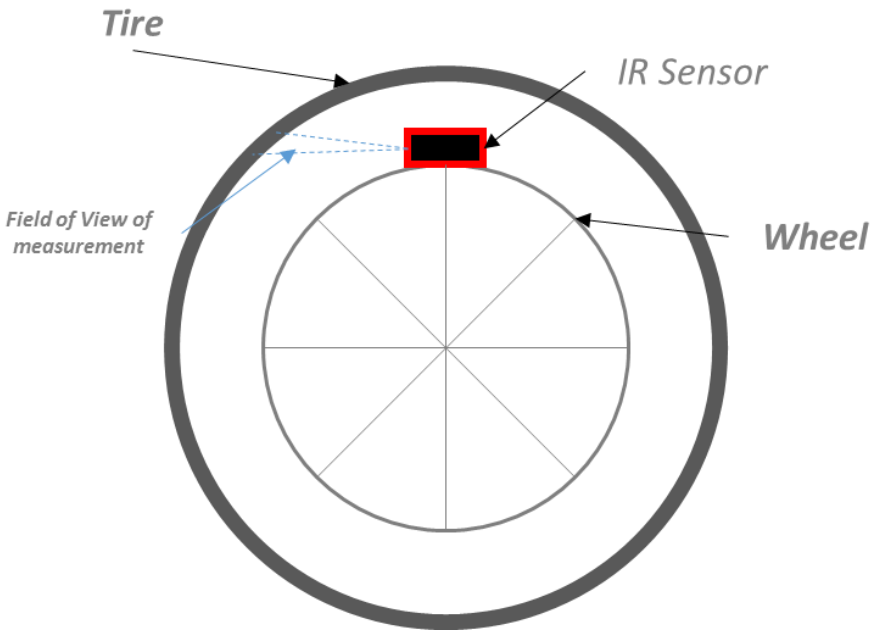


Figure 24 – Schematic of IR sensor mounted inside the wheel to measure the internal tire temperature

The field of view of the sensor is based on the distance between the inner liner of the tire and the IR sensor. Using a 17" wheel with a 215/55R17 tire, the distance between the sensor and the inner liner is approximately 250mm. At this distance, the sensor covers 190mm of width on the inner liner. This distance is covered with eight measurement circles with each being 37.5 mm in diameter. This schematic is shown in Figure 25. The reported temperature at each is the average temperature in that circle [36].

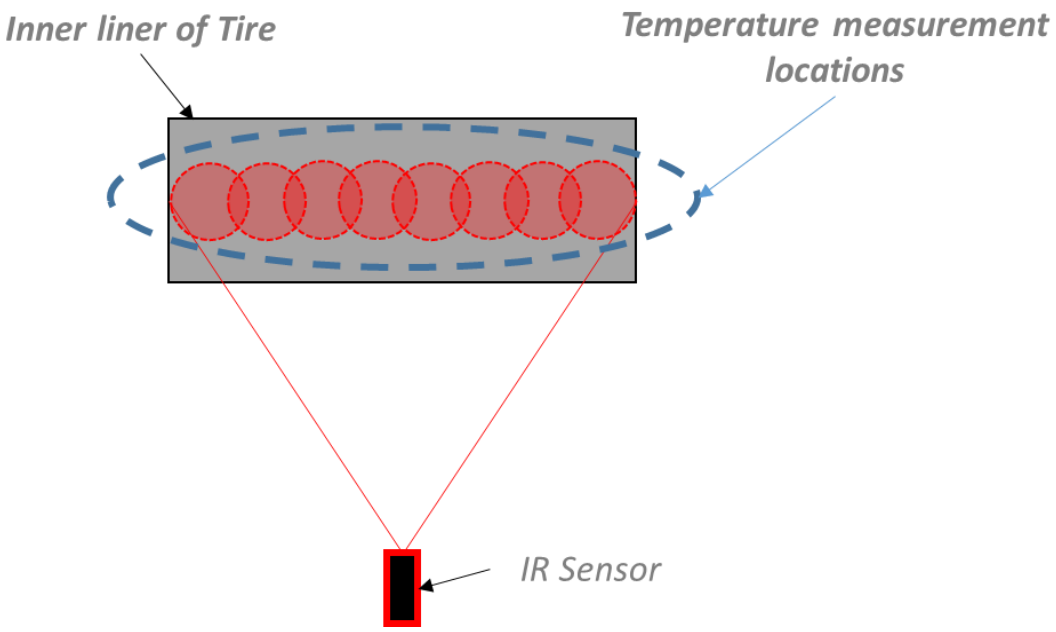


Figure 25 – Schematic of operation of IR sensor to measure temperature on the inner liner of the tire.

Figure 26 shows the internal tire temperature sensor along with the 3D printed housing mounted on the wheel. The surface of the wheel was first sanded with 600 grit sandpaper to create a rough surface. It was then cleaned with alcohol wipes to remove any dust, dirt and grime. The sensor was then mounted using hot glue and allowed to cure for 5 minutes. The tire was then mounted on the wheel. The internal tire temperature sensor wirelessly communicates with a master CAN bus which is then connected to the data acquisition system.

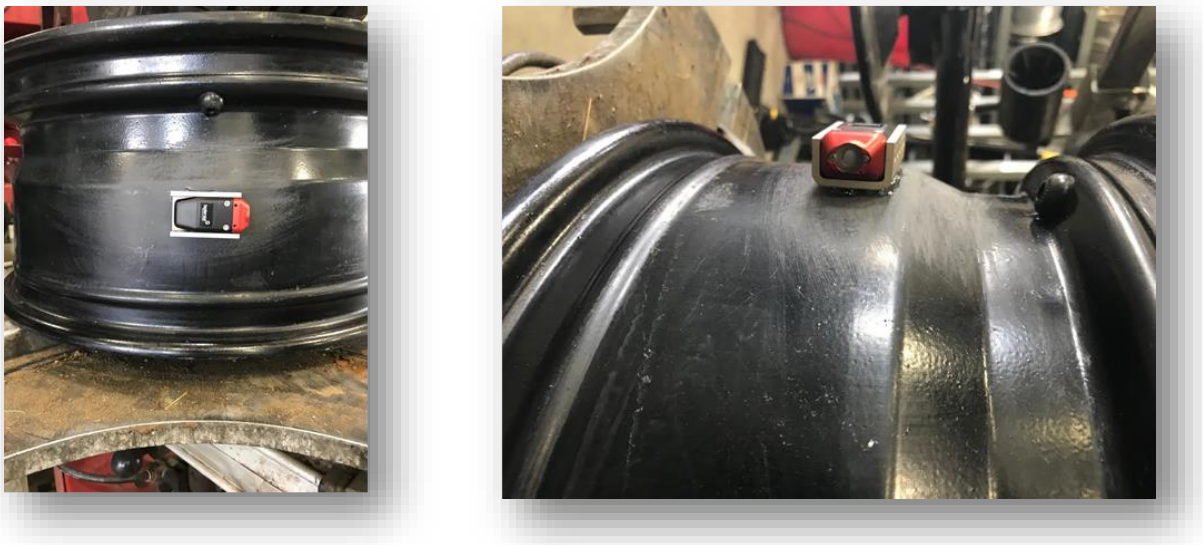

Figure 26 – IRN8-WS4 internal tire temperature sensor mounted on the 3D printer housing which is glued on to the wheel.

g. Tire tread surface temperature sensor

The tire tread surface temperature was measured using an infrared array of sensors, Texense IRN-RC, mounted under the fender of the vehicle. These sensors can measure from -20C to +200C with a response time of 100ms at full scale. The sensor samples at 50Hz and can transmit data via CAN bus between 125k to 1Mbps [37]. Figure 27 shows the sensor with the red infrared sensors. The sensors were mounted using 3M dual lock right above the steering axis of the wheel, seen in Figure 28. This way, the sensors do not lose sight of the tire tread surface during steering. These sensors are connected to the data acquisition via CAN bus.

Figure 27 – Texense IR temperature sensor for measuring tread surface temperature. [37]

Figure 28 – IRN-RC Texense infrared temperature sensors mounted underneath the fender

Figure 29 shows the Texense IRN-RC sensor measuring the tread surface temperature on three locations – inside, middle and outside. The part of the tire tread which is facing the inside of the vehicle is labeled ‘inside’, the part of the tread which is towards the outside of the car is labeled ‘outside’. The part of the tread which is in the middle of the tire tread is labeled ‘middle’.

Figure 29 – Texense IRN-RC temperature sensors measuring the tread surface in three locations – inside, middle and outside.

h. CAN bus communication

All the equipment was set up to communicate with the data acquisition systems via the CAN protocol. CAN bus communication offers the ability to transmit several channels over the same piece of cable thereby minimizing the number of wires needed to integrate multiple sensors [38]. For example, the wheel force transducer measures and transmits three forces, three moments, two accelerations, angular position and angular velocity for a total of 10 channels per WFT. Analog or digital transmission would require 10 different cables running from the CT2 box to the data acquisition system. Instead, using CAN only one wire is needed from the CT2 box to the data acquisition system. All 10 channels are

transmitted over the same cable. The individual channels can be identified by their unique hexadecimal identification numbers [38].

Since multiple channels are being transmitted on the same bus, the channel with the highest priority gets transmitted first and then the lower priority channels gets delayed but not destroyed. The lower priority channel will eventually be transmitted once higher priority message is transmitted [38]. With the IMU and GPS Kalman filtering enabled, the CAN delay in the VBOX is fixed at 20ms for speed and velocity [39].

i. MTS Flat-Trac III CTTire Test System

The tires are tested on a tire testing machine at Smithers Rapra in Ravenna, Ohio. The test machine is an MTS Flat-Trac III CTTire Test System as shown in Figure 30. The capabilities of the machine are shown in Table 1 [26]

Table 1 – MTS Flat-Trac III CTTire Test System specifications

| | |
|---|---|
| **Speed** | ± 250 km/h |
| **Vertical Force** | 25 kN |
| **Lateral Force** | ± 15 kN |
| **Spindle Torque** | ± 2800 Nm |
| **Slip Angle** | ± 30 deg |
| **Inclination Angle** | -12 to +45 deg |
| **Tire OD** | ≤ 910 mm |
| **Tire Width** | ≤ 400mm |

The machine can be programmed to take any combination of vertical load, inclination angle, slip angle and speed inputs within the limits as specified in Table 1. The Flat-Trac III machine at Smithers Rapra uses 120 grit 3M safety walk as the test surface. The machine measures tire forces and moments at the spindle and can also translate them to the contact patch. The Flat-Trac III is extensively used in the automotive industry to

characterize tire performance. In this research this machine is used to generate empirical tire models and correlate the friction between the road surface and surface used on the Flat-Trac III. The tests will be done at 60mph which is significantly below the speed limit of the machine.

Figure 30 – MTS Flat-Trac III CTTire Test System [26]

The machine can measure forces and moments along all three axes at the hub and at the contact patch. It can also measure the ambient temperature, belt surface temperature and tread surface temperature. The tread surface temperature is measured by three infrared sensors mounted on the machine which face the tire tread surface. Figure 31 shows the three infrared sensors (highlighted in red) mounted on the MTS FlatTrac III system to

measure tread surface temperature. The sensors always point in the same direction relative to the tire. Thus as the tire moves due to slip angle, camber or normal load inputs, the same part of the tire tread is always measured. The internal tire temperature used for on-track testing was not available for use on the tire test machine. Thus no internal tire temperature was recorded during the test.

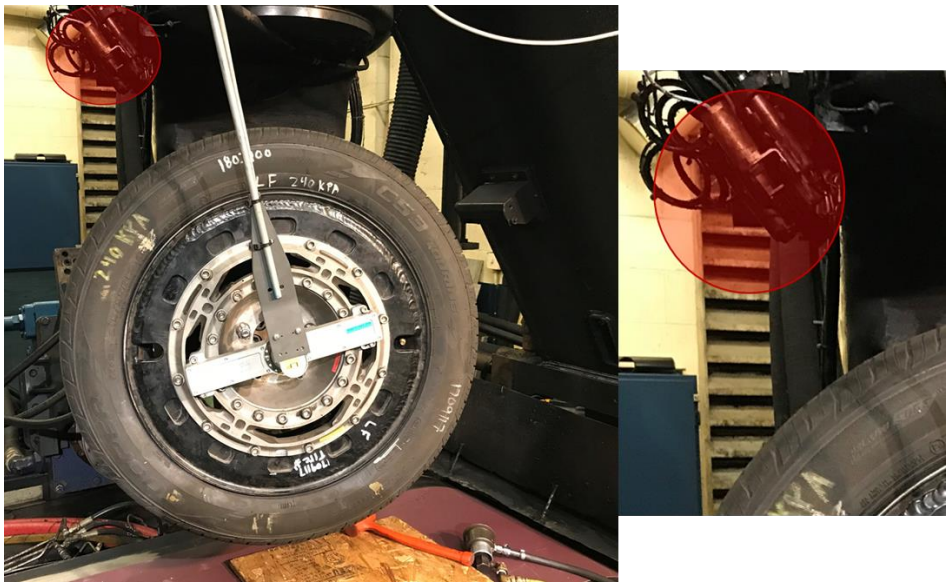

Figure 31 – Tread surface temperature measurement on the MTS FlatTrac III using three infrared (highlighted in red) sensors (left). Zoomed in view of the sensors (highlighted in red) facing the tire tread (right).

# Chapter 4. On-Vehicle Testing

a. Integration of data acquisition systems on the test vehicle

Both the VBOX 3i and L180 were used for data acquisition. The slip angle sensor, internal and tire surface temperature sensors were connected to the VBOX on the only available CAN bus. All sensors were set to log at the maximum allowed logging frequency of 100Hz at 500kbps baud rate. These sensors were provided with industry standard CAN database files which were used to configure the communication between the sensors and the VBOX 3i.

The wheel force transducers need higher logging frequency due to potential aliasing of the signal from tire rotational harmonics and engine vibration frequencies which can range from 30Hz to 350Hz [40] [41] [42] on a modern passenger car internal combustion engine. The WFT were connected to the L180 on one of the CAN bus and configured to log at 1000Hz at a baud rate of 1Mbps. While the WFT data was logged at 1000Hz, an FFT (Appendix A) of the data shows that the data could have been logged at lower frequencies since there was no significant data in the higher frequencies. Future testing can be logged at the minimum manufacturer recommended logging frequency of 250Hz.

A schematic of the communication network between the different data acquisition systems and the sensors is shown in Figure 33. Logging data on two different data acquisition systems poses the challenge of time syncing the data. To facilitate this, a trigger

signal and lateral acceleration signal from the VBOX were transmitted to the L180 over the second CAN bus at logging frequency of 100Hz and at a baud rate of 500Kbps. Recording of the data was controlled by the VBOX using an external file manager as seen in Figure 32. At the instant the VBOX 3i starts recording data, a trigger is sent to the L180 indicating that data is being recorded. This trigger is used by the L180 to start logging wheel force transducer data.

Figure 32 – Racelogic VBOX file manager used to control the start/stop of data recording on the VBOX 3i.

Time syncing the data between the VBOX 3i and L180 is important since that will determine the relationship between the forces and moments measured by the WFT and the measured slip angle and tire internal/tread surface temperatures. In addition, the normal load, camber and slip angle channels are used to drive the tire on a Flat-Trac III machine at Smithers. Having the channels synced will allow direct correlation between the forces and moment measured on the road surface and Flat-Trac III surface.

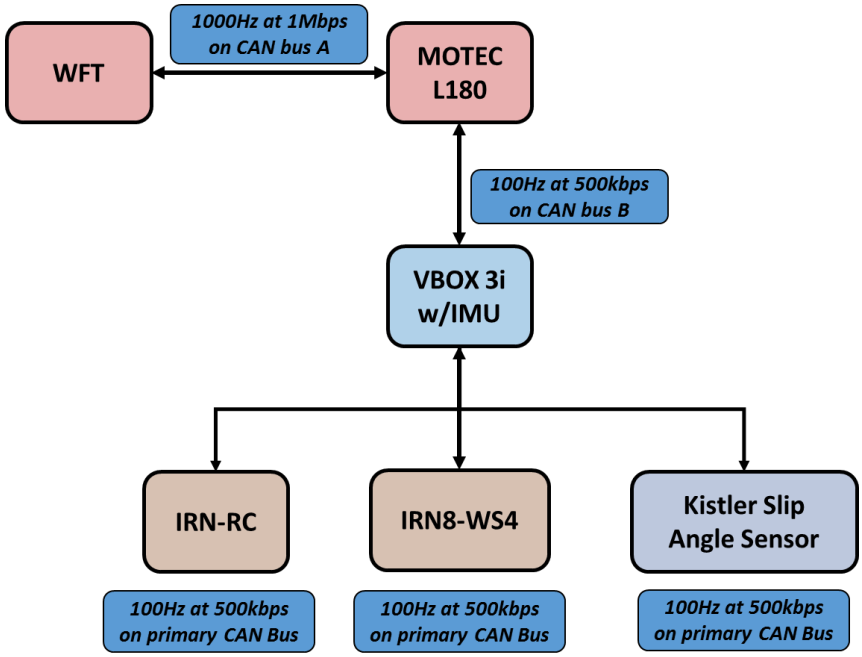


Figure 33 – Schematic of connection between sensors and data acquisition system

There was a noticeable delay between the data recorded by the L180 and the VBOX 3i, see Figure 34. This is mostly likely due to signal delay in transmitting the signals from VBOX 3i to the L180. To achieve synchronization between the two datasets, the data was imported into MATLAB and the cross correlation [43] between the two recorded lateral acceleration signals was measured. The result of the cross correlation provided the necessary time shift required to perfectly line up the data, see Figure 35. This time shift is then applied to all the channels to ensure that WFT data logged in the L180 is synchronized with the slip angle, temperature and camber angle channels logged in the VBO 3i. The data logged in the VBOX 3i are all internally synchronized by a fixed CAN delay of 20ms [39]. Thus while the cross correlation (and thus the time shift) is calculated for lateral acceleration, it can be applied across all the recorded channels.

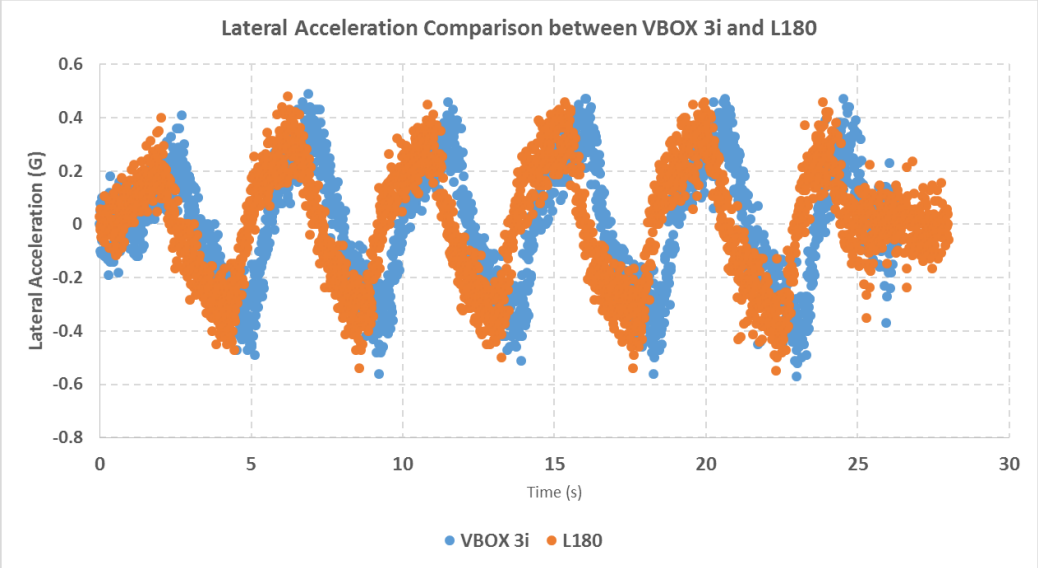


Figure 34 – Lateral acceleration logged between the VBOX 3i and L180. The figure shows that the VBOX 3i lateral acceleration is leading the L180 lateral acceleration signal

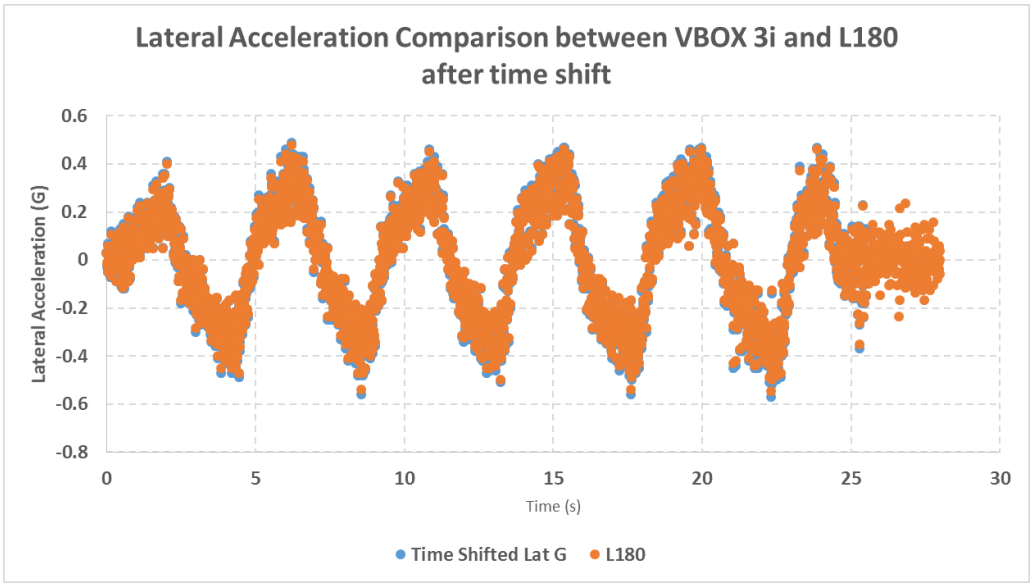


Figure 35 – Lateral acceleration comparison after the time shift applied using the cross correlation between the two signals

Two runs per tire were done and it was noticed that the time lag was not uniform. The time lag between VBOX 3i and MoTeC L180 was calculated for each run and the corresponding data was time shifted. Table 2 summarizes the time shift for each run and each tire necessary to synchronize the data. Figure 34 and Figure 35 correspond to the data from Run 2 of the Broadline Tire time shifted by 0.67 seconds

Table 2 – Time shift (in seconds) applied to each run for each tire to synchronize the data

| | UHP Tire | Broadline Tire |
|---|---|---|
| **Run 1** | 0.80 | 1.04 |
| **Run 2** | 0.85 | 0.67 |

b. Daily driving log

Since the goal of the thesis was to understand the operating range of the tire during normal highway driving, a vehicle similar to the test vehicle was instrumented with a data acquisition system to log the speed, steering wheel angle and the lateral acceleration. This data provided guidance to the on-track testing procedure. A VBOX 3i was installed on a personal car and data was logged for a span of 20 days which translates to approximately 50 hours of driving. This included driving from home, work, gym, grocery store etc. to reflect normal highway driving scenarios.

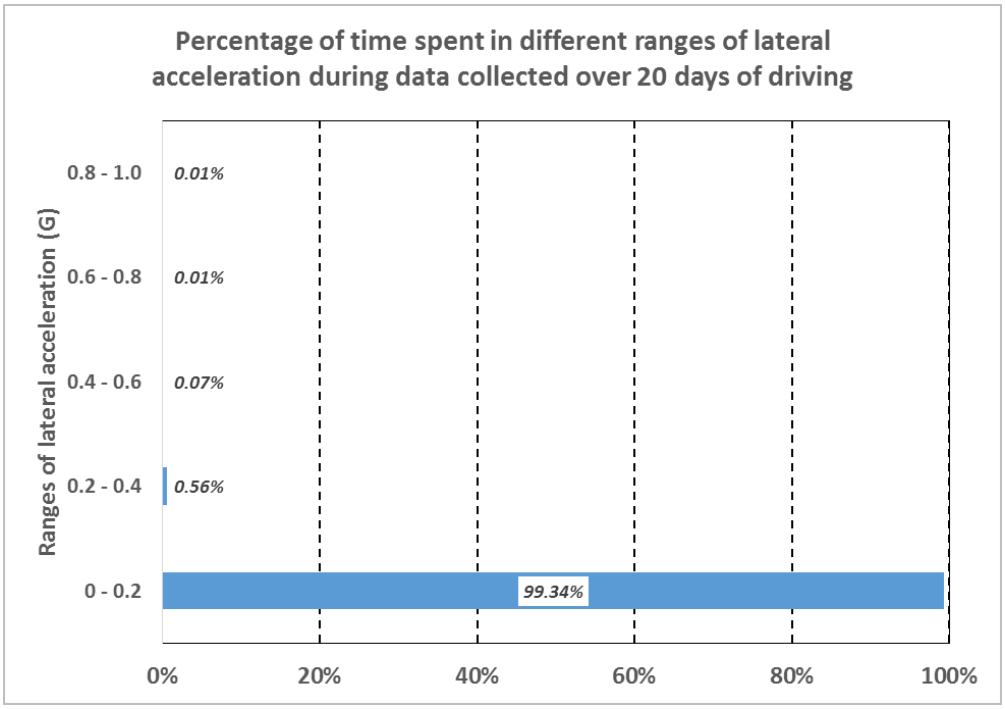


Figure 36 – Percentage of time spent in different ranges of lateral acceleration during data collected over 20 days of driving

Figure 36 shows that over 99% of the time is spent between 0g and 0.2g lateral acceleration. The next region with most activity is between 0.2g to 0.4g of lateral acceleration. That is not surprising given that majority of the driving involved straight-line driving on the highway along with some lane changes to pass vehicles. The data does also include city driving which is at much lower speeds compared to highway speeds.

c. On Track Testing

Track testing was conducted on the handling oval of the Cooper Tire & Vehicle Test Center in Pearsall, Texas. Figure 37 shows an aerial layout of Cooper Tire and Vehicle Test Center along with the test area highlighted in red.

Figure 37 – Layout of Cooper Tire & Vehicle Test Center. Testing area of the handling oval highlighted in red (Right).

Using data from the daily driving log, track testing was conducted on the test vehicle at a speed of 60mph to operate within the identified lateral acceleration region. Prior to conducting the test procedure, the tires were warmed up by driving around the 2 mile oval for two laps at 60mph. Figure 38 shows a profile of lateral acceleration during track testing. It can be seen that the lateral acceleration is within the lateral acceleration range as observed in Figure 36.

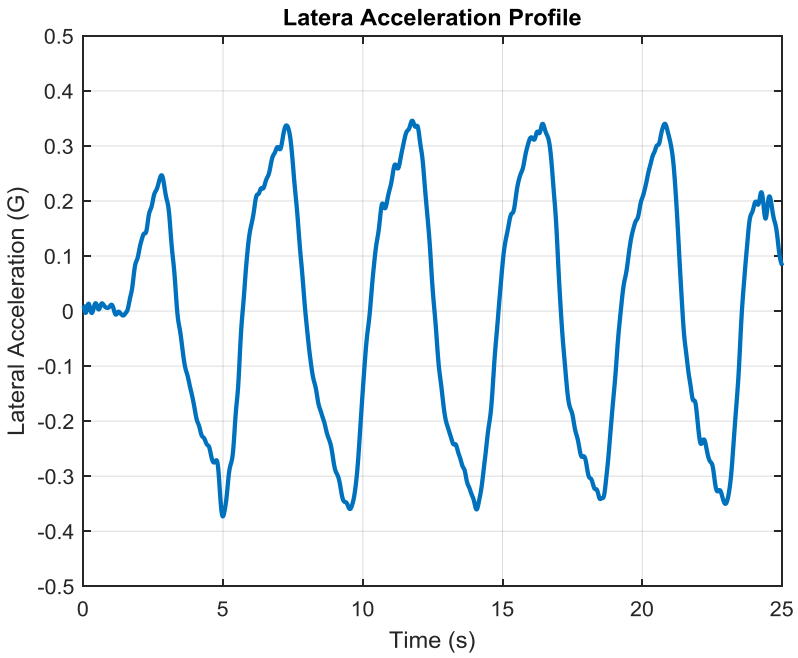


Figure 38 – Lateral Acceleration profile from on track testing

Two sets of tires, both of size 215/55R17, were used for the testing – Ultra High Performance (UHP) and Broadline Tire. The UHP was a Cooper RS3-G1 and the Broadline Tire was a CS5 Ultra Touring. The UHP tire is reported to have more response and better dry traction at the compromise of ride performance [44]. The Broadline tire is designed for comfort at the sacrifice of responsiveness [45]. Utilizing these two contrasting tires will give an idea of the range of tire operating conditions that can be expected. Figure 39 shows a picture of both the Broadline and UHP tires.

Figure 39 – CS5 Ultra Touring Broadline Tire (Left). RS3-G1 UHP Tire (Right) [45] [44]

Figure 40 shows the measured lateral acceleration profiles and slip angle profiles for both the Broadline and UHP tires used for the test. It can be seen that the slip angle for both tires is less than 2 degrees. The slip angle range for the UHP tire is lower than the Broadline tire. This is due to higher cornering stiffness in the UHP Tire. Figure 41 shows the tire camber versus lateral acceleration for both sets of tires. The camber for both tires changes between -1.5 degrees to approximately 2.5 degrees.

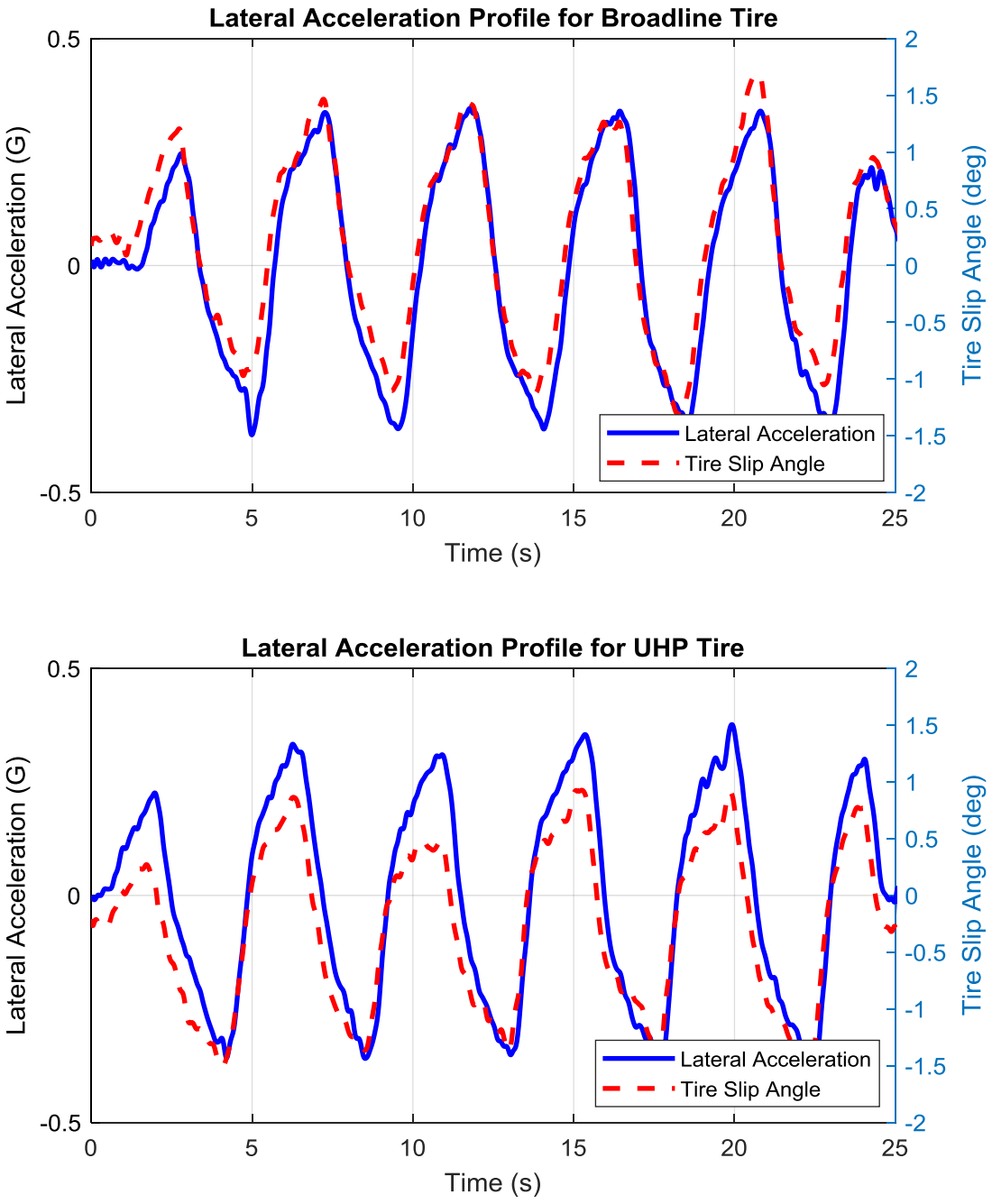


Figure 40 – Measured lateral Acceleration and slip angle profiles from on track testing

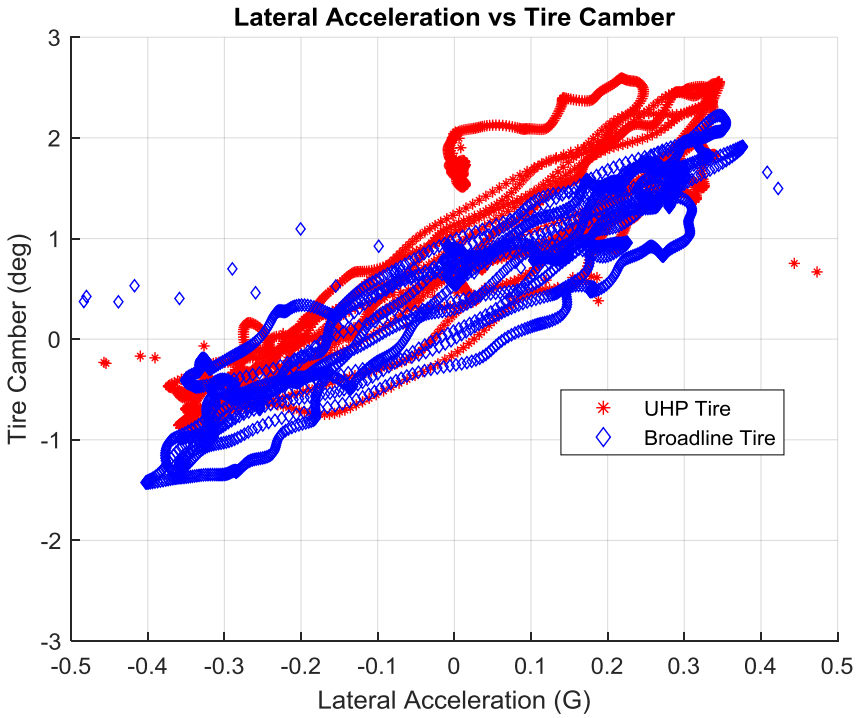


Figure 41 – Lateral acceleration versus camber showing the range of tire camber for both UHP and Broadline tires

Figure 42 shows the range of variation in normal load with lateral acceleration. The normal load for both sets of tires vary between 3000N to 5500N for the test. These data shows the range of slip angles, camber and normal load that a tire would experience during normal highway driving. Figure 43 and Figure 44 show the tread surface temperatures for the Broadline and UHP tires respectively. The rear UHP tire seems to operate at about 5 degrees C hotter than the Broadline tire probably due to the fact that they are the driving tires and have higher rolling resistance than the Broadline tire. The front tires of both the UHP and Broadline tire sets seem to operate within similar temperatures.

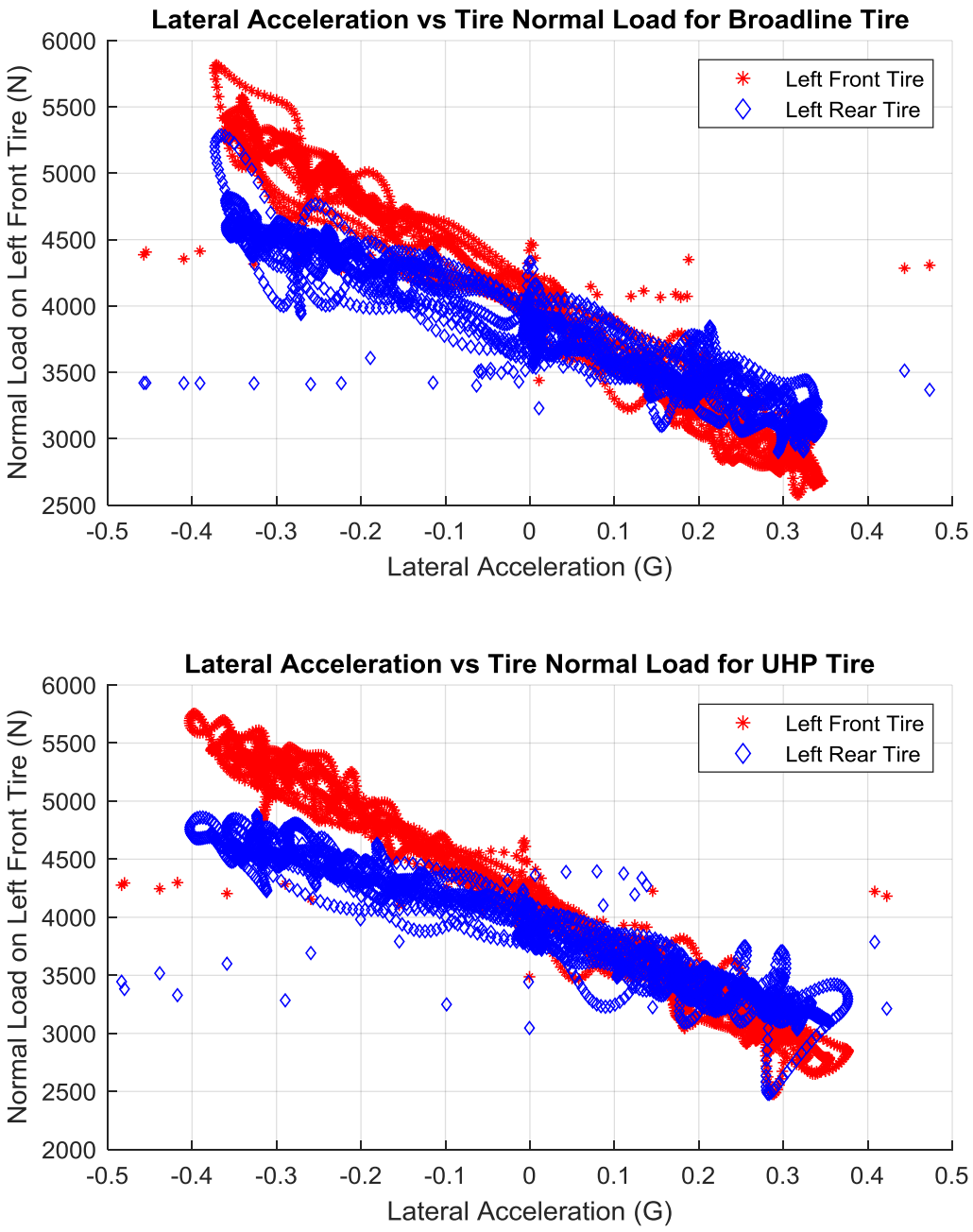


Figure 42 – Lateral Acceleration versus Normal Load profiles for left front and left rear tires for Broadline Tire (top) and UHP Tire (bottom).

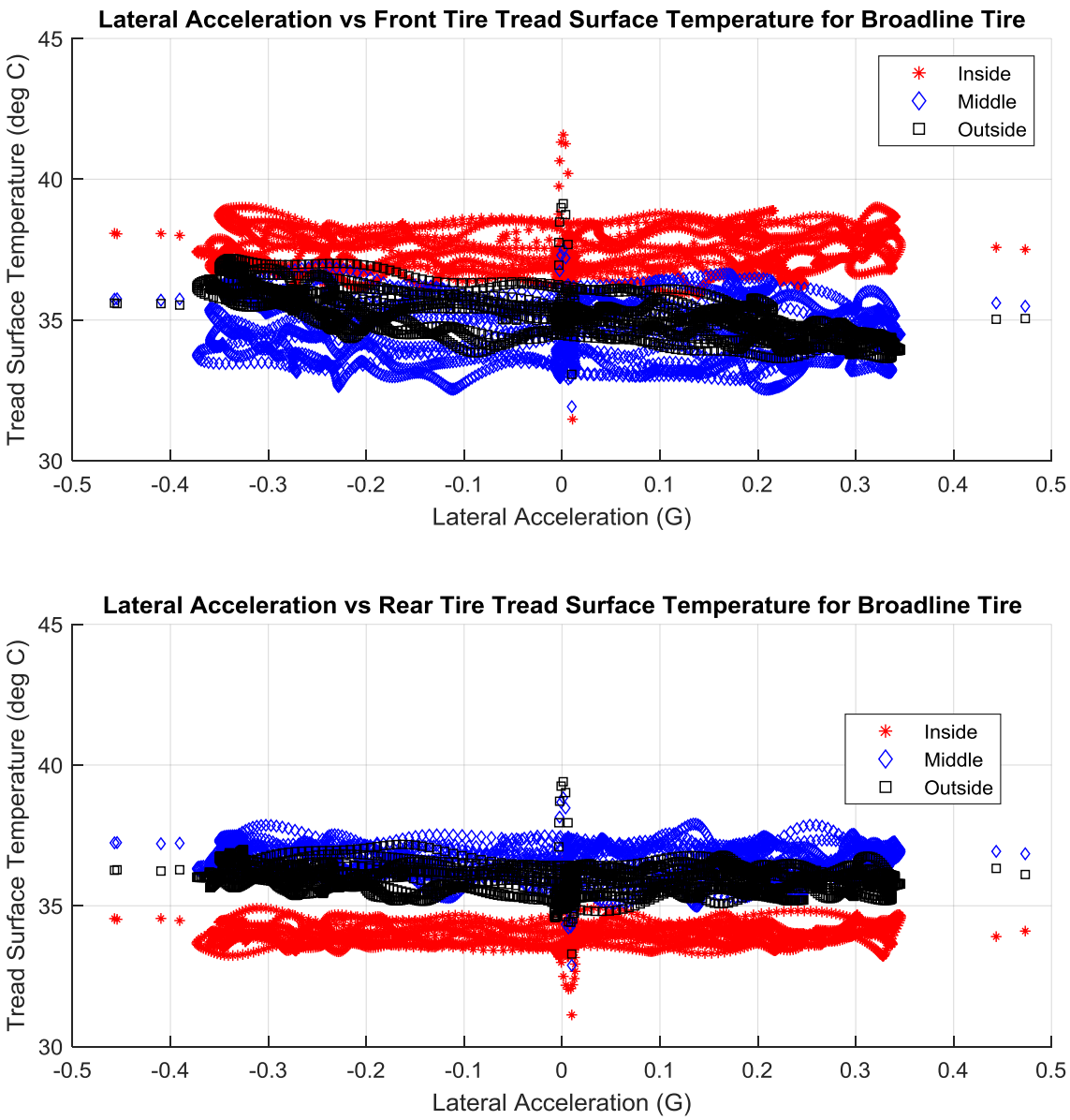


Figure 43 – Lateral acceleration versus front tire tread surface temperature (top) and rear tire tread surface temperature (bottom) for Broadline tire.

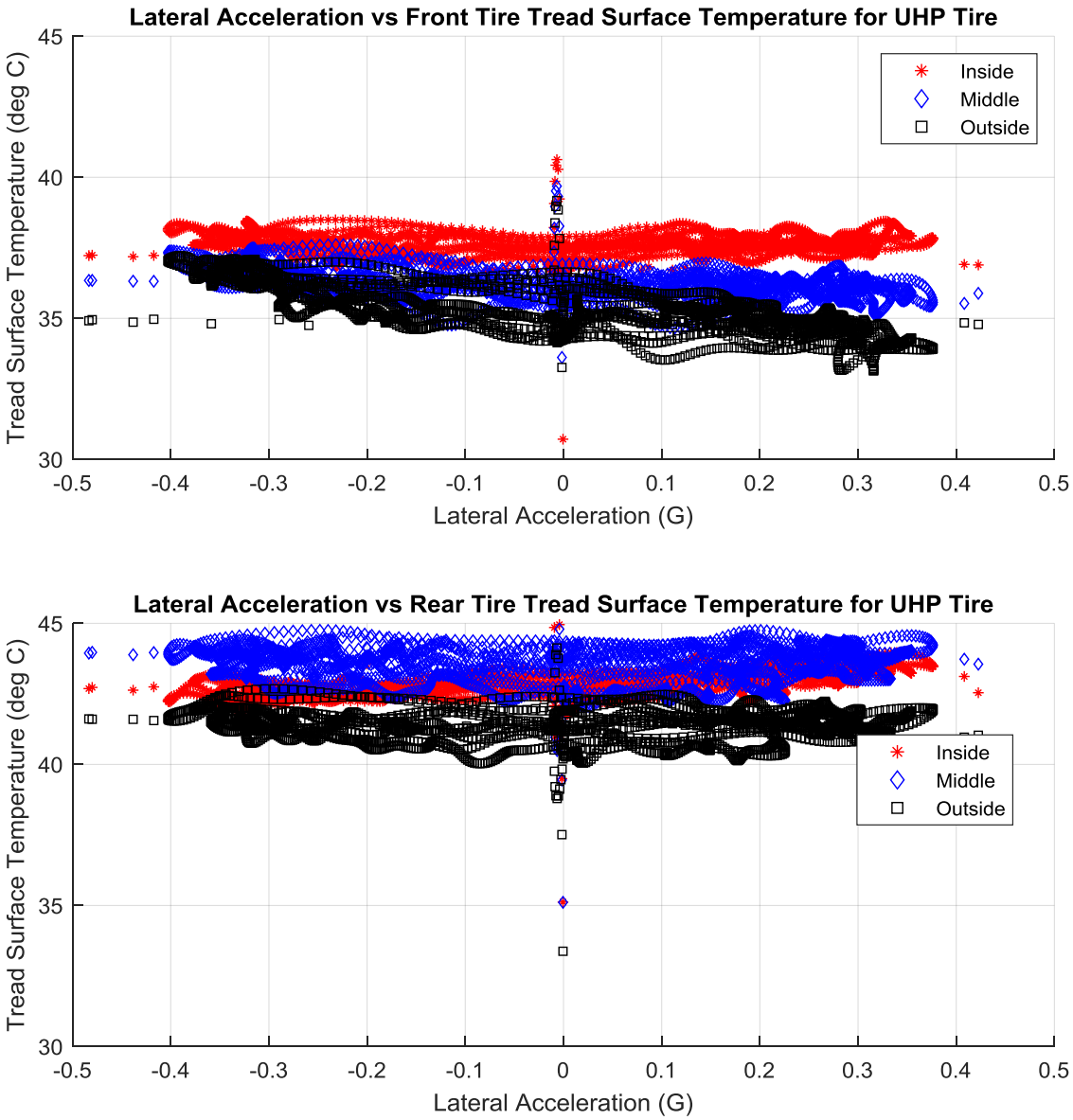


Figure 44 – Lateral Acceleration versus Tread Surface temperature for front (top) and rear tire (bottom) for UHP Tire

Figure 45 shows the inner liner temperature of Broadline and UHP tire versus lateral acceleration. It is interesting to note that the front and rear tires of the Broadline tire operate at similar temperatures with the rear slightly warmer.

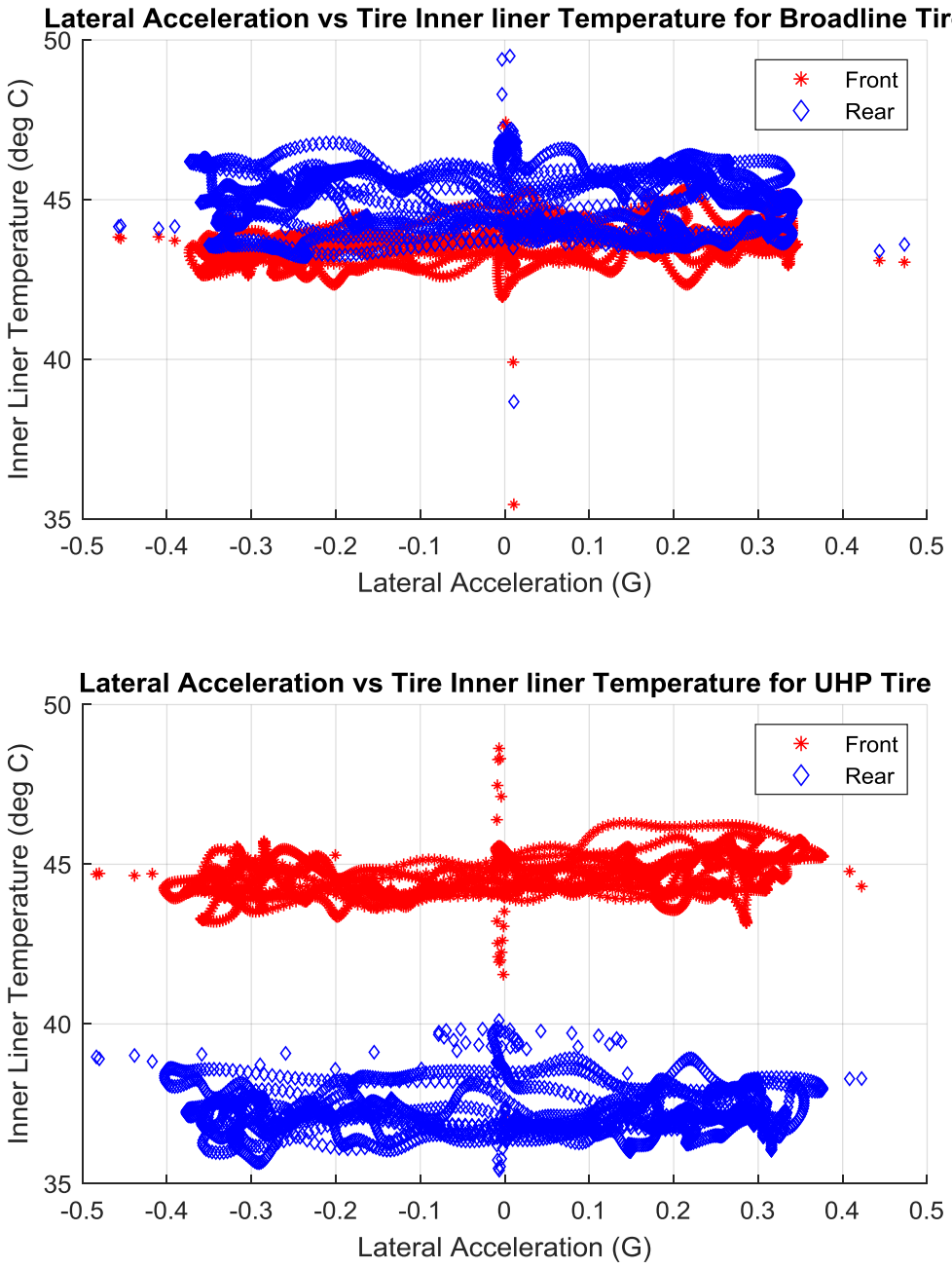


Figure 45 – Lateral Acceleration versus Tire Inner liner temperature for Broadline tire (top) and UHP tire (bottom)

However, there is approximately 5 degree Celsius temperature difference between the front and rear tire inner liner temperature on the UHP tire. Figure 44 and Figure 45

show that the inner liner temperature of the rear tire on the UHP tire is lower than the tread surface temperature. This observation is in contrast with the inner liner and tread surface temperatures of Broadline tire. This seems to be measurement issue since the temperature of the inner liner on the front UHP tire and both tires of the Broadline tire were higher than their respective tread surface temperatures.

The normal load, camber and slip angle ranges observed in Figure 40, Figure 41 and Figure 42 are used to design the tire testing on the FlatTrac III machine at Smithers.

# Chapter 5. Tire Testing on FlatTrac III

Tire performance can be characterized by testing tires on a tire testing machine such as a FlatTrac III [2] [26]. Testing a tire on such a machine is often faster and more convenient due to the ability to control both operating and environmental conditions of the tire. In addition, while on vehicle testing requires a full set of four tires of the same design to test, often only one or two tires of the same design are needed to test on a FlatTrac III machine [14] [29]. By choosing the appropriate range of normal load, slip angle, inclination angle (or camber), and longitudinal speed the tire performance can be characterized in the desired operating range.

In this case, the test was designed to operate the tire through the operating conditions as identified earlier. In addition, the tire was also tested through a high slip angle range in an attempt to capture the variation in tire characteristics due to testing it under operating conditions. This data and the corresponding model fit was used to generate tire performance metrics similar to low slip angle testing. The tire was warmed by running it at 60 mph at 100% reference load for 15 minutes.

The actual physical tires from on-vehicle testing were used for testing on the MTS FlatTrac III machine at Smithers to eliminate any influence from tire manufacturing or uniformity on the test data. The left front UHP and Broadline tires were used.

Figure 46 – One of the test tires from on track testing being fitted with the wheel force transducer to be tested on the MTS FlatTrac III machine at Smithers.

a. sLAT02

The tire test corresponding to low slip angle was referred to as sLAT02. Figure 47 shows the slip angle, inclination angle and normal load command profiles for the sLAT02 test procedure. It can be noticed that the tire is swept between ±2 deg slip angles at 2 deg/s. Smith et al [14] mentioned that a 2 deg/s slip angle generated the least amount of hysteresis in the data. No data was provided when the tire transitions between inclination angles and normal loads. Appendix B shows a zoomed in view of the transition between inclination angle and normal load across the slip angle sweep.

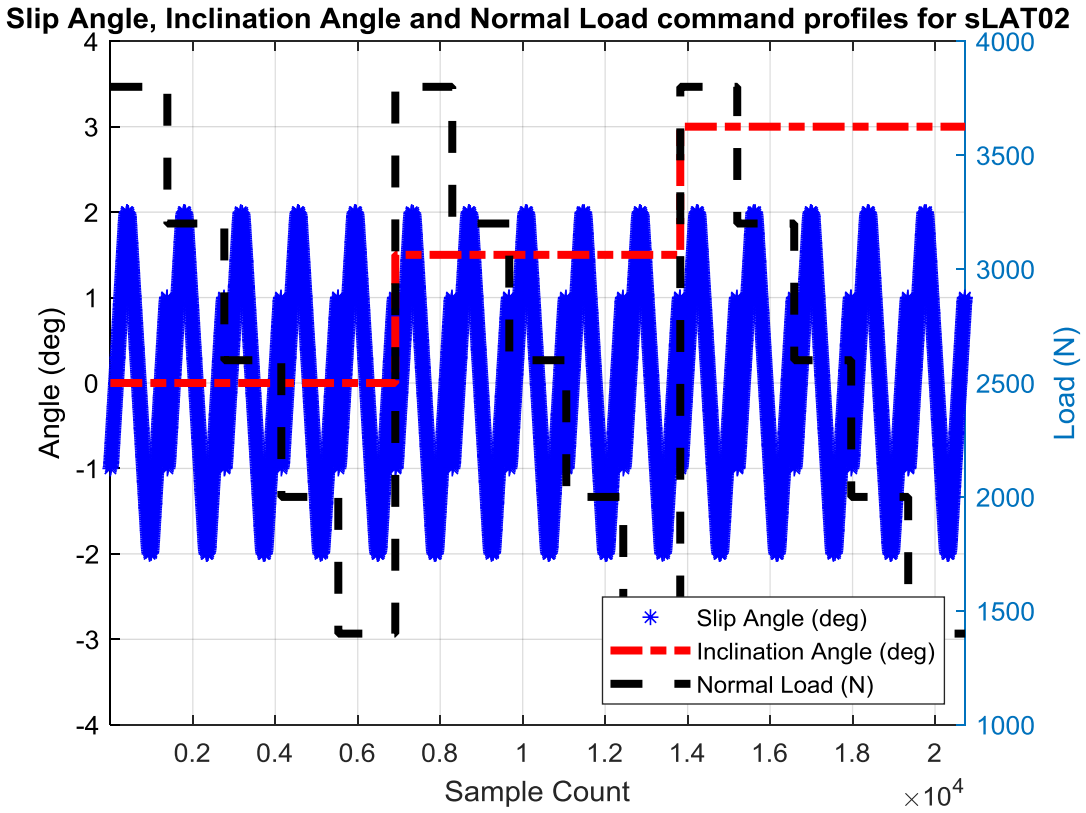


Figure 47 – Slip Angle, Inclination angle and Normal Load command profiles for sLAT02.

The tire is first tested at 0 degree inclination angle at all five normal load conditions. Subsequently the tire is changed to 1.5 and 3 degree inclination angles while being tested at the same five normal loads at each inclination angle. Figure 48 shows a plot of raw lateral force versus slip angle test data for the Broadline tire under sLAT02 test procedure. As expected the tire makes more lateral force at higher normal loads. The plot also shows that inclination angle shifts the entire curve toward a positive lateral force indicating positive lateral force at 0 deg slip angle with inclination angle which is also referred to as plysteer [8].

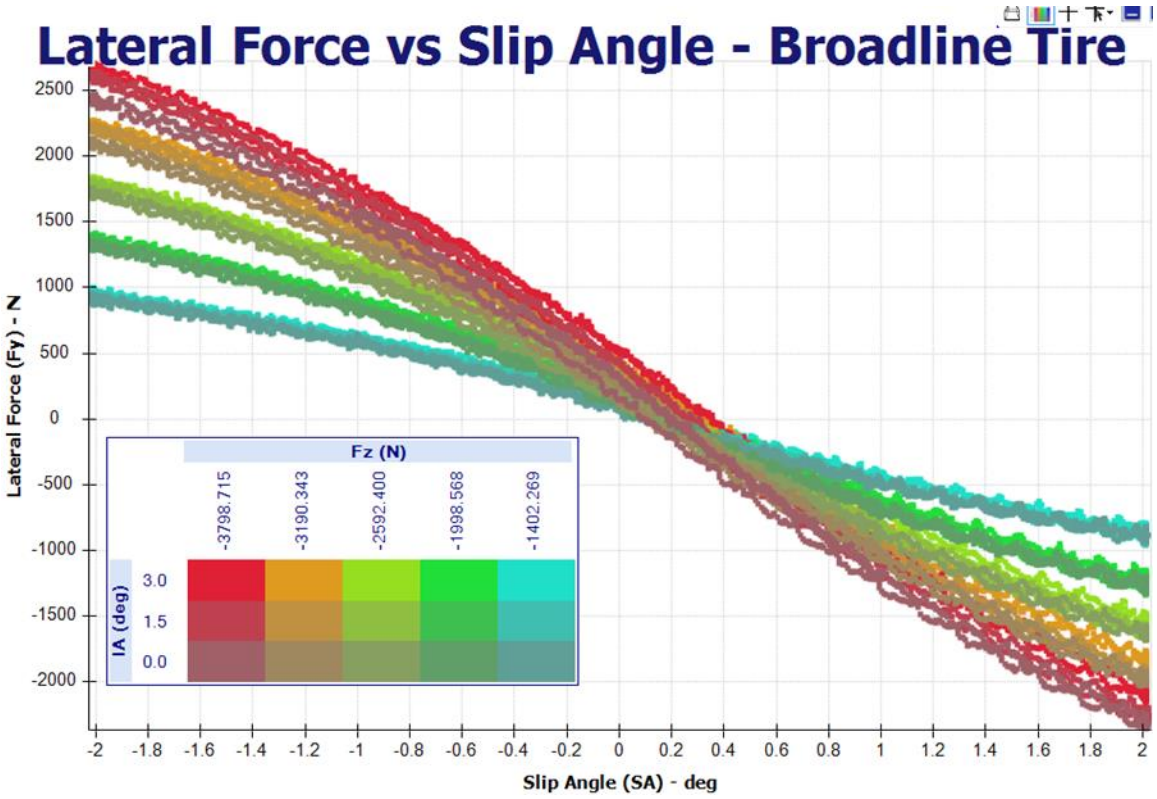


Figure 48 – Lateral force versus Slip Angle at different inclination angles and normal loads from sLAT02 test for the Broadline tire

b. sLAT12

The tire test corresponding to high slip angle test was referred to as sLAT12. Figure 49 shows the slip angle, inclination angle and normal load command profiles for sLAT12 test procedure. It can be observed that the tire is now swept between ±12 degrees slip at 12 deg/s. Smith et al [14] observed that 12 deg/s slip angle sweep rate provided consistent tire temperature during the high slip angle test. Similar to sLAT02, no data during the inclination angle and normal load change was provided. Appendix B shows a zoomed in view of this transition.

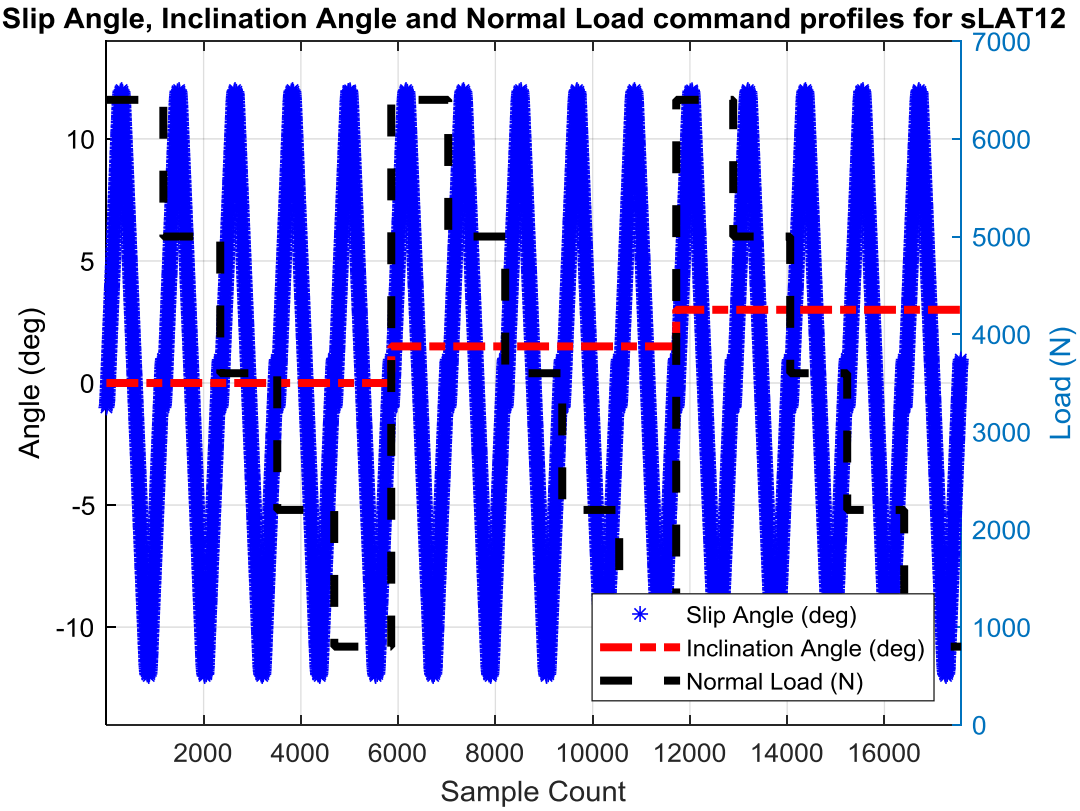


Figure 49 – Slip Angle, inclination angle and normal load command profiles for sLAT12 test procedure.

Figure 50 shows the raw lateral force versus slip angle test data from sLAT12 test for the Broadline tire at different normal loads and inclination angles. The tire generates the most amount of lateral force at the highest normal load as expected. Similar to the data from sLAT02, higher inclination angle seems to move the curve towards positive lateral force indicating a positive lateral force at 0 degree slip angle.

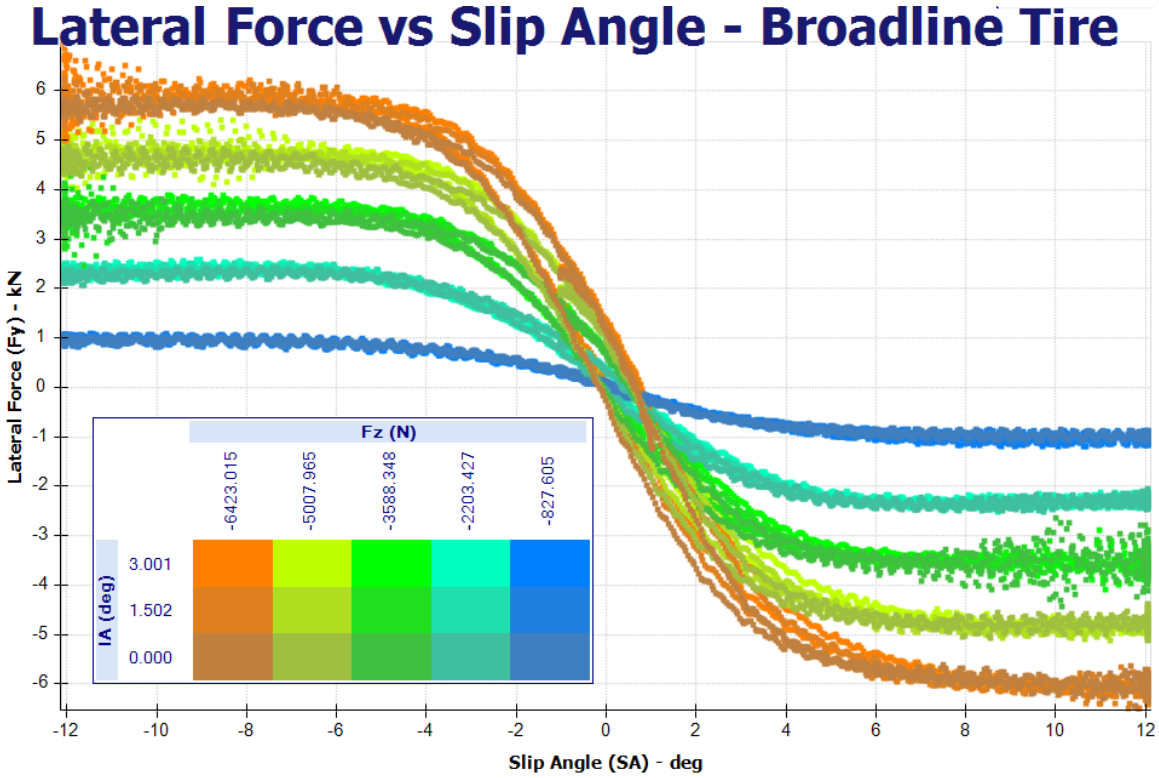


Figure 50 – Lateral force versus slip angle at different inclination angles and normal loads from sLAT02 test for the Broadline tire.

c. Track Replay

In addition to the standard slip angle sweeps, a track replay profile consisting of time history data of slip angle, normal load and inclination angle that the tire experienced from track testing was input in to the FlatTrac III machine. The goal here was to measure the lateral force by both the FlatTrac III and the WFT on the belt surface when the tire is subject to the exact same load, slip angle and inclination angle conditions that it would experience on the road. This will provide a direct correlation of the friction between the two surfaces – belt and asphalt for both the Broadline and UHP tires. Since the same physical tires are used, any difference in friction is a result of the difference in surface and not due to tire

variation. Each tire was subject to the track replay five times on the FlatTrac III. The average lateral force of the five runs was used for the correlation studies.

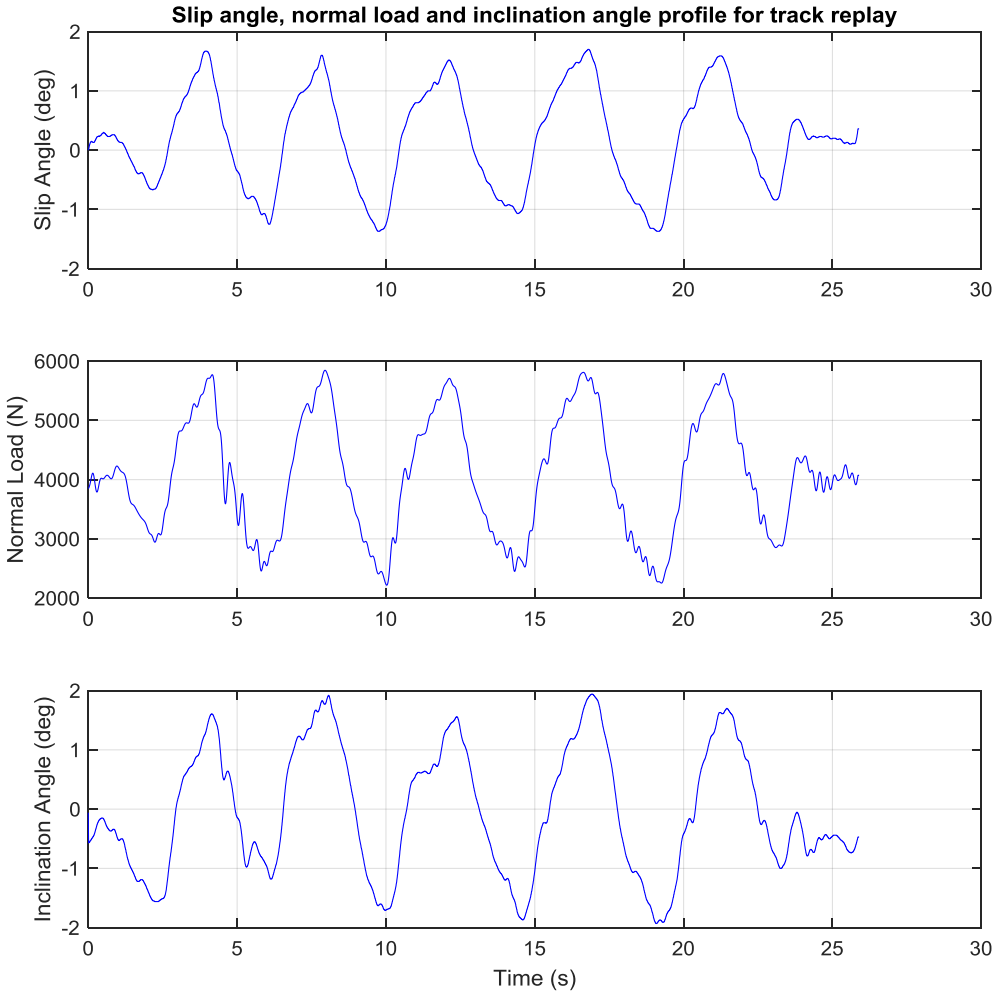


Figure 51 – Time history profile of slip angle, normal load and inclination angle from driving on the oval at CTVTC. This time history profile is fed into the MTS FlatTrac III machine to get a direct correlation between the belt surface and CTVTC asphalt surface for both Broadline and UHP tires.

d. Data Analysis

a. Pre-Processing the data

The test data was sampled at 250Hz and filtered using a low pass 5 pole elliptic filter with a cutoff frequency at 100Hz. However, as can be noticed in Figure 48 and Figure 50, there is still noise in the data. The data was further filtered using a low pass 5 pole Butterworth [46] filter at 5.46 Hz. The data was filtered using a phaseless filter which filters the data twice – one forward and once backward. This eliminates any phase shift in the data due to the filter. Due to the fact that the phaseless filter filters the data twice, the amplitude gets attenuated twice as well. Thus the filter cutoff frequency for this type of filter must be slightly higher than the cutoff frequency for a filter which will filter the data only once. In this case, the target cutoff frequency was 5Hz [47].

b. Wheel force transducer to MTS FlatTrac III Data Comparison

Since the tire was fitted with the wheel force transducer for both on track testing and on the FlatTrac III, it allowed for direct comparison between both the surface and the measurement device. Figure 46 shows the tire fitted with the wheel force transducer mounted for testing on the MTS FlatTrac III test machine. Unlike the CAN based communication setup used for on track testing, the WFT was setup to communicate with via analog due to unavailability of CAN input the on Smithers' data acquisition system.

Figure 52 – The Michigan Scientific CT2 communications box connected to an analog breakout box (in yellow) providing the analog signals from the WFT into the Smithers data acquisition system. Power to the CT2 is provided by a bench top DC power supply at 12V (in red)

Figure 53 shows the comparison between the normal force measured on the FlatTrac III machine and the WFT during both sLAT02 and sLAT12 tests for the Broadline tire. It is interesting to note that across both ranges of slip angle sweep testing, the FlatTrac III reads the normal load to be approximately 3% higher than measured by the WFT linearly across the entire load range. There is also a static offset in measurement between the two measurement systems, with the FlatTrac III measuring normal load approximately 230N more than measured by the WFT. This static offset is due to the weight of the tire and wheel force transducer assembly which is roughly 50lbs or approximately 230N. But

this offset is not consistent between sLAT02 and sLAT12. However, the linear correlation between these two measurement systems allows easy scaling of tire data.

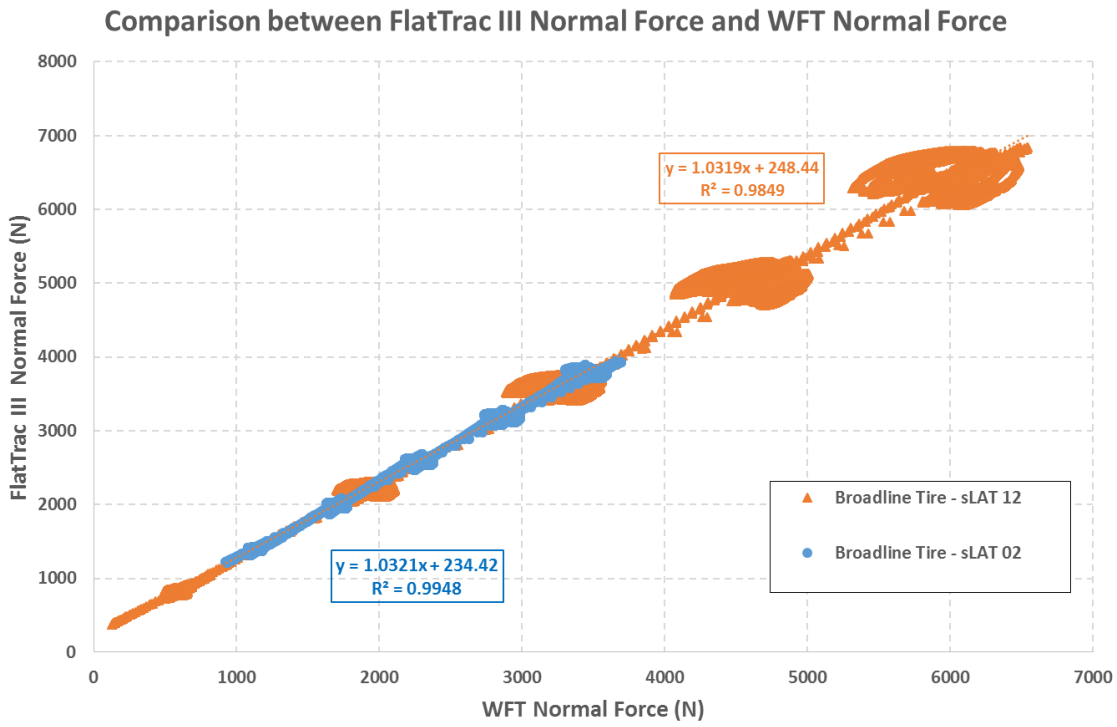


Figure 53 – Comparison between FlatTrac III Normal Force and WFT Normal Force for both sLAT02 and sLAT12 test procedures for Broadline Tire.

Similar to the normal force correlation, Figure 54 shows the correlation between the lateral forces measured by the FlatTrac III and WFT for both sLAT02 and sLAT12 test procedures using the Broadline tire. The lateral force measured seems to be linearly correlated with the FlatTrac III measuring approximately 10% less force laterally compared to the lateral force measured by the WFT. In addition, there is a static offset of 71N for sLAT02 and 80N for sLAT12. Interestingly the static offset for the normal load correlation is also large for sLAT12 compared to sLAT02 as seen in Figure 53. It is important to note that these normal and lateral force correlations are across the entire sLAT02 and sLAT12

procedures which consist of different inclination angles as well (Figure 47 and Figure 49). Thus these correlations seem to hold across the entire slip angle, normal load and inclination angles for these two measurement systems.

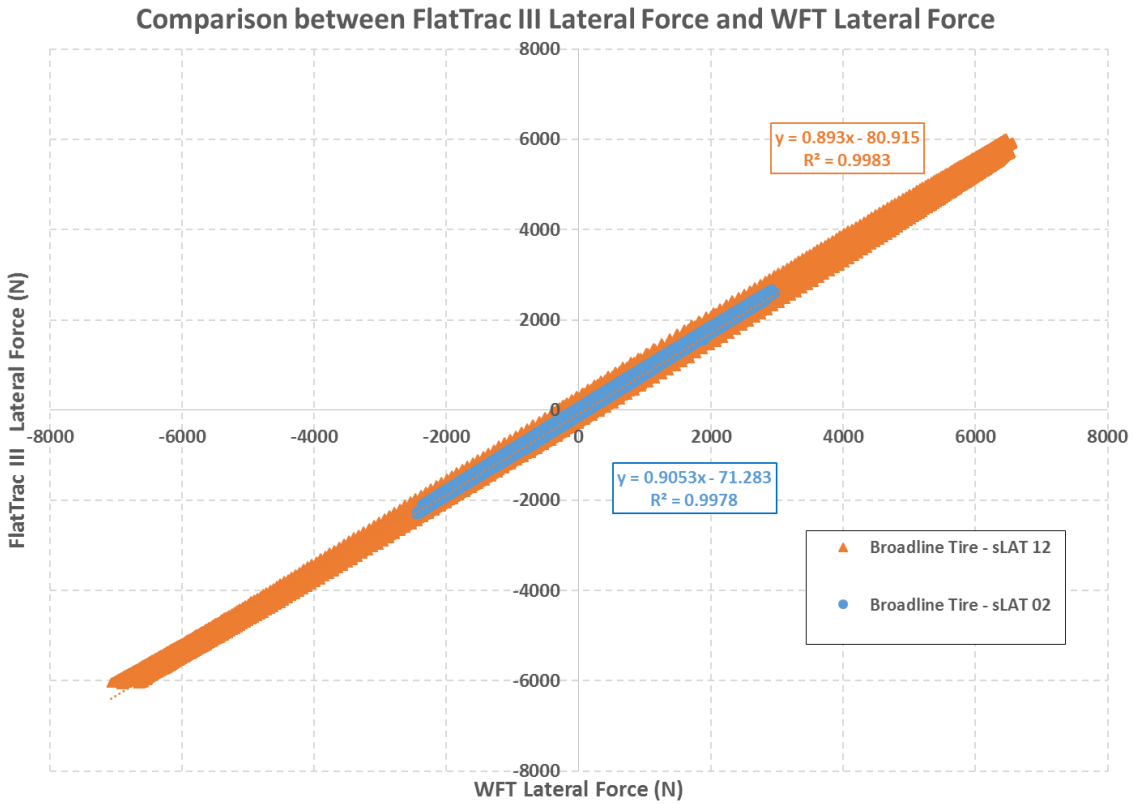


Figure 54 – Comparison between FlatTrac III Lateral Force and WFT Lateral Force for both sLAT02 and sLAT12 test procedures for Broadline Tire.

While the correlations presented in the figures above were for the standard sLAT02 and sLAT12 slip angle sweep tests, Figure 55 shows the comparison in lateral force measured by the WFT on the track and the FlatTrac III belt surface for the track replay input. The lateral force measured on both the surfaces seems to be linearly correlated with

a slope of almost 1 indicating that the lateral friction on the belt surface and the asphalt at the test track are almost identical for the Broadline tire.

The track replay input has constantly varying slip angle, inclination angle and normal load whereas the inclination angles and normal load for sLAT02 and sLAT12 are constant for a given slip angle sweep. Figure 55 indicates that the lateral force correlates linearly across all these operating conditions for the Broadline tire on these two surfaces. The linear correlation between the two surfaces for the Broadline tire allows for simple scaling of tire data and tire models to predict lateral force on each surface. The $R^2$ and Root Mean Square Error (RMSE) for all the correlation fits are summarized in Table 3 and Table 4

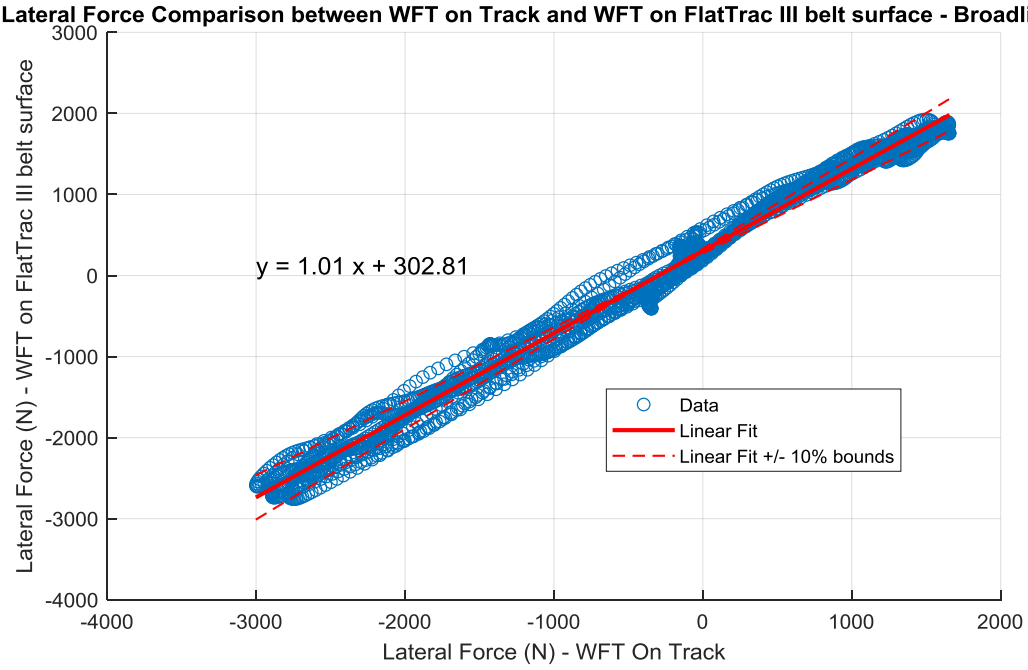


Figure 55 – Lateral force correlation between WFT on the Test Track (CTVTC) and WFT on the FlatTrac III belt surface for Broadline tire for track replay input. The solid

red line shows the linear fit to the data and the dashed line shows the linear fit +/- 10% bound

Figure 56 shows the comparison between the lateral force as measured by the WFT on the track and the measurement system on the FlatTrac III. The lateral force measured by the FlatTrac III system is 13% lower than the lateral force measured by the WFT on track for same input conditions. This correlation is useful since it can be used to directly scale the tire data from the track to the belt surface across two measurement systems.

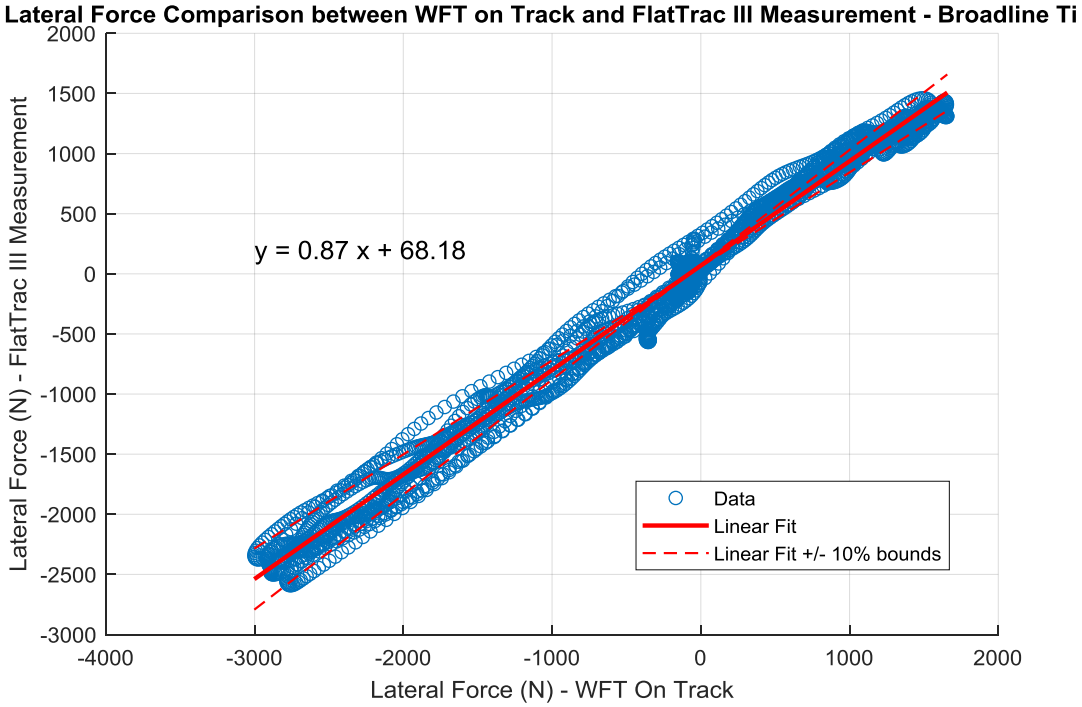


Figure 56 – Lateral force comparison between WFT on Track and FlatTrac III Measurement for Broadline Tire for track replay input. The solid red line shows the linear fit to the data and the dashed line shows the linear fit +/- 10% bound

Figure 57 shows a time history plot of the lateral force as measured by the WFT on the FlatTrac III belt surface, WFT on the test track and the lateral force as measured by the FlatTrac III measurement system. The profiles closely follow the correlations observed in Figure 55 and Figure 56.

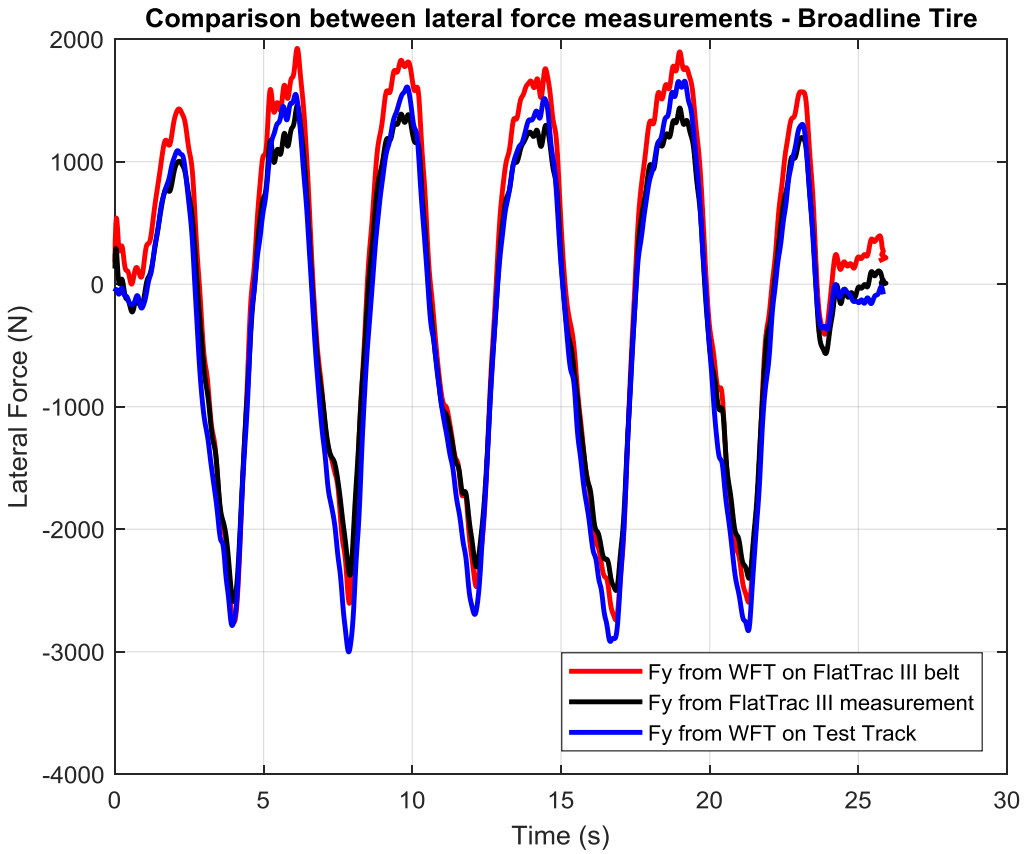


Figure 57 – Time history plot of lateral force profiles as measured by WFT on FlatTrack III belt, WFT on test track and lateral force measured by FlatTrac III measurement system

Applying the same processing does not yield similar results in the case of UHP tire as shown in Figure 58. The lateral forces measured by the WFT on the test track at CTVTC

(asphalt surface) and on the FlatTrac III belt surface seem to be nonlinearly correlated across the track replay.

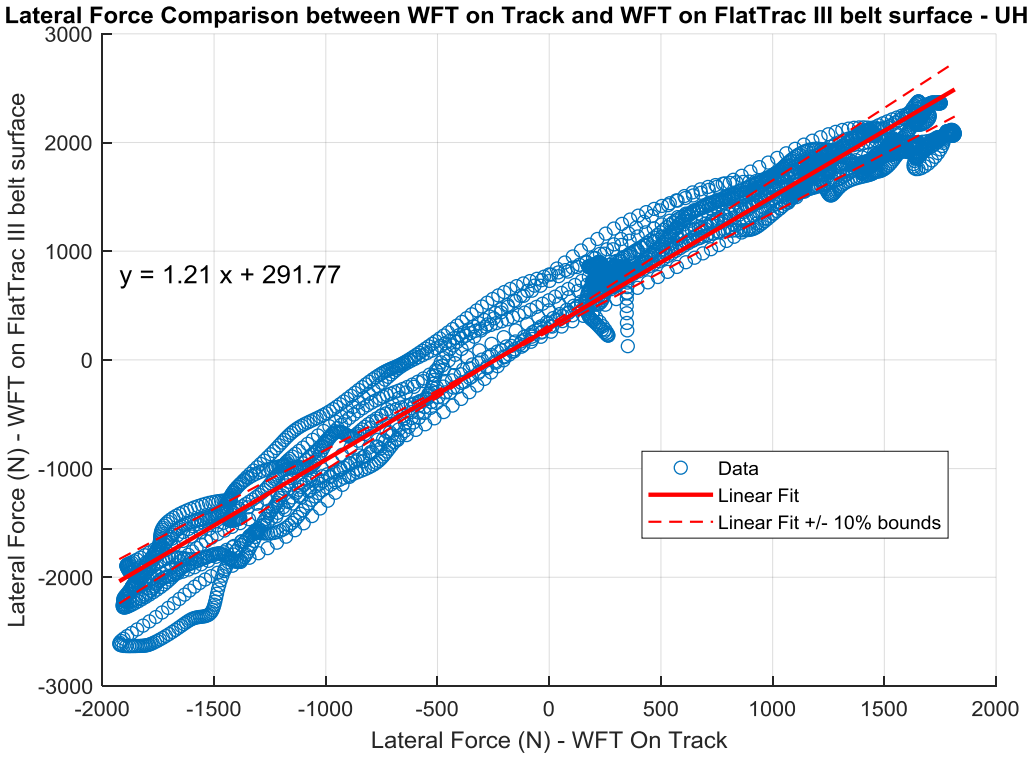


Figure 58 – Lateral force comparison between WFT on the Test Track (CTVTC) and WFT on the FlatTrac III belt surface for the UHP Tire for track replay input. The solid red line shows the linear fit to the data and the dashed line shows the linear fit +/- 10% bound

Upon closer inspection of the data, the correlation seems to tend towards nonlinearity as the slip angle gets larger than 0.75 degrees as shown in Figure 59. A quadratic function was used instead to capture the correlation. Figure 60 shows the lateral force comparison between the WFT on track and on the FlatTrac III surface with a quadratic curve fit. The quadratic function does a better job at capturing the trend of the

correlation. These results indicate that the surface friction correlation from one tire cannot necessarily applied to another tire.

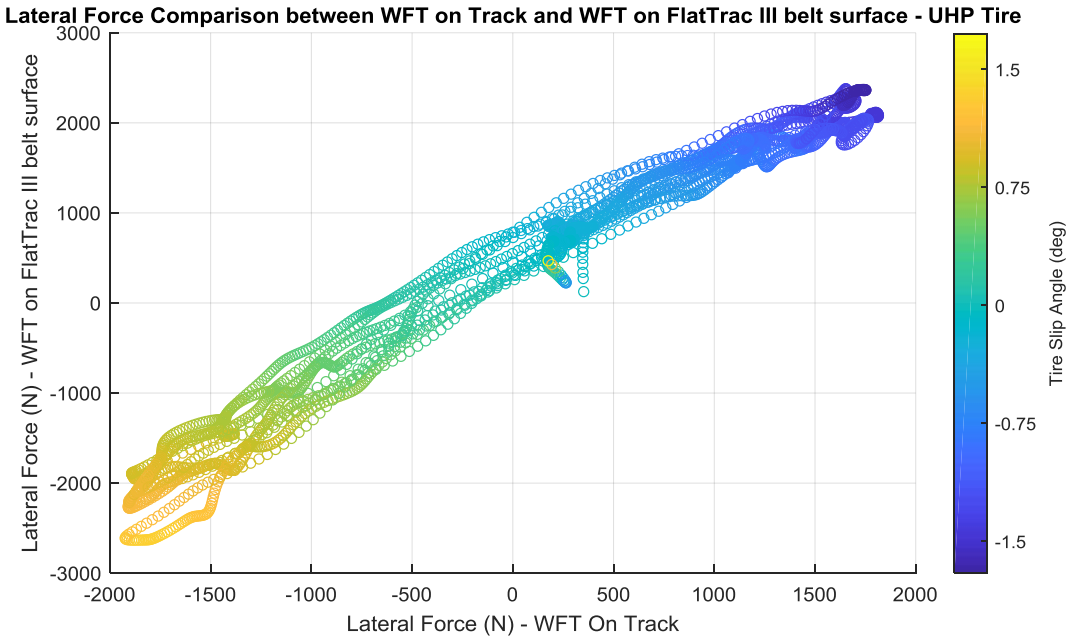


Figure 59 – Lateral force comparison between WFT on the Test Track (CTVTC) and WFT on the FlatTrac III belt surface for the UHP Tire for track replay input. The gradient indicates the tire slip angle.

Figure 61 shows the comparison and correlation between the lateral force measured by the WFT on track and the lateral force as measured by the FlatTrac III system. As noticed in Figure 58, there seems to be a nonlinear relationship between the two measurements and is thus captured more effectively by a quadratic function.

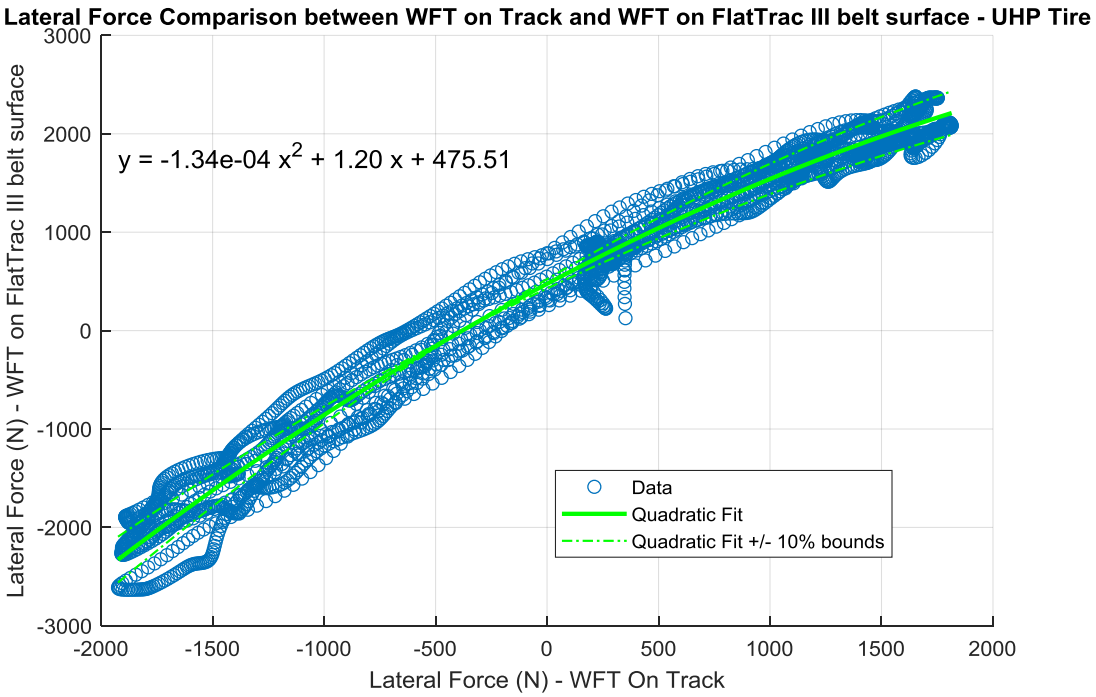


Figure 60 – Lateral force comparison between WFT on the Test Track (CTVTC) and WFT on the FlatTrac III belt surface for the UHP Tire for track replay input. The solid green line shows the quadratic fit to the data and the dashed line shows the quadratic fit +/- 10% bound.

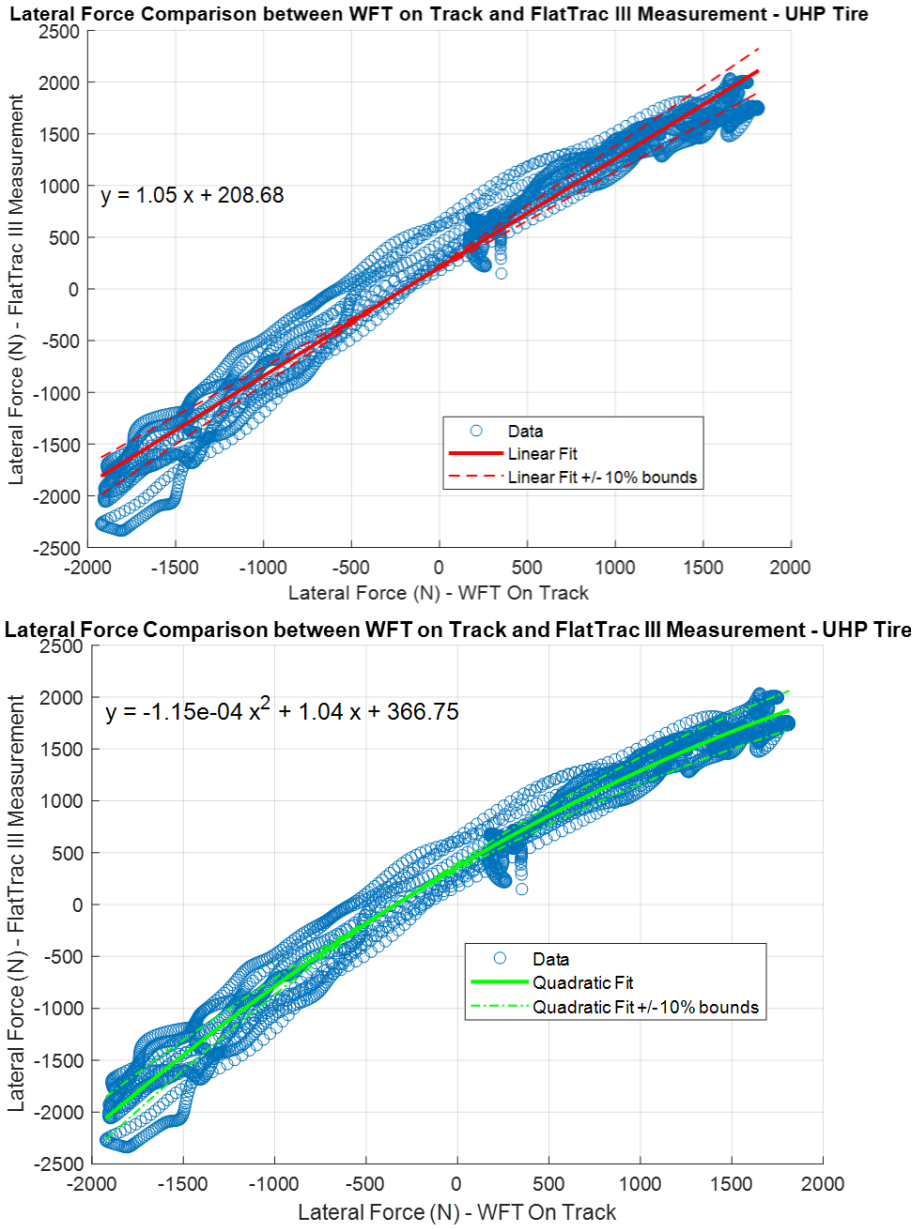


Figure 61 – Lateral force comparison between WFT on Track and FlatTrac III Measurement for UHP Tire for track replay input (top and bottom). (Top) The solid red line shows the linear fit to the data and the dashed line shows the linear fit +/- 10% bound. (Bottom) The solid green line shows the quadratic fit to the data and the dashed line shows the quadratic fit +/- 10% bound.

Figure 62 shows a plot of lateral force vs slip angle for track replay colored by normal load on the FlatTrac III for the UHP Tire. As expected, the tire generates higher lateral force at higher normal loads compared to the slip angle at lower normal load.

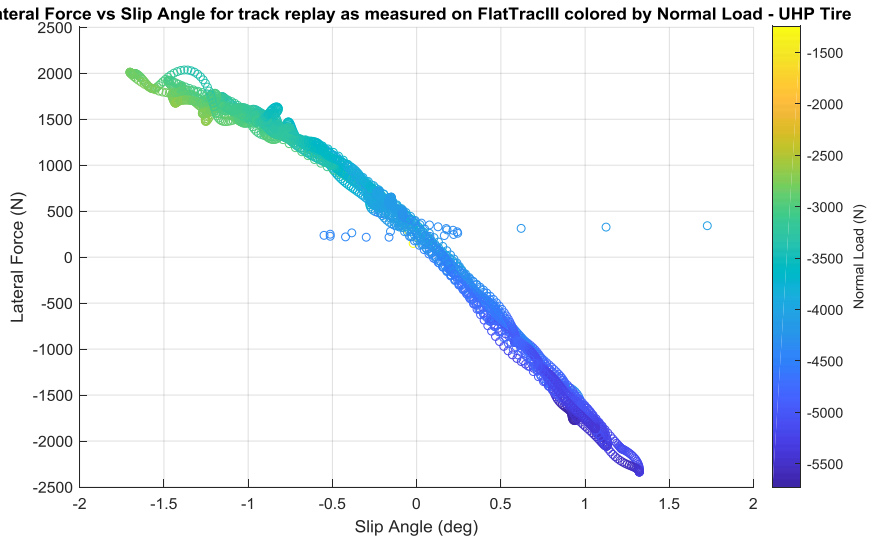


Figure 62 – Lateral Force vs Slip Angle for track replay as measured on the FlatTrac III colored by Normal Load for UHP Tire

Figure 63 shows the lateral force vs slip angle as measured by the WFT on the Track and WFT on the FlatTrac III for the UHP Tire for track replay. In the entire slip angle region, the lateral force vs slip angle curves between the WFT on the Track and the WFT on the FlatTrac III have different lateral force values and slopes. This indicates the tire lateral force to same conditions of slip angle, normal load and inclination angle are different on the track surface compared to the FlatTrac III surface. Thus causing the non-linearity in surface correlation observed in Figure 58 and Figure 60.

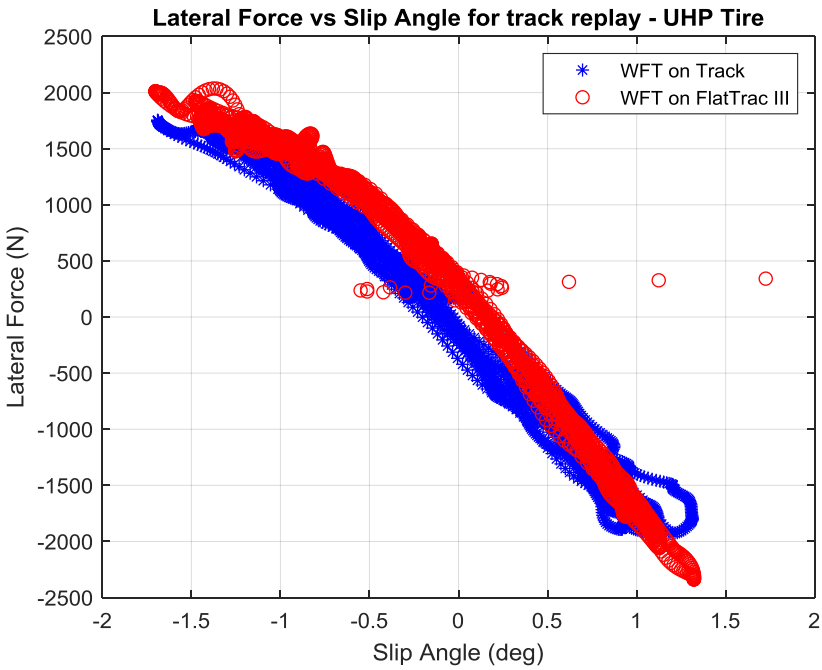


Figure 63 – Lateral Force vs Slip Angle for track replay comparison between WFT on Track and WFT on FlatTrac III for UHP Tire.

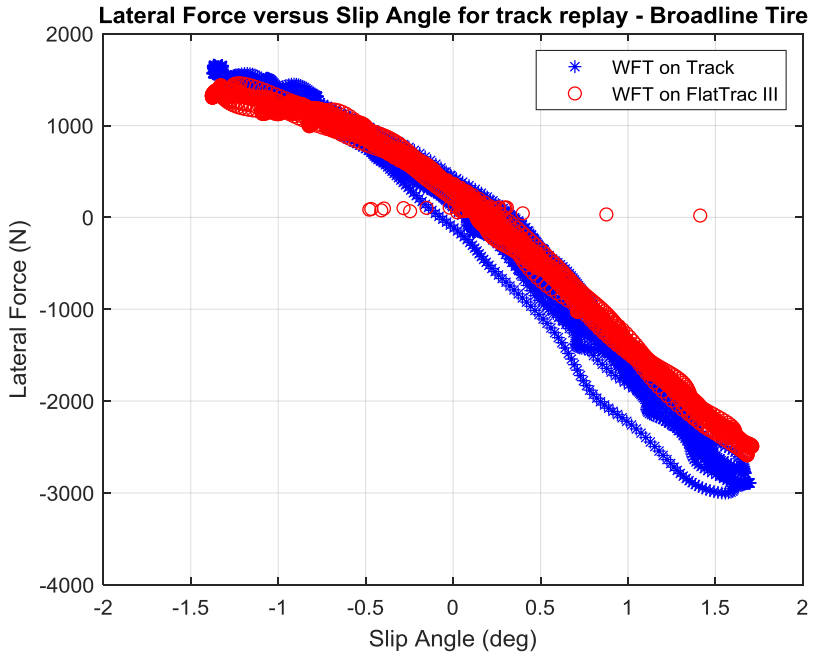


Figure 64 – Lateral Force versus Slip Angle for track replay comparison between WFT on Track and WFT on FlatTrac III for Broadline Tire.

In comparison, Figure 64 shows the lateral force versus slip angle for track replay for Broadline tire as measured by WFT on Track and WFT on FlatTrac III. The lateral force curves are almost identical in slope and value for most of the region except between 0.75 deg and -1.4 deg slip angle. This indicates that the Broadline tire has similar cornering stiffness and similar variation in cornering stiffness on both track surface and FlatTrac III surface which contributed to its linear surface correlation as observed in Figure 55

Table 3 and Table 4 summarize the $R^2$ and Root Mean Square Error (RMSE) between the linear correlation fits and quadratic correlation fit respectively. Using a quadratic fit significantly reduces the RMSE in the correlation for the UHP tire. The equations used to evaluate $R^2$ and RMSE are outlined in Appendix C.

Table 3 – Summarize $R^2$ and Root Mean Square Error (RMSE) of linear fits of correlation

| | Broadline Tire - Linear Fit | | UHP Tire - Linear Fit | |
|---|---|---|---|---|
| | WFT from Track to WFT on FlatTrac III | WFT on Track to FlatTrac III Measurement | WFT from Track to WFT on FlatTrac III | WFT on Track to FlatTrac III Measurement |
| **$R^2$** | 0.99 | 0.98 | 0.96 | 0.96 |
| **RMSE** | 137.26 | 123.23 | 252.81 | 216.81 |

Table 4 – Summarized $R^2$ and Root Mean Square Error (RMSE) of quadratic fit of correlation for UHP Tire

| | UHP Tire - Quadratic Fit | |
|---|---|---|
| | WFT from Track to WFT on FlatTrac III | WFT on Track to FlatTrac III Measurement |
| **$R^2$** | 0.97 | 0.97 |
| **RMSE** | 208.06 | 178.15 |

c. Tire F&M Analysis

Cornering stiffness has been established as one of the most important metrics of tire performance since it is a direct contributor of vehicle handling and stability [1] [3] [8]. Cornering stiffness can be calculated as –

$$C_\alpha = \frac{dF_y}{d\alpha} \; at \; \alpha = 0$$

Equation 1 – Equation to calculate cornering stiffness

Equation 1 describes the calculation of cornering stiffness as the slope of the lateral force versus slip angle curve when slip angle is 0 degrees [8] [29]. From a practical standpoint, it is recommended by the SAE that the cornering stiffness is calculated as the slope of the linear fit to the lateral force versus slip angle curve between -1 to +1 degree slip angle [29]. Pacejka et al [8] propose calculating cornering stiffness as the analytical derivative of the tire model fit to the data at 0 slip angle. This approach was adopted by fitting Magic Formula 6.1 (MF 6.1) to the tire data using commercially available software OptimumTire©. MF 6.1 is the latest iteration of the widely used empirical tire model first developed by Pacejka et al [7] [8]. A Comparison between the linear fit and MF 6.1 tire model fit between -1 and +1 deg slip angle is presented in Appendix D.

Figure 65 shows the comparison between the MF 6.1 model fit and the test data for the Broadline tire at different normal loads and inclination angles for the sLAT02 test dataset. The model does a good job of fitting the data with a total error of 1.89% across the entire data set. The total error is calculated within the OptimumTire © software and the equation used is outlined in Appendix C.

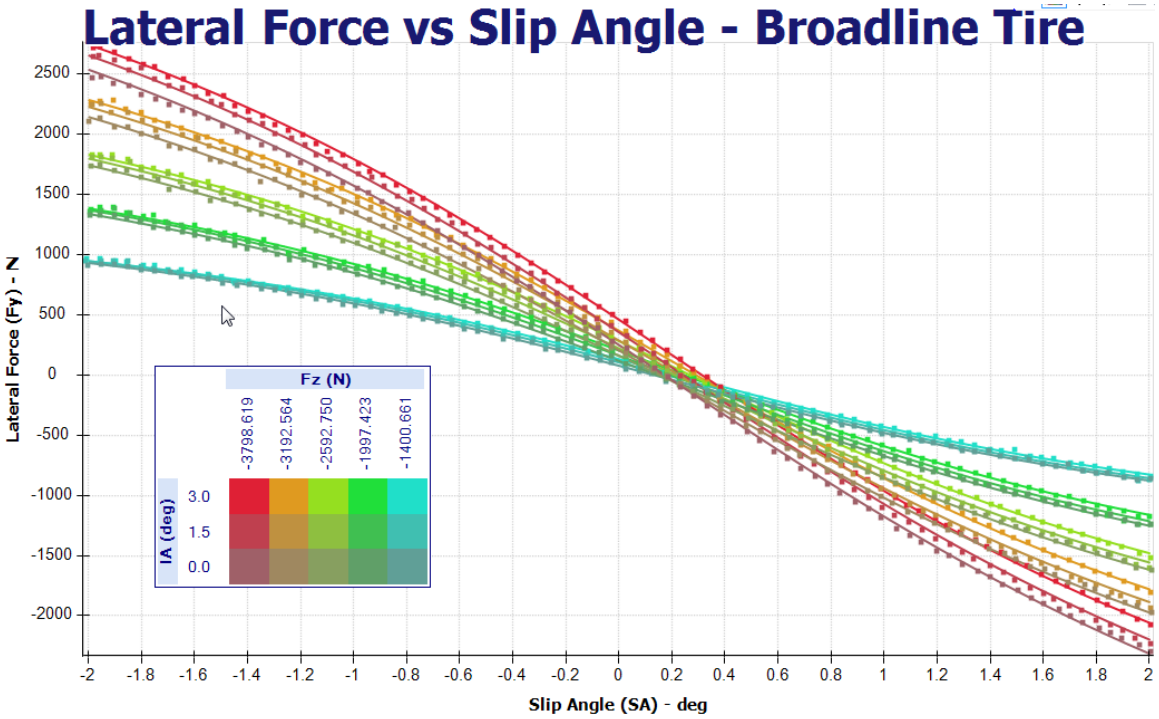


Figure 65 – Lateral force versus Slip Angle plot with test data (dots) and MF 6.1 model (solid line) at different inclination angles and normal loads for Broadline Tire from sLAT02.

Similarly Figure 66 shows the quality of the model fit to test data for the UHP tire data from sLAT02. The model does a good job of fitting the data with a total error of 1.35% across the entire dataset.

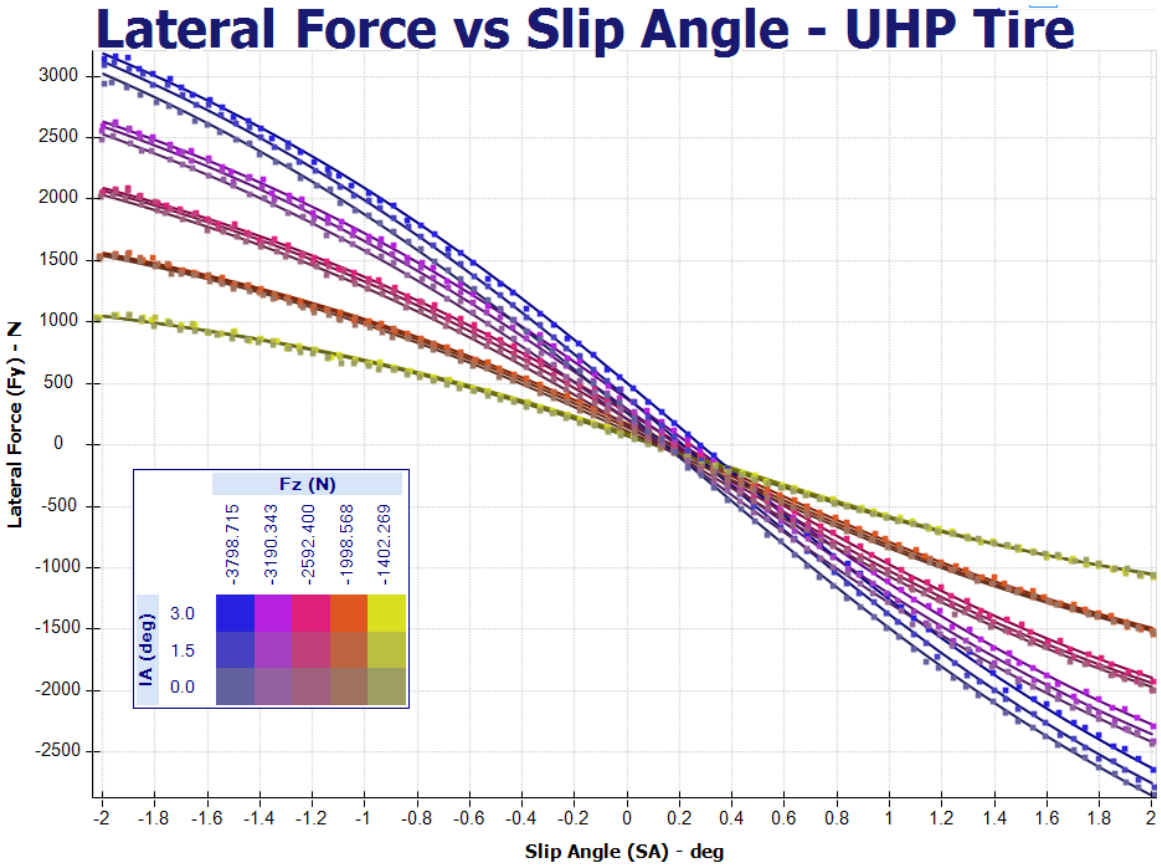


Figure 66 – Lateral force versus Slip Angle plot with test data (dots) and MF 6.1 model (solid line) at different inclination angles and normal loads for UHP Tire from sLAT02.

Figure 67 shows the cornering stiffness comparison between the UHP tire and Broadline tire from sLAT02 test. The cornering stiffness for the UHP is higher than the Broadline tire across the load range. This indicates that the UHP tire generates more lateral force for the same slip angle compared to the Broadline tire.

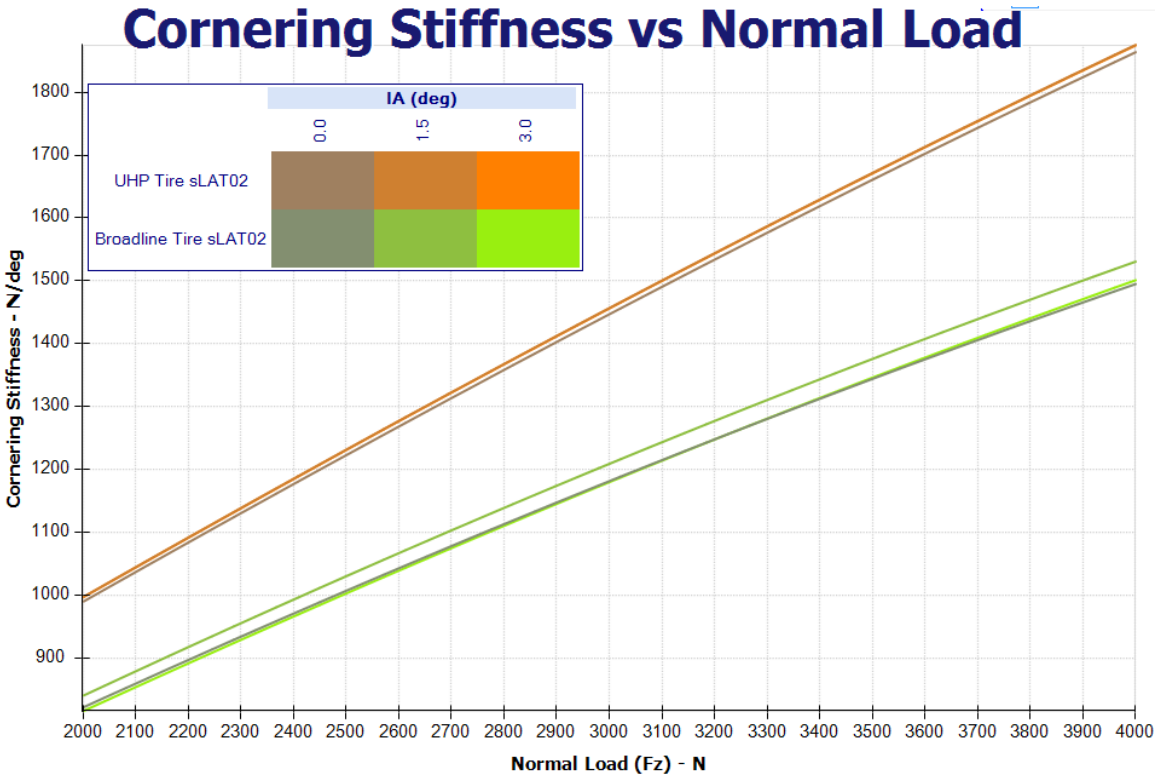


Figure 67 – Cornering stiffness versus Normal Load for both Broadline and UHP tire calculated using the MF 6.1 tire model fit to the data.

Similar to the model fits for test data from sLAT02, MF 6.1 models were also fit to tire test data from sLAT12 test procedure. Figure 68 shows the test data (in dots) and the MF 6.1 model (solid line) to both Broadline Tire and UHP tire. The total error in the model for the Broadline tire was 1.95% and the error for the UHP model was 2.4%.

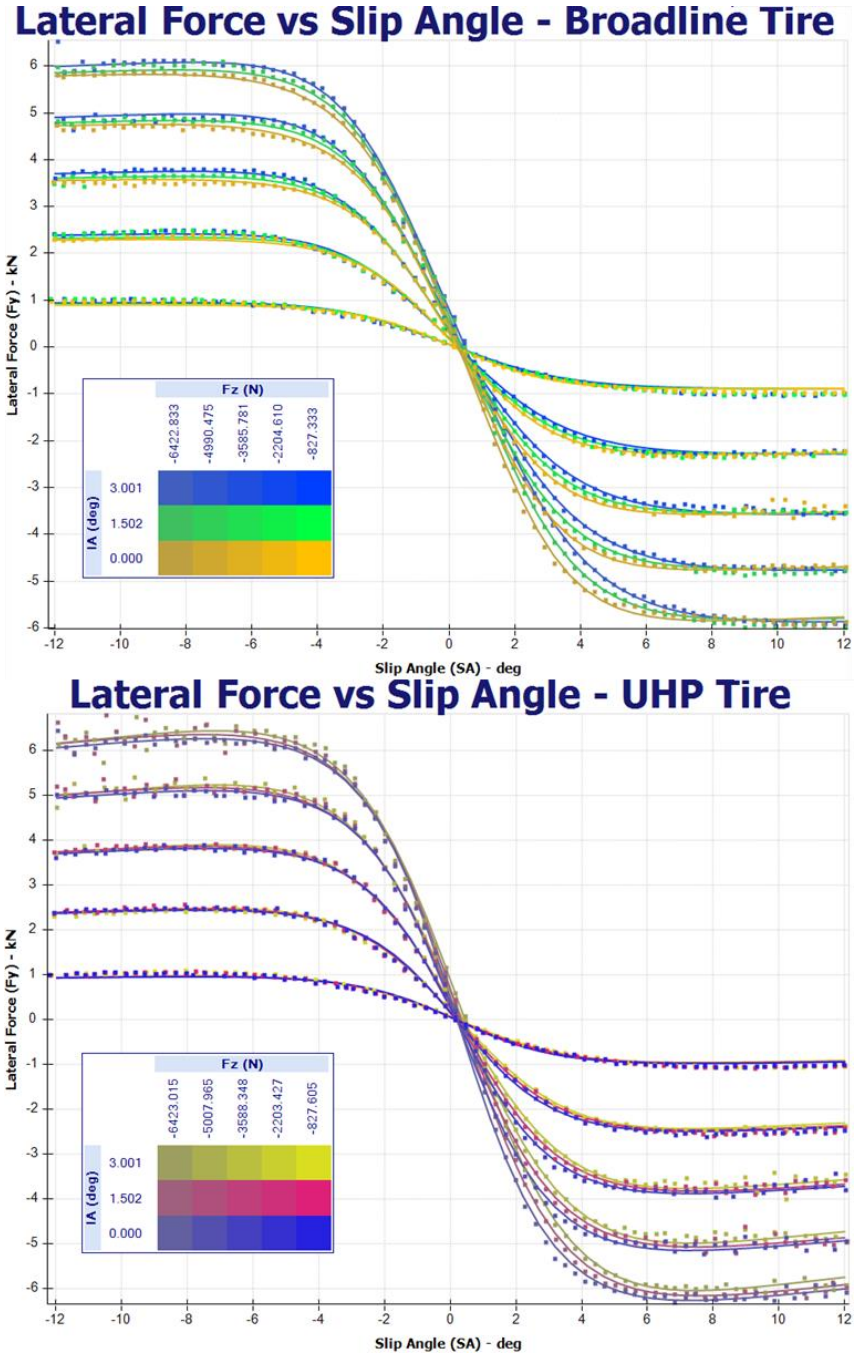


Figure 68 – MF 6.1 model fit (solid lines) to test data (dots) from Broadline Tire (top) and UHP Tire (bottom) from sLAT12 test procedure.

Even though the same tire is run through both sLAT02 and sLAT12, their cornering stiffness across the same load range can be different. Figure 69 shows the lateral force versus slip angle curve for UHP tire from sLAT02 and sLAT12 tire data. The data from sLAT02 has a higher slope indicating a higher cornering stiffness compared to the sLAT12 tire data.

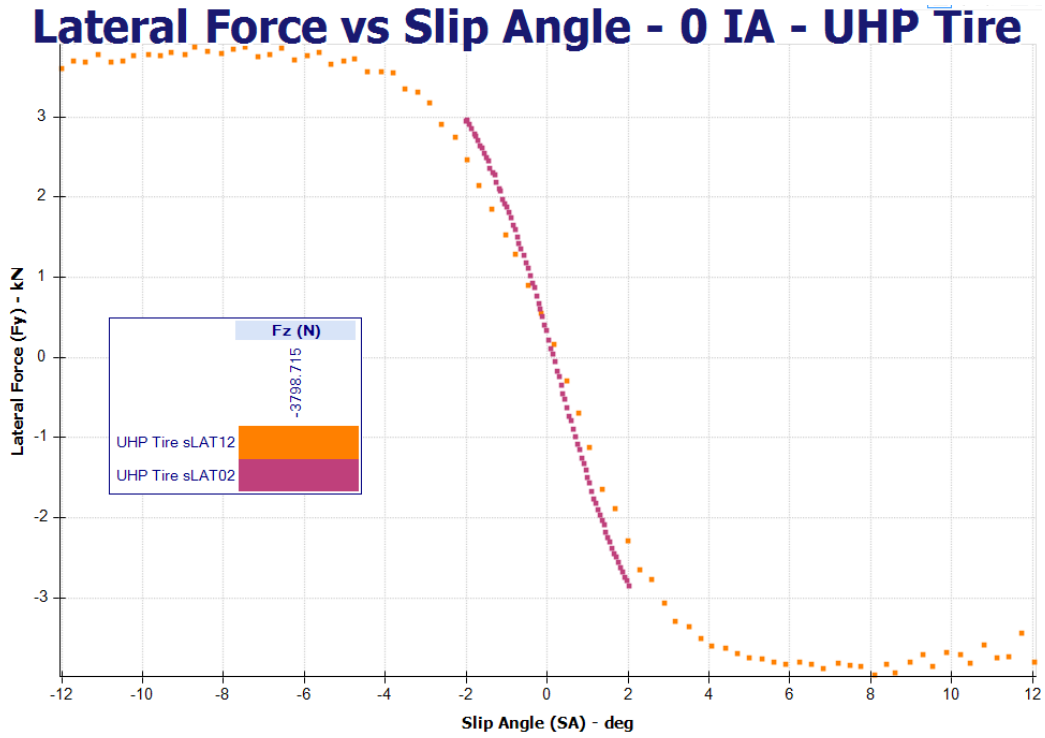


Figure 69 – Lateral Force versus Slip Angle Magic data for UHP tire from sLAT02 and sLAT12 tests. Note that the tire data from sLAT02 predicts higher cornering stiffness than the sLAT12 with a higher slope.

Figure 70 and Figure 71 show the cornering stiffness versus normal load derived from the MF 6.1 tire models fit to sLAT02 and sLAT12 data for Broadline tire and UHP tire respectively. The cornering stiffness from the high slip angle test is significantly lower

than the cornering stiffness from the low slip angle test. In addition, tire camber seems to make a larger influence on cornering stiffness at a given load for the data from sLAT12 data than the sLAT02 data.

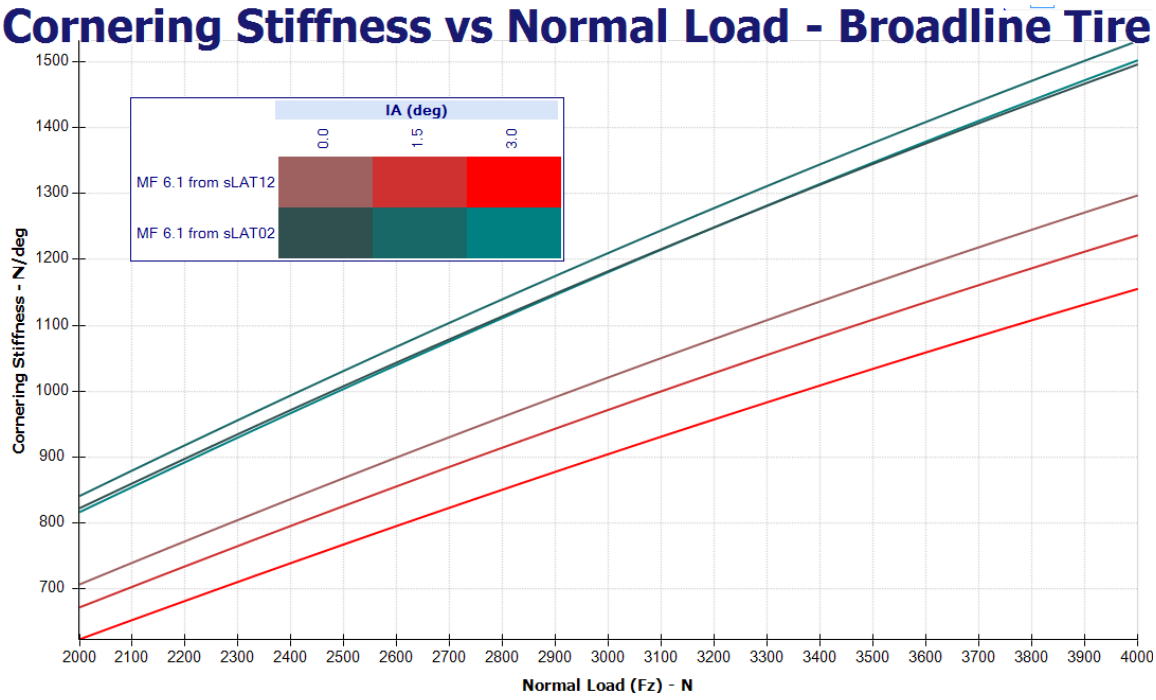


Figure 70 – Cornering stiffness versus Normal load comparison for Broadline tire between tire models fit for sLAT02 and sLAT12 test data.

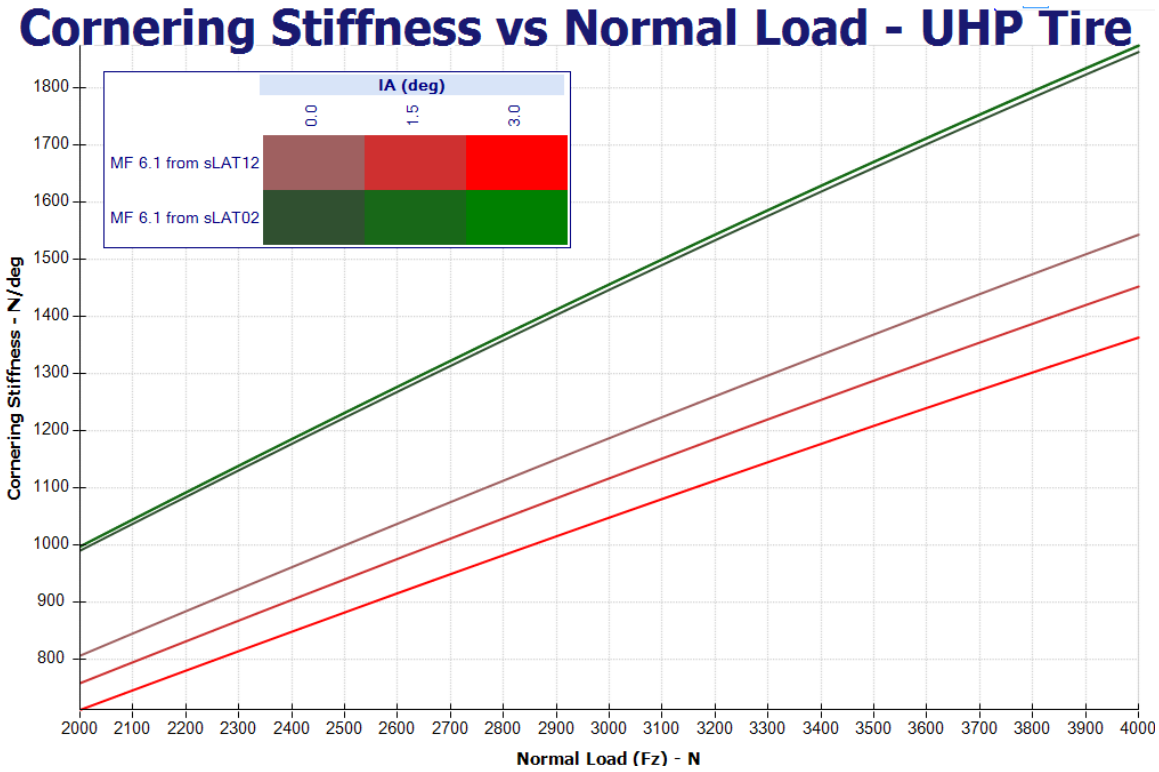


Figure 71 – Cornering stiffness versus Normal Load comparison for UHP tire between tire model fit for sLAT02 and sLAT12 test data.

Figure 65, Figure 66 and Figure 68 show that the model fits for the respective data are good, thus the difference in cornering stiffness is not due to any error in model but due to a difference in the tire behavior itself. Singh [5] and Angrick et al [9] determined that tire temperature influences tire cornering stiffness. Figure 47 and Figure 49 show that the tire experiences different slip angle sweep, peak slip angle and normal load for sLAT02 and sLAT12 test procedures. As a result the tire has different tread surface temperature profiles.

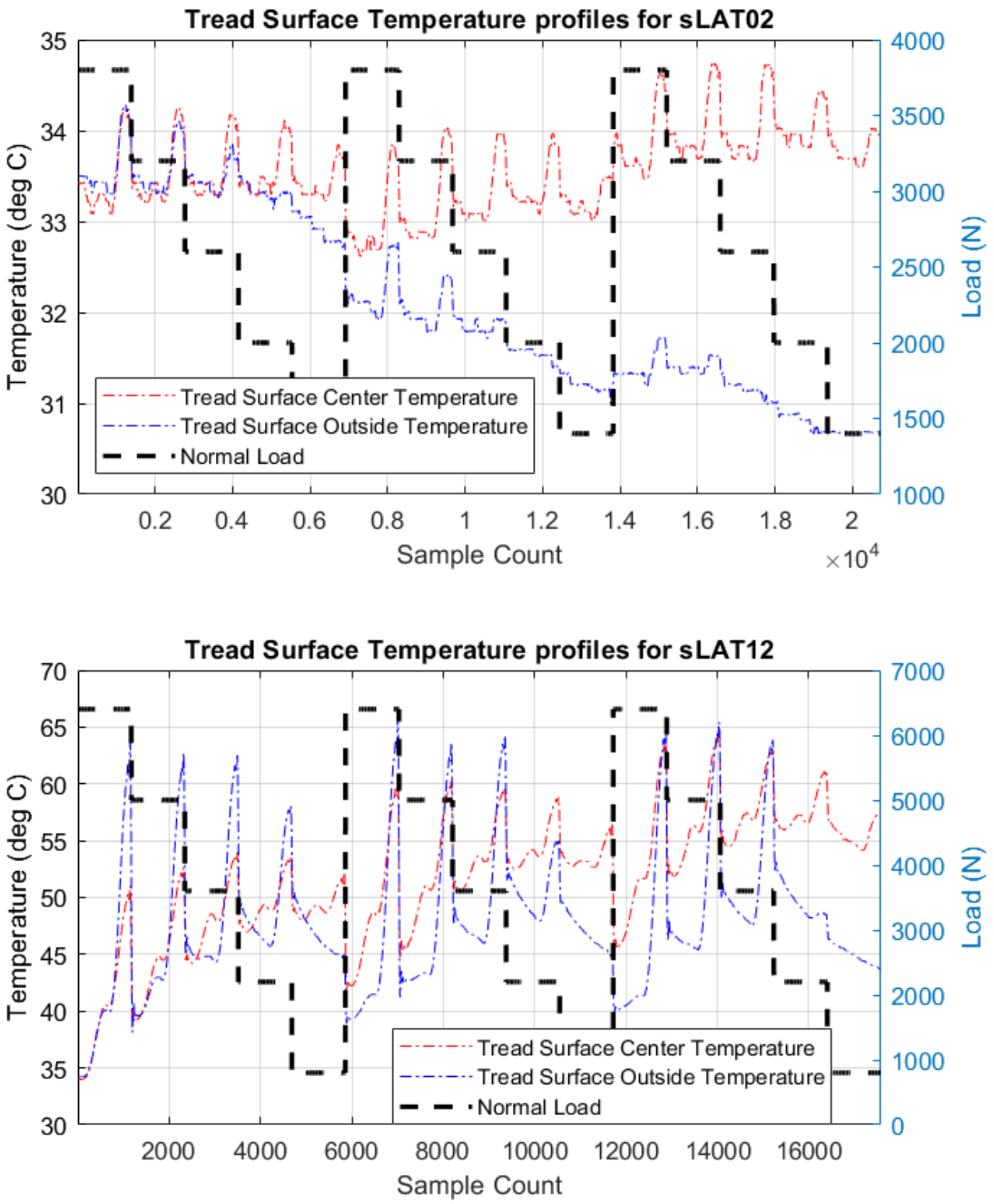


Figure 72 – Tread surface temperatures for sLAT02 and sLAT12 test procedures

Figure 72 shows the tread surface temperature profiles for both sLAT02 and sLAT12 test procedures. The tread surface temperature stays between 30 degrees C to 35

degrees C for both outside and center parts of tread for sLAT02 but it jumps to almost 65 degrees C over the course of the sLAT12 test. Internal tire temperature measurement was not available at Smithers for this test, thus no such measurement was possible. But if such measurement could be made in the future, it may follow similar trend given the results from Singh [5] and Angrick et al [9].

d. Tread Surface temperature and Cornering Stiffness

The tire passes through 0 degree slip angle three times for every inclination angle and normal load combination as seen in Figure 73. Thus three values of cornering stiffness can be calculated for every combination of inclination angle and normal load.

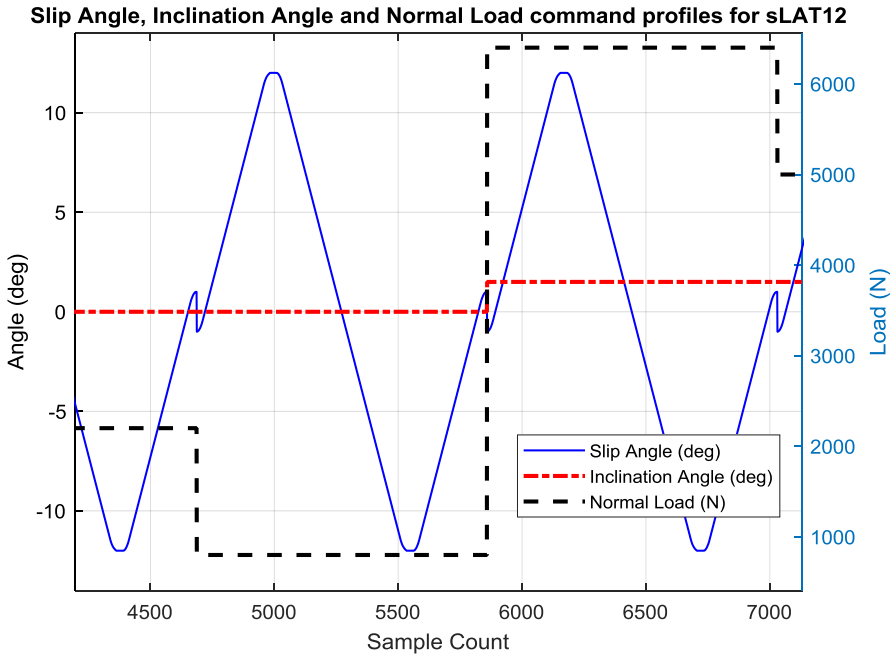


Figure 73 – Slip Angle profile for sLAT12. Notice that the slip passes through 0 three times for each combination of load and inclination angle (camber).

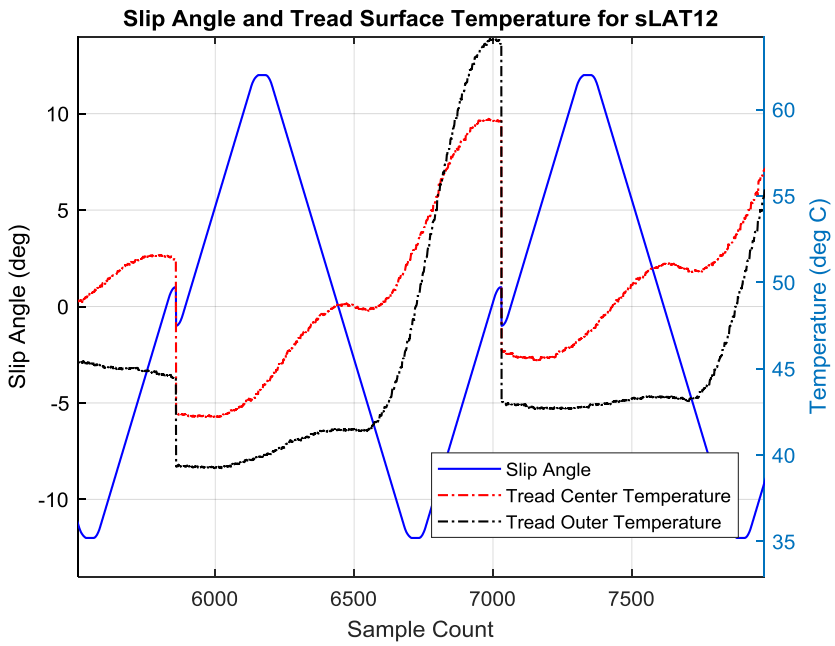


Figure 74 – Slip angle profile and tread surface temperature for sLAT12

In addition, Figure 74 shows that the tread surface temperature at each of those three sweeps also changes as the tire sweeps through the slip angle. Figure 75 and Figure 77 show the cornering stiffness versus normal load at all three inclination angles for UHP tire and Broadline tire at each of these three sweeps. Figure 76 and Figure 78 show the corresponding tread surface center temperature for these sweeps. While the 1$^{st}$ sweep has the lowest center temperature, it does not have the highest cornering stiffness as would be expected. The 2$^{nd}$ sweep and 3$^{rd}$ sweep seem to have identical cornering stiffness even though they have significantly different temperatures and higher temperature than the 1$^{st}$ sweep. While this seems contradictory, work done by Angrick et al [9] and Singh et al [5] show that tread surface temperature is a poor indicator of cornering stiffness. However, tread surface temperature has been shown to be a strong indicator of peak lateral coefficient of friction of the tire [5].

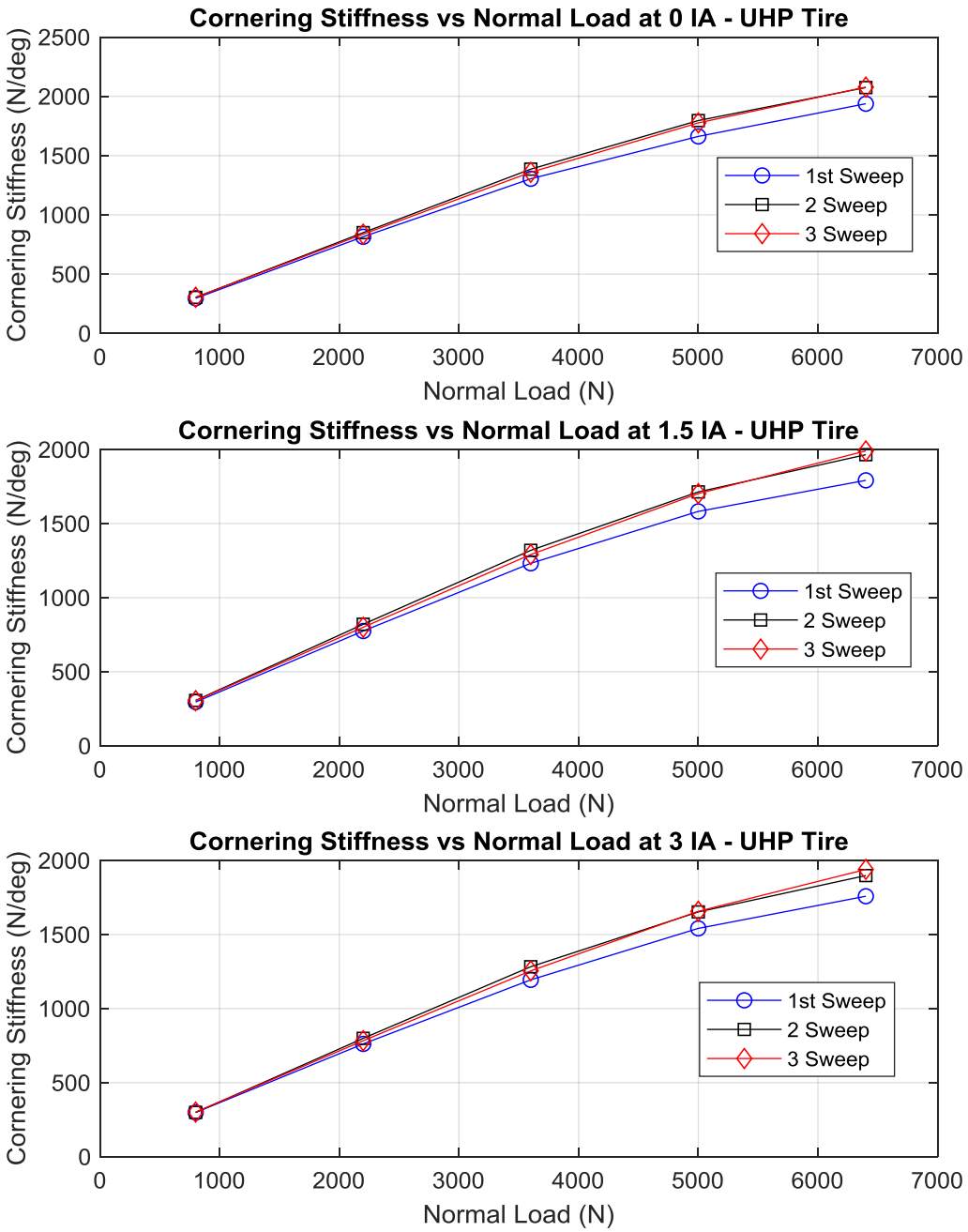


Figure 75 – Cornering stiffness versus normal load plots for UHP tire all three inclination angles for each sweep through 0 degree slip angle. Notice that the highest load is first test condition for each inclination angle condition as outlined in section b above.

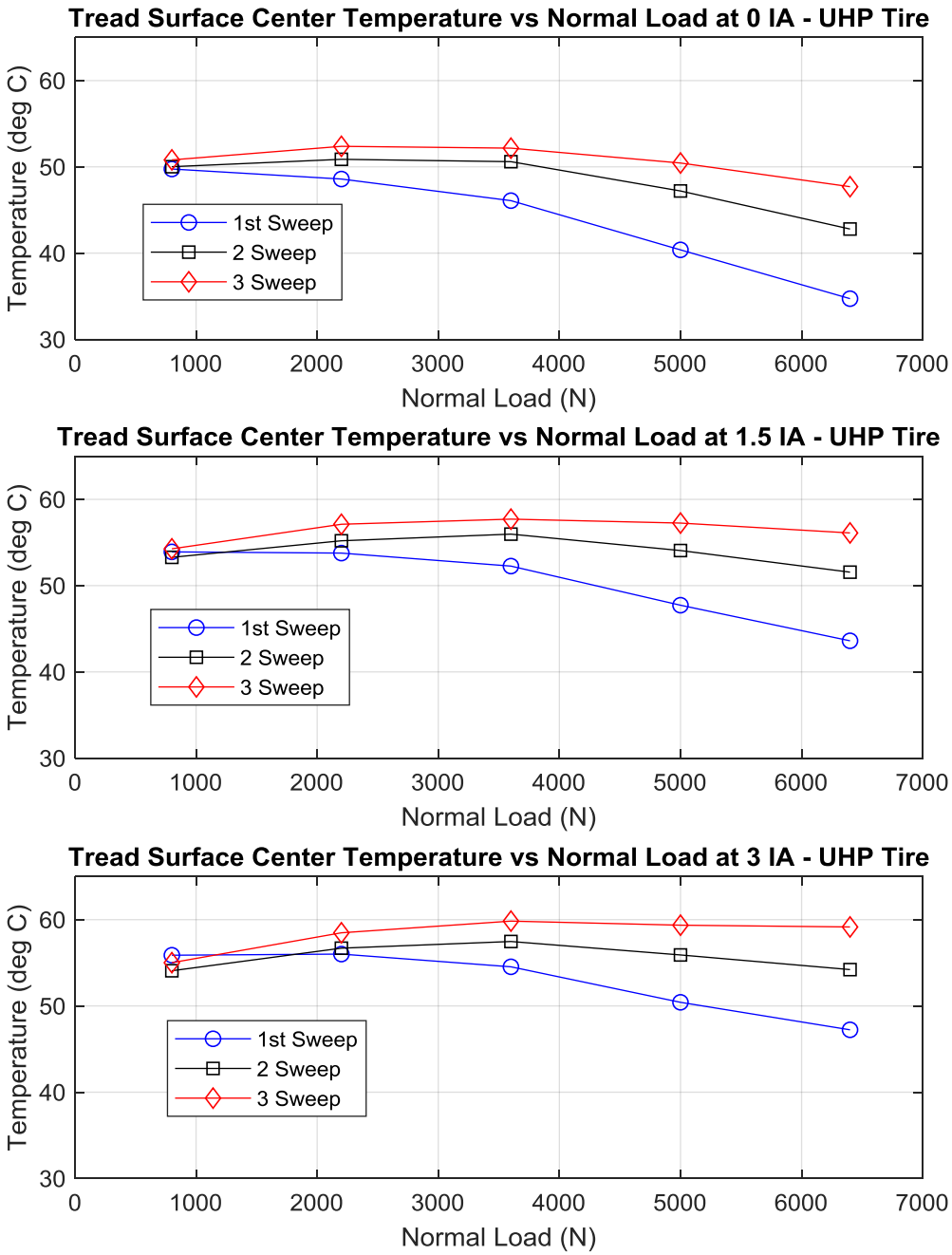


Figure 76 – Tread Surface Center Temperature versus Normal load at all three inclination angles for UHP Tire for each sweep through 0 degree slip angle. Notice that the highest load is first test condition for each inclination angle condition as outlined in section b above

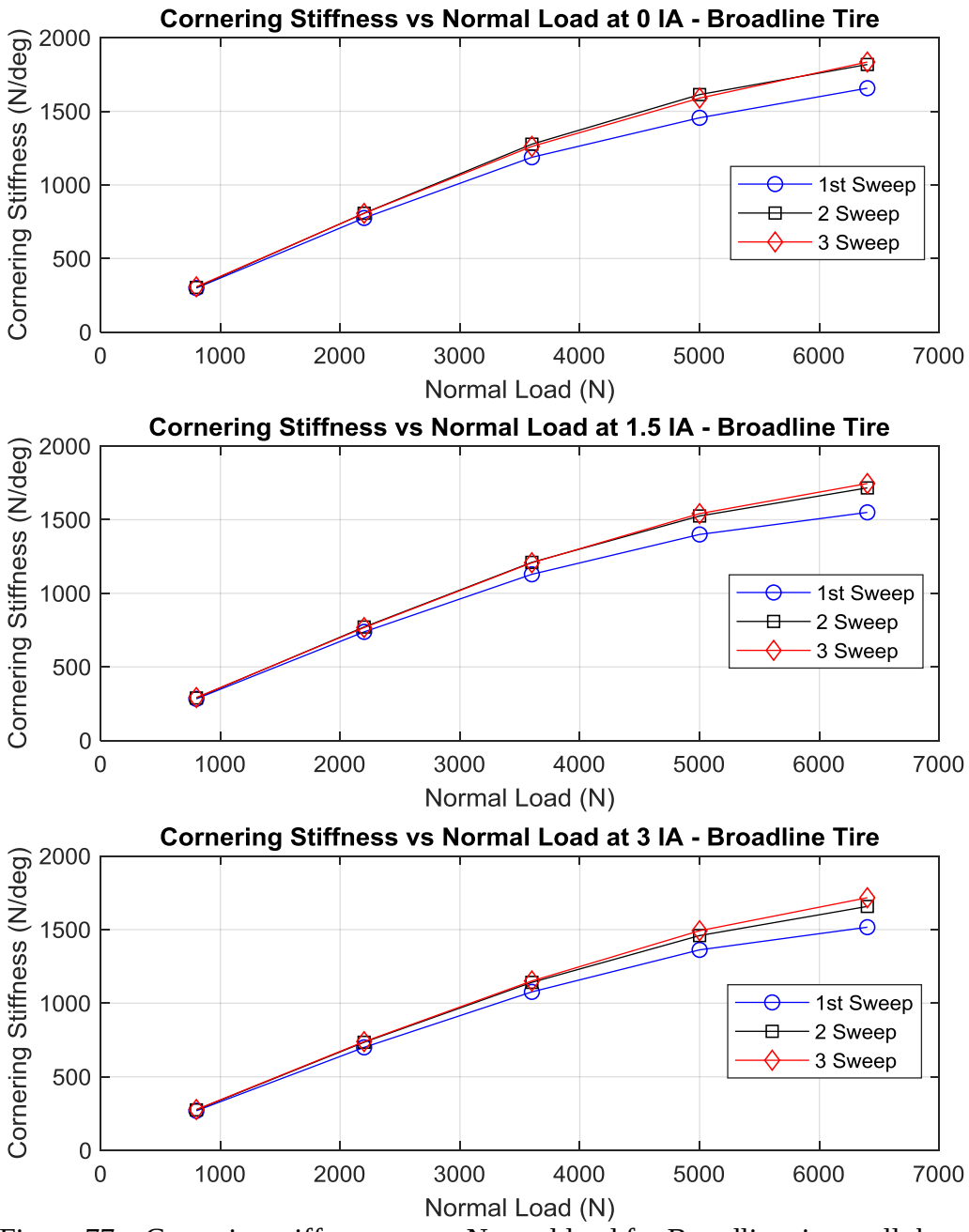


Figure 77 – Cornering stiffness versus Normal load for Broadline tire at all three inclination angles for each sweep through 0 degree slip angle. Notice that the highest load is first test condition for each inclination angle condition as outlined in section b above.

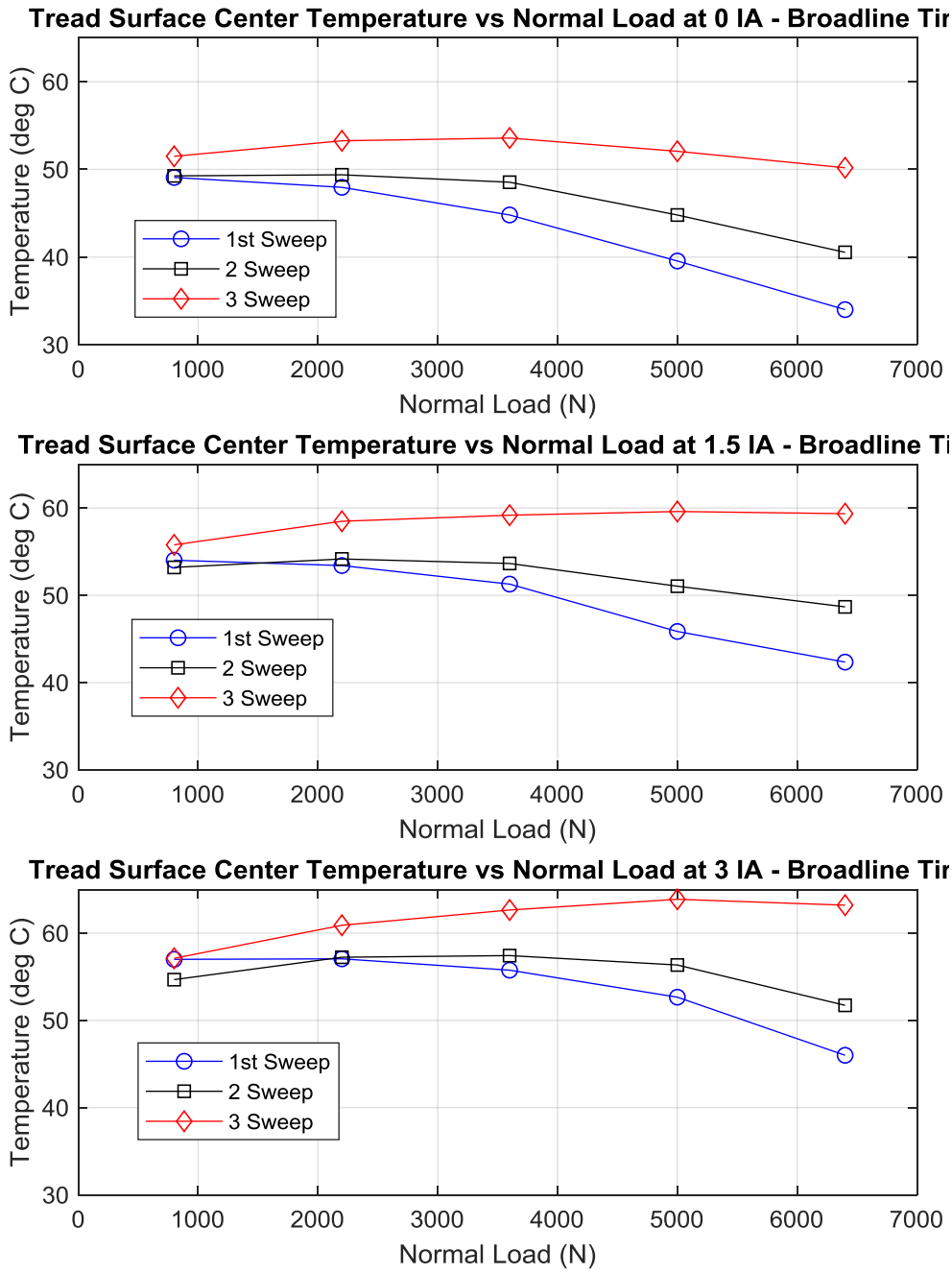


Figure 78 – Tread surface temperature versus Normal Load for Broadline Tire at all three inclination angles for each sweep through 0 degree slip angle. Notice that the highest load is first test condition for each inclination angle condition as outlined in section b above

e. Modification of Tire Test Procedure

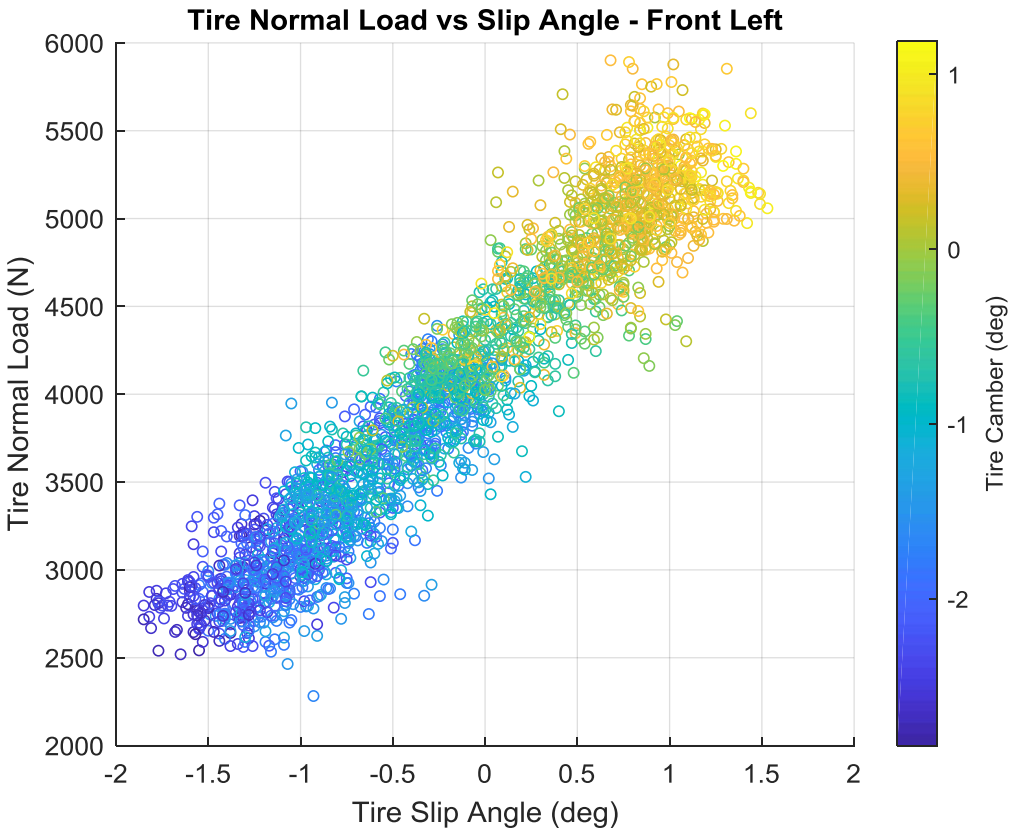


Figure 79 – Tire normal load versus slip angle colored by tire camber as measured from on track testing

As observed in the track testing data from Figure 42 and Figure 41, the tire does not operate at all combinations of normal load and camber. Figure 79 shows a concise overview of the ranges of normal load, slip angle and camber angle the tire will experience during driving. It can be seen that the tire has a larger negative camber value at lower loads and a smaller positive camber angle at higher normal loads. This data was used to modify tire model fitting process from sLAT12. Table 5 shows the normal load and camber

conditions for sLAT12 test procedure. The symmetry of test conditions based on SAE [29] recommends that all combinations of normal load and camber be tested.

Table 5 – Normal load and camber angle conditions for sLAT12. Notice the symmetry in test conditions

| **Tire F&M Test Conditions - Symmetric** | | ***Normal Load (N)*** | | | | |
|---|---|---|---|---|---|---|
| | | *800* | *2200* | *3600* | *5000* | *6400* |
| ***Camber Angle (deg)*** | *0.0* | x | x | x | x | x |
| | *1.5* | x | x | x | x | x |
| | *3.0* | x | x | x | x | x |

Using on track data, the sLAT12 test procedure was modified by only including combinations that are relevant for the tire. Table 6 shows the modified normal load and camber angle conditions proposed. This asymmetric test procedure reduces the number of testing conditions from 15 down to 9 directly translating to 40% reduction in testing time and cost. It must be noted that these combinations of normal load and camber are unique to the test vehicle due to its inertia, weight distribution and suspension layout. Similar testing can be done on other vehicles to determine the combination of testing conditions needed for useful tire testing.

Table 6 – Normal load and camber angle conditions for asymmetric sLAT12 after modification

| **Tire F&M Test Conditions - Asymmetric** | | ***Normal Load (N)*** | | | | |
|---|---|---|---|---|---|---|
| | | *800* | *2200* | *3600* | *5000* | *6400* |
| ***Camber Angle (deg)*** | *0.0* | | | x | x | x |
| | *1.5* | | x | x | x | |
| | *3.0* | x | x | x | | |

a. Scaling the tire model

As shown in Figure 70 and Figure 71 the cornering stiffness of the tire can change depending on test condition. Thus the cornering stiffness from asymmetric sLAT12 model will be different from the cornering stiffness measured from sLAT02.

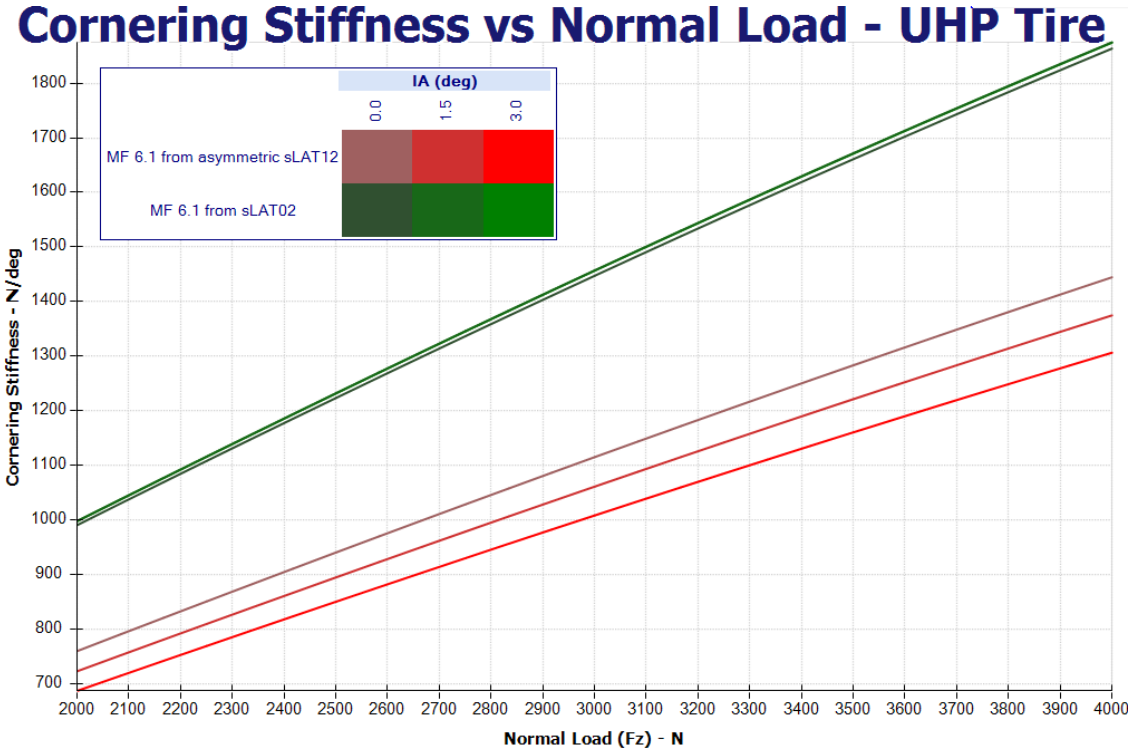


Figure 80 – Cornering stiffness versus normal load comparison between tire model from sLAT02 and asymmetric sLAT12

Figure 80 shows the comparison between cornering stiffness at different normal loads for the tire model fit from sLAT02 and asymmetric (modified) sLAT12 test. As expected, the cornering stiffness from asymmetric sLAT12 is lower than the cornering stiffness from sLAT02. However, MF 6.1 model allows manipulation of the model by using scaling factors or modifying the parameters themselves. This could allow prediction

of cornering stiffness from sLAT02 using tire data from asymmetric sLAT12 which will further reduce testing time and cost.

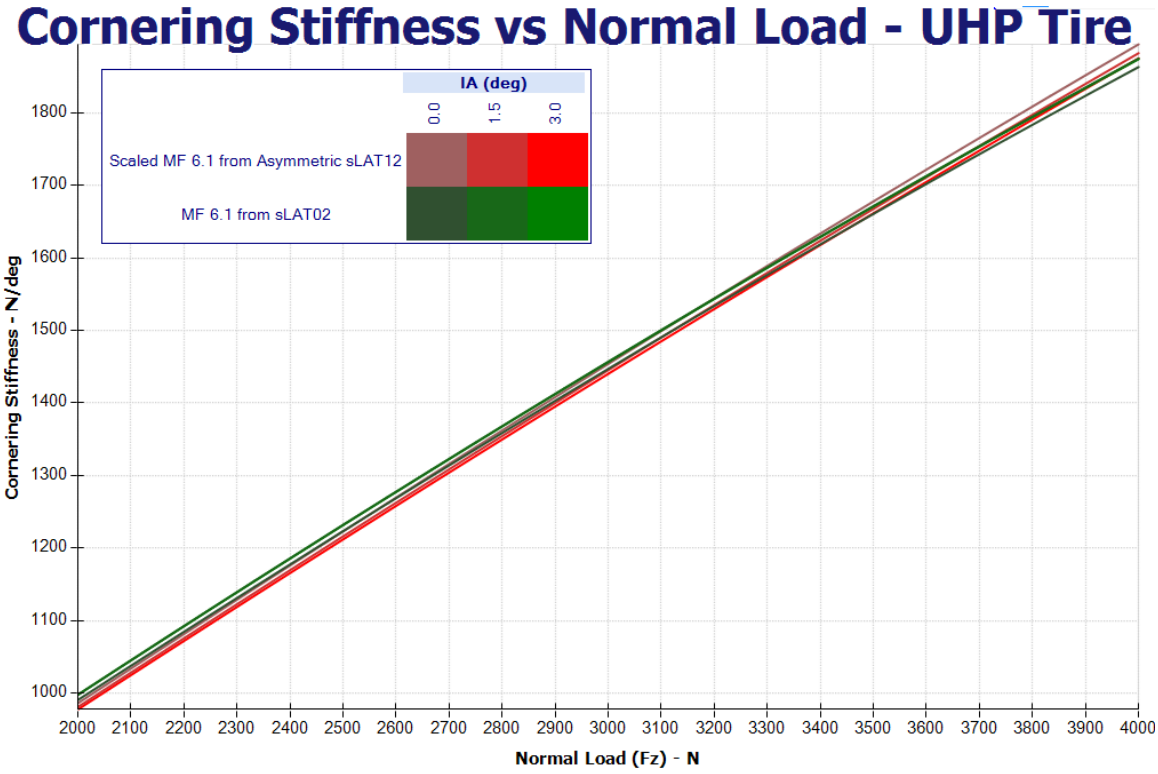


Figure 81 – Cornering stiffness versus normal comparison between tire model from sLAT02 and asymmetric sLAT12 after scaling the model for UHP tire

Figure 81 shows the cornering stiffness predicted by the scaled MF 6.1 tire model from asymmetric sLAT12 with good agreement with the cornering stiffness as predicted by MF 6.1 from sLAT02. In addition, Figure 82, Figure 83 and Figure 84 show the lateral force versus slip angle at 0 degrees, 1.5 degrees and 3 degree inclination angle within ±2 deg slip angle for the scaled MF 6.1 model from asymmetric sLAT12, unscaled MF 6.1 model from asymmetric sLAT12 and MF 6.1 from sLAT02. While the scaled model does

not perfectly match the lateral force as predicted by MF 6.1 model from sLAT02, it is significantly better than the original unscaled tire model.

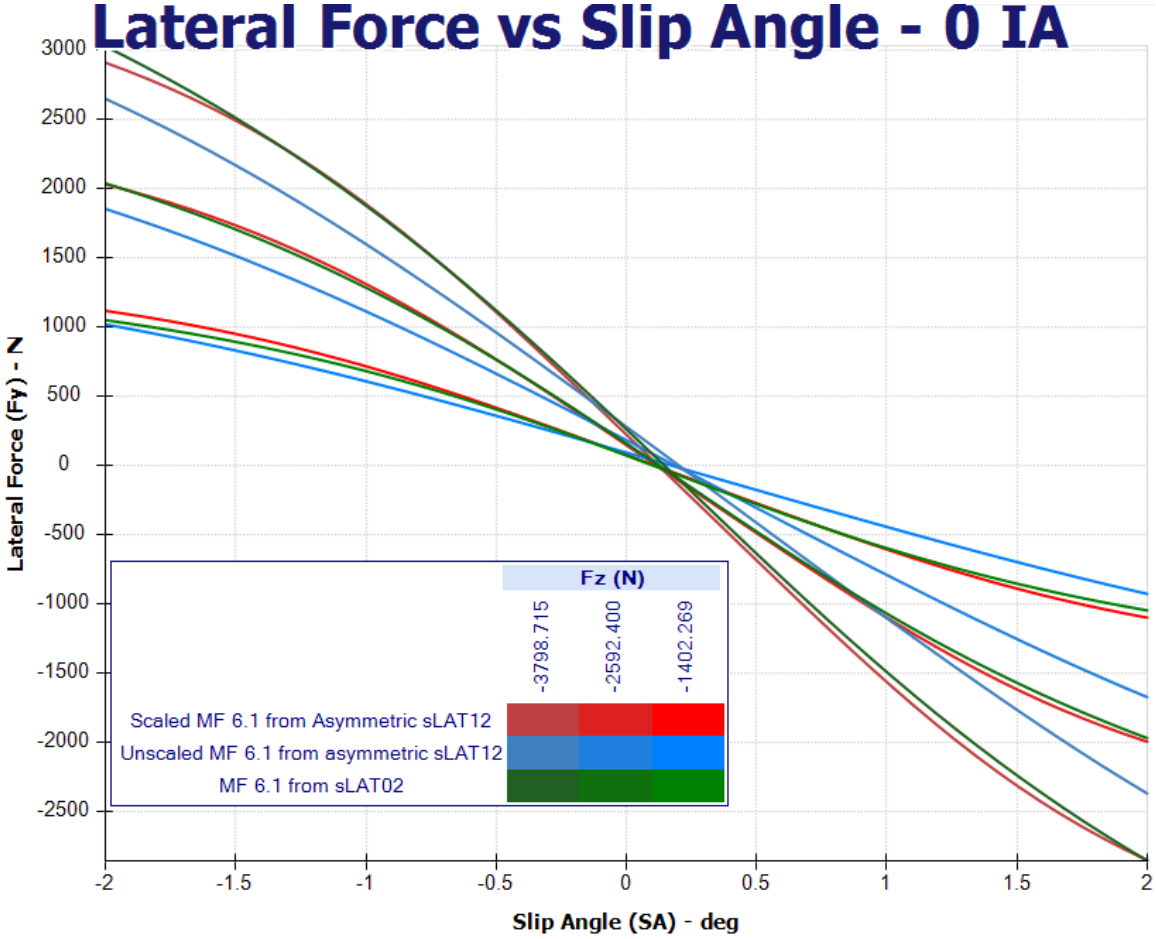


Figure 82 – Lateral force versus slip angle at 0 deg inclination angle (camber) for scaled, unscaled MF 6.1 tire models from asymmetric sLAT12 and MF 6.1 from sLAT02 for UHP tire

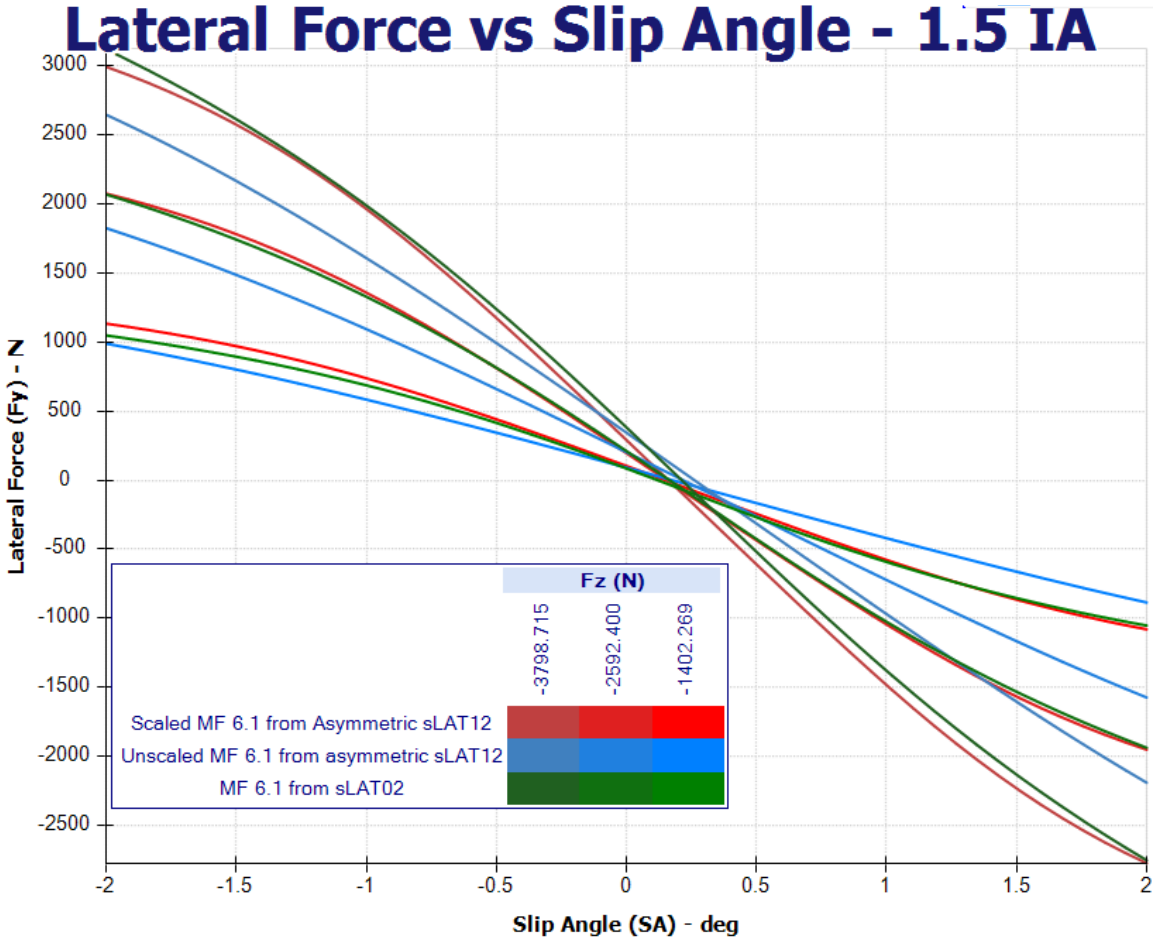


Figure 83 – Lateral force versus slip angle at 1.5 deg inclination angle (camber) for scaled, unscaled MF 6.1 tire models from asymmetric sLAT12 and MF 6.1 from sLAT02 for UHP tire.

The scaling was achieved by using an interactive scaling feature in OptimumTire [48] which allows instant comparison between scaled and unscaled tire models. Given that the primary interest was to predict cornering stiffness, the scaling factors corresponding to modifying cornering stiffness and the lateral force within ±2 degree slip angle were modified. Pacejka et al [8] and Braghin et al [49] outline the coefficients and scaling factors that affect the tire model in this range. This was used as guidance to modify tire model by

using the interactive scaling feature tool in OptimumTire. The scaled asymmetric MF 6.1 tire model for the UHP tire had a total error of 4.5% in predicting lateral force while the unscaled model had an error of 20.18% in predicting lateral force. The MF 6.1 tire model from sLAT02 had an error of 1.35%.

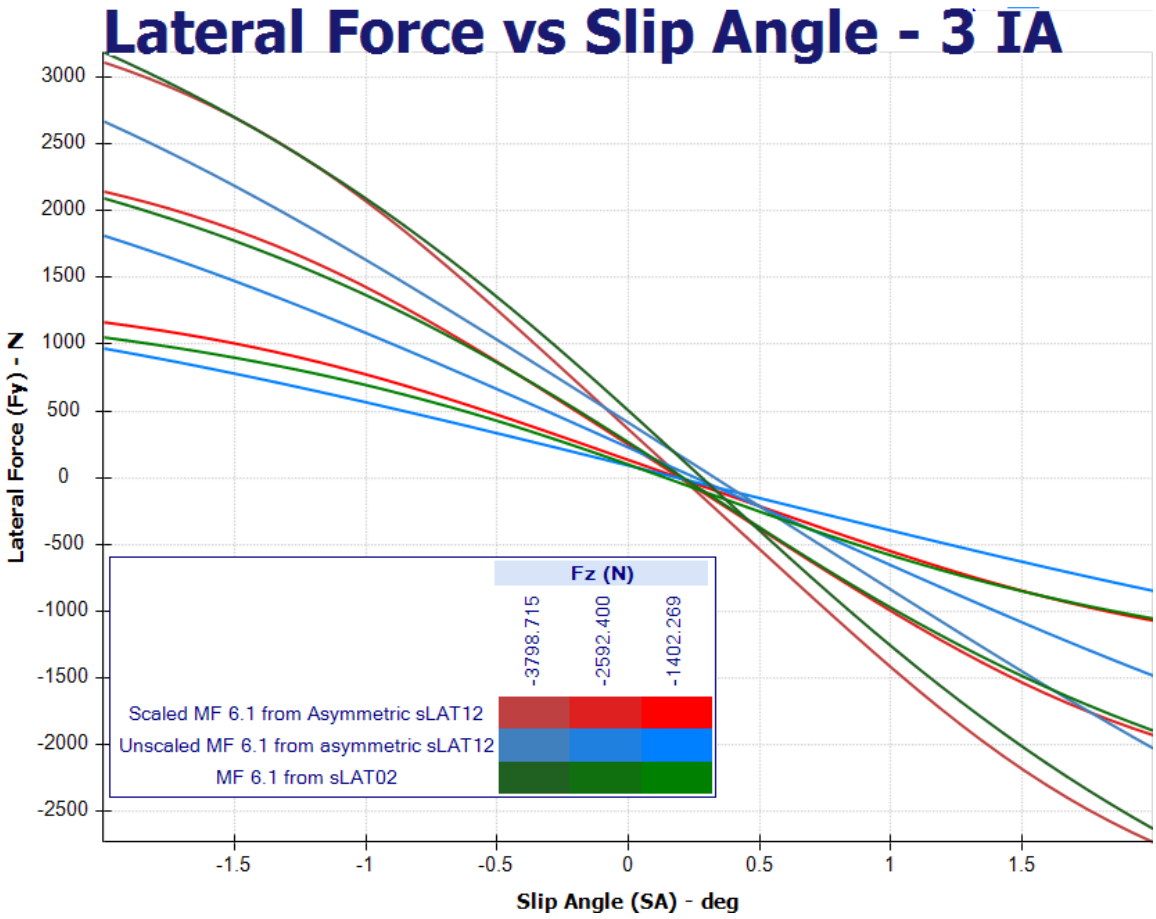


Figure 84 – Lateral force versus slip angle at 3 deg inclination angle (camber) for scaled, unscaled MF 6.1 tire models from asymmetric sLAT12 and MF 6.1 from sLAT02 for UHP tire.

Similarly, scaling factors for the Broadline tire were also calculated. The total error for scaled asymmetric MF 6.1 model for the Broadline was 5.42% in predicting lateral force while the unscaled model had an error of 18.77% in predicting lateral force. The MF

6.1 tire model from sLAT02 had an error of 1.46%. Thus the scaled model significantly improved the cornering stiffness prediction under the low slip angle maneuvers. Table 7 presents a summary of total error between different MF 6.1 model predicted lateral force and measured lateral force from sLAT02 test for both Broadline tire and UHP tires.

Table 7 – Summary of total error between different MF 6.1 tire models and tire test data from sLAT02 for both Broadline and UHP Tires

| **Error in Lateral Force Prediction between +/- 2 deg slip angle** | | | |
|---|---|---|---|
| | *MF 6.1 Model from sLAT02* | *Unscaled MF 6.1 Model from asymmetric sLAT12* | *Scaled MF 6.1 Model from asymmetric sLAT12* |
| **Broadline Tire** | 1.46% | 18.77% | 5.42% |
| **UHP Tire** | 1.35% | 20.18% | 4.50% |

Table 8 and Table 9 shows a summary of the coefficients and scaling factors of MF 6.1 that were modified for the asymmetric sLAT12 tire model for both UHP and Broadline tire respectively. The terms with λ are the scaling factors whereas the terms with 'p' are the model coefficients. λKyα is a direct modifier of tire cornering stiffness. Thus as expected, this factor is increased in the scaled model for both Broadline and UHP Tires. It can also be noticed that the bulk of the coefficients that were modified have the prefix 'pKy', this is due to the fact that these coefficients directly affect the cornering stiffness value and cornering stiffness sensitivity to camber, inflation pressure and normal load.

Table 8 – Coefficients and scaling factors of MF 6.1 that were modified for the asymmetric sLAT12 tire model for UHP Tire

| | | UHP Tire | |
|---|---|---|---|
| | Coefficient | Unscaled (original) | Scaled |
| **Model Coefficients** | *pCy1* | 1.27 | 0.90 |
| | *pKy1* | 76.32 | 88.95 |
| | *pKy2* | 2.82 | 3.20 |
| | *pKy3* | 1.91 | 0.30 |
| | *pKy4* | 0.82 | 0.84 |
| | *pKy5* | -2.73 | -5.64 |
| | *pKy6* | -0.73 | -0.73 |
| | *pKy7* | -1.02 | 0.10 |
| | *pHy1* | -3.69E-03 | -7.20E-03 |
| **Scaling Factors** | *λKyα* | - | 1.23 |
| | *λHy* | - | 0.31 |

Table 9 – Coefficients and scaling factors of MF 6.1 that were modified for asymmetric sLAT12 tire model for Broadline Tire

| | | Broadline Tire | |
|---|---|---|---|
| | Coefficient | Unscaled (original) | Scaled |
| **Model Coefficients** | *pCy1* | 1.15 | 1.85 |
| | *pEy1* | -1.42 | 0.55 |
| | *pKy1* | 58.68 | 56.80 |
| | *pKy2* | 2.70 | 3.00 |
| | *pKy3* | -0.65 | 0.12 |
| | *pKy4* | 0.91 | 1.13 |
| | *pKy5* | 20.00 | 5.00 |
| | *pKy6* | -0.58 | -0.84 |
| | *pKy7* | -0.80 | 1.65 |
| | *pHy1* | -4.1E-03 | -1.9E-03 |
| | *pHy2* | -1.2E-03 | -3.6E-03 |
| **Scaling Factors** | *λKyα* | - | 1.11 |
| | *λHy* | - | 1.61 |

Coefficient pKy3 modifies the camber sensitivity of cornering stiffness and Figure 80 indicates that the asymmetric MF6.1 asymmetric sLAT12 model without scaling has higher camber sensitivity than the MF 6.1 model from sLAT02. Decreasing this term significantly reduced the influence of camber on cornering stiffness across the normal load range. While not perfect, the scaling factors do seem to be able to modify the tire model enough to predict cornering stiffness for on-center highway maneuvers as is seen in highway driving. Eliminating sLAT02 from the tire test procedure will reduce the testing conditions by 50%. In addition, the asymmetric sLAT12 will further reduce testing cost and time for 40%. In addition, it can also be noted that the scaling factors for both tires are different despite having the same testing surface and load conditions. This could indicate that the scaling factors could potentially depend on the type of tire being tested. Thus both sLAT02 and sLAT12 tests are recommended at the start of a tire development program to understand the range of scaling factors expected. Once understood, future tire tests can greatly reduce sLAT02 and apply scaling factors to reduce testing time and cost. A larger variety of tires can be chosen for future studies to get a potentially wider range of scaling factors. In addition, a constrained optimization algorithm can be implemented to calculate scaling factors. Unfortunately due to scheduling conflicts with Smithers on testing time, tire data was not available early enough to develop an optimization algorithm.

b. Track replay using tire model

The tire models were then input with the normal load, slip angle and inclination angle inputs from the track replay outlined earlier to predict the lateral force.

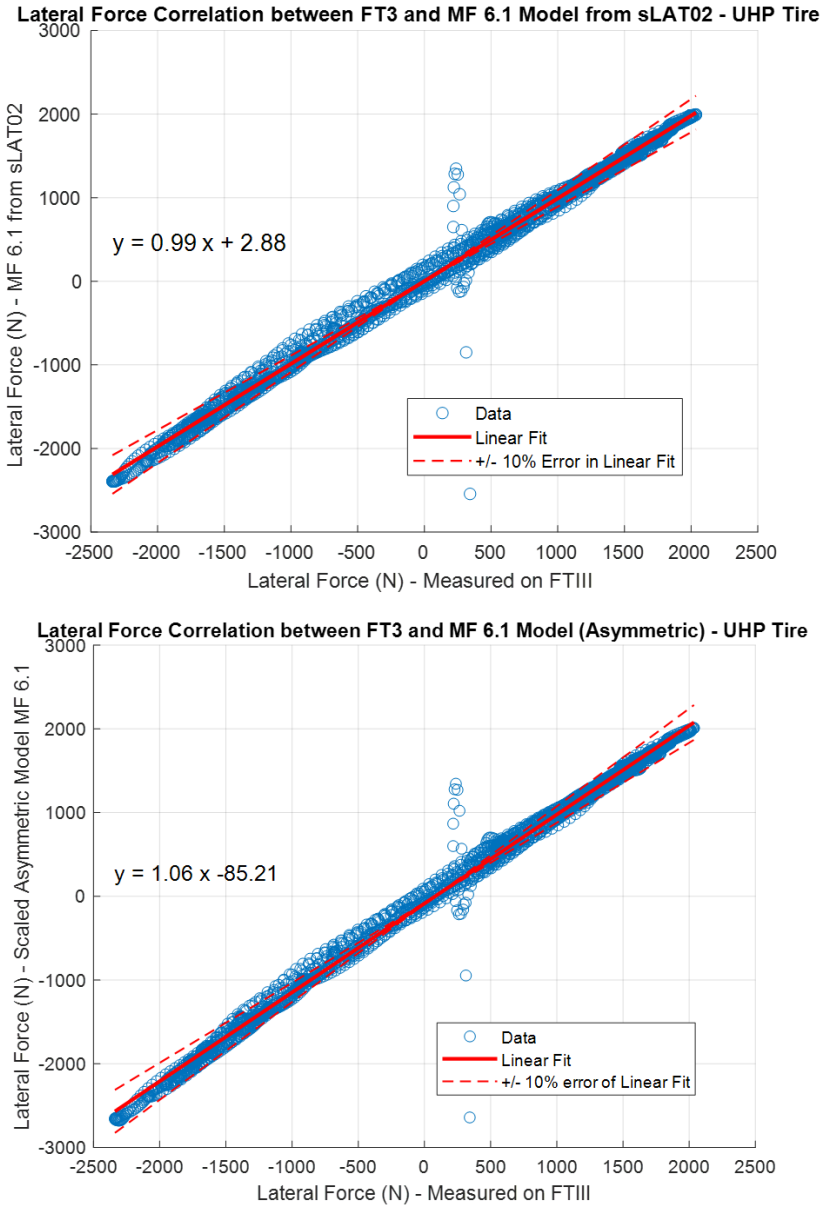


Figure 85 – UHP Tire: Scatter plot of Lateral force predicted by MF 6.1 model from sLAT02 model (top) and measured by FT III for the track replay. Similarly, scatter plot of Lateral Force predicted by scaled MF 6.1 model from asymmetric sLAT12 (bottom) and measured by FT III for track replay input. Also presented is the linear fit, coefficients and ±10% error bounds

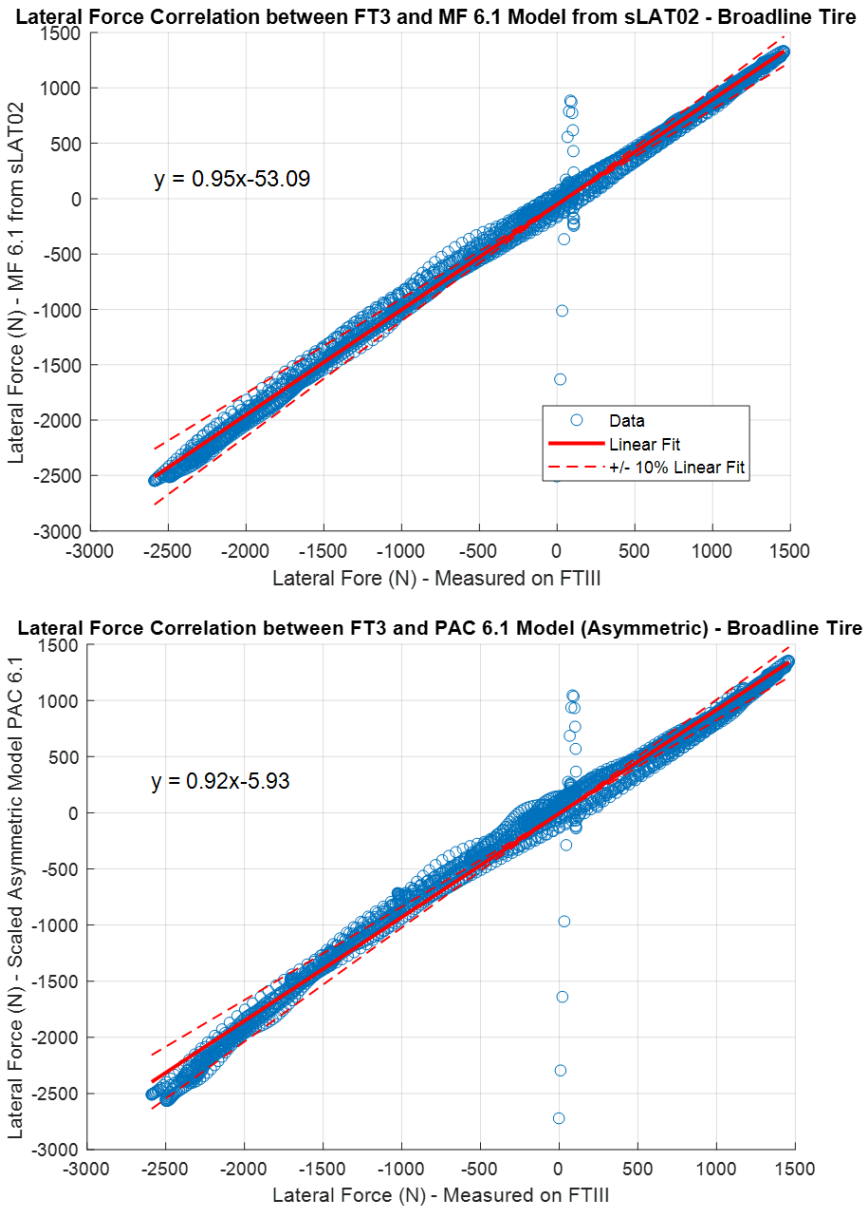


Figure 86 - Broadline Tire: Scatter plot of Lateral force predicted by MF 6.1 model from sLAT02 model (top) and measured by FT III for the track replay. Similarly, scatter plot of Lateral Force predicted by scaled MF 6.1 model from asymmetric sLAT12 (bottom) and measured by FT III for track replay input. Also presented is the linear fit, coefficients and ±10% error bounds

Figure 85 and Figure 86 show the correlation between lateral forces measured by FT III and predicted lateral force by MF 6.1 from sLAT02 and scaled MF 6.1 tire model from asymmetric sLAT12 for UHP and Broadline tire respectively. It can be observed that the MF 6.1 tire model from sLAT02 correlates linearly with the lateral force as measured on the FTIII for both Broadline and UHP Tire. Given that the MF 6.1 model from sLAT02 has an error of less than 1.5% for both UHP and Broadline tires, this serves as the upper bound for the quality of the linear fit.

The scaled MF 6.1 model from asymmetric sLAT12 also seems to be linearly correlated with the measured lateral force on the FT III. While there does seem to be some non-linearity in Figure 86 for the Broadline tire, the linear fit seems to do a reasonable job of capturing the trend in data. Table 10 summarizes the error between the predicted lateral force from tire model and measured lateral force on the FT III for track replay.

Table 10 – Summarized errors between tire model and measured lateral force on FT III from track replay

| | **UHP Tire** | | **Broadline Tire** | |
|---|---|---|---|---|
| | *MF 6.1 from sLAT02* | *Scaled MF 6.1 from Asymmetric sLAT12* | *MF 6.1 from sLAT02* | *Scaled MF 6.1 from Asymmetric sLAT12* |
| **$R^2$** | 0.99 | 0.98 | 0.98 | 0.98 |
| **RMSE** | 114.29 | 152.74 | 127.07 | 156.81 |

# Chapter 6. Conclusion and Future Remarks

## a. Concluding Remarks

A process to identify relevant tire operating conditions for tire force and moment testing has been presented. The test vehicle was equipped with wheel force transducers, slip angle sensors, accelerometers, temperature sensors and data acquisition system to measure the operating condition of the tires. Data collected during 'daily driving' using a vehicle with a data acquisition provided guidance to design the on vehicle testing at the test track.

This data was used to design the appropriate normal load, slip angle and camber angle inputs for tire force and moment testing on the FlatTrac III. Driving the tire on the FlatTrac III machine using actual normal load, slip angle and camber angle measured on the road surface provided correlation between the road surface at test track and the belt surface on the FlatTrac III machine. In addition, the correlation between the wheel force transducer and the FlatTrac III machine was provided. By utilizing the exact physical tire from physical testing any variations due to tire uniformity were eliminated. A correlation between tread surface temperature and cornering stiffness was not found, which validated the observations found in literature.

It was shown that by using the data from on vehicle testing, a reduction of 40% in testing time and cost can be achieved by using an asymmetric test matrix approach. In

addition, use of scaling factors will reduce the amount of tire testing by 50%. But care must be taken to identify the appropriate range of scaling factors. The tire models were also simulated with the track replay inputs consisting of measured normal load, camber and slip angle inputs from the road. The correlation between the measured lateral force from FlatTrac III and the simulated lateral force from MF 6.1 tire models with different parameters and the errors were presented. These correlations along with the track surface to belt surface and WFT to FlatTrac III measurement can be used to predict the lateral force and the cornering stiffness of a tire on a road surface.

b. Future Work

It is evident that further testing is necessary to understand the relationship between tire internal temperature and cornering stiffness since that was not done due to scheduling conflicts with the testing lab. It is recommended to test a wide variety of tires on track and on the FlatTrac III surface to understand the range of scaling factors necessary to reliably scale the models.

Both tires showed that they had the highest cornering stiffness at 0 deg inclination angle in sLAT12 test. This could be due to the fact that both tires were started at 0 deg inclination angle and thus the tire at 0 deg inclination angle was cooler than at 1.5 and 3 degree inclination angle. It is recommended to reverse the order of the inclination angle to investigate any temperature related influence on cornering stiffness sensitivity to inclination angle. In addition, it is also recommended to run both sLAT02 and sLAT12 at different sweep rates and monitor the tire internal temperature to measure influence of sweep rates on internal tire temperature and thus the cornering stiffness of the tire.

No work was done here with regards to understanding the influence of tire wear on the correlation or the model fits. It is recommended to design a study that can incorporate tire wear as a metric to understand tire behavior. It is also recommended to repeat the test on different types of road surfaces – concrete and different types of asphalt. These could further affect the correlation and scaling factors. The methodology presented here can also be used to study the longitudinal and limit performance of the tire.

# References


[1] T. D. Gillespie, Fundamentals of Vehicle Dynamics, Society of Automotive Engineers, 1992.

[2] W. F. Milliken and D. L. Milliken, Race Car Vehicle Dynamics, Warrendale: Society of Automotive Engineers, 1995.

[3] T. Bundorf and R. Leffert, "The Cornering Compliance Concept for Description of Vehicle Directional Control Properties; 760713," SAE International, 1976.

[4] P. Riede, R. Rasmussen and R. Leffert, "Understanding Tire Intermix Through the Cornering Compliance Concept; 741104," SAE International, 1974.

[5] K. B. Singh and S. Sivaramakrishnan, "An Adaptive Tire Model for Enhanced Vehicle Control Systems; 2015-01-1521," *SAE International Passenger Cars - Mechanical Systems,* vol. 8, no. 1, pp. 128-145, 2015.

[6] H. Olsson, D. Gentz and M. Strang, "Characterization of thermal influence on tire force and moment properties," in *36th Annual Tire Society Meeting and Conference*, Akron, Ohio, 2017.

[7] H. B. Pacejka and E. Bakker, "The Magic Formula Tyre Model," *Vehicle System Dynamics - International Journal of Vehicle Mechanics and Mobility,* vol. 21, no. 1, pp. 1-18, 1992.

[8] H. B. Pacejka and I. Besselink, Tire & Vehicle Dynamics, Elsevier, 2012.

[9] C. Angrick, S. V. Putten and G. Prokop, "Influence of Tire Core and Surface Temperature on Lateral Tire Characteristics; 2014-01-0074," *SAE International Journal of Passenger Cars,* vol. 7, no. 2, pp. 468-481, 2014.

[10] Calspan Corporation, "Force and Moment Testing," [Online]. Available: https://www.calspan.com/services/transportation-testing-research -equipment/tire-performance-testing/force-moment-testing/. [Accessed July 2018].

[11] M. Mizuno, "Development of tire side force model based on magic formula with the influence of tire surface temperature," *R&D Review of Toyota CRDL,* vol. 38, no. 4, pp. 17-22, 2003.

[12] M. W. Arndt, M. Rosenfield and S. M. Arndt, "How tires change a SUV's performance in fishhook and sine-with-dwell testing," *21st International Technical Conference on Enhanced Safety of Vehicles,* 2009.

[13] Highway Tire Commitee, "Force and Moment Test Method," SAE International, 1998.

[14] G. Smith and M. Blundell, "A new efficient free-rolling tyre testing procedure for the parametrization of vehicle dynamics tyre models," *Institution of Mechancial Engineers,* vol. 23, no. 10, pp. 1436-1448, 2016.

[15] L. Lidner, "EXPERIENCE WITH THE MAGIC FORMULA TYRE MODEL," *Vehicle System Dynamics,* vol. 21, no. 1, pp. 30-46, 1992.

[16] S. Sivaramakrishnan and S. Taheri, "Using Objective Vehicle-Handling Metrics for Tire Performance Evaluation and Selection; 2013-01-0743," *SAE Journal of Passenger Cars - Mechanical Systems,* vol. 6, no. 2, pp. 732-740, 2013.

[17] K. B. Singh, P. Lee and S. Sivaramakrishnan, "Influence of Tire Operating Conditions on ABS Performance," *Tire Science and Technology,* vol. 43, no. 3, pp. 216-241, 2015.

[18] F. Cheli, E. Sabbioni, M. Sbrosi, M. Brusarosco, S. Melzi and V. d'Alesandro, "Enhancement of ABS Performance through On-Board Estimation of the Tires' Response by Means of Smart Tires; 2011-01-0991," in *SAE 2011 World Congress & Exhibition,* 2011.

[19] M. Pottinger and A. M. Fairlie, "Characteristics of Tire Force and Moment Data," *Tire Science and Technology,* vol. 17, no. 1, pp. 15-51, 1989.

[20] D. A. Crolla, R. P. King and H. Ash, "Subjective and Objective Assessment Of Vehicle Handling," in *Seoul 2000 FISITA World Automotive Congress*, Seoul, Korea, 2000.

[21] T. Mimuro, M. Ohsaki, H. Yasunaga, K. Satoh and R. G. Dubensky, "Four Parameter Evaluation Method of Lateral Transient Response; 901734," *Journal of Passenger Cars,* vol. 99, no. 6, pp. 1499-1508, 1990.

[22] C. Schroder and S. Chung, "Influencec of Tire Characteristic Properties on the Vehicle Lateral Transient Response," *Tire Science and Technology,* vol. 23, no. 2, pp. 72-95, 1995.

[23] S. Monsma, "Feel the Tire - Tire Influence on Driver's Handling Assessment," Aalto University, Helsinki, Finland, 2015.

[24] M. Gipser, "FTire – the tire simulation model for all applications related to vehicle dynamics," *Vehicle System Dynamics,* vol. 45, no. 1, pp. 139-151, 2007.

[25] A. Gallrein and M. Backer, "CDTire: A Tire Model For Comfort And Durability Applications," *Vehicle System Dynamics,* vol. 45, no. 1, pp. 69-77, 2007.

[26] MTS Systems Corporation, "MTS Flat-Trac III CTTire Test System For Dynamic Force and Moment Testing of Passenger Car Tires," MYS Systems Corporation, Eden Prairie, MN, 2003.

[27] SoVa Motion, "Tire Testing Services," [Online]. Available: http://www.sovamotion.com/flat-belt.html. [Accessed July 2018].

[28] M. G. Pottinger, K. D. Marshall and G. A. Arnold, "Effects of Test Speed and Surface Curvature on Cornering Properties of Tires; 760029," in *1976 Automotive Engineering Congress and Exposition*, Warrendale, 1976.

[29] SAE International, "Force and Moment Test Method," SAE International, Warrendale, 1998.

[30] E. M. Kasprzak and D. Gentz, "The Formula SAE Tire Test Consortium—Tire Testing and Data; 2006-01-3606," in *Proceedings of the 2006 Motorsports Engineering Conference and Exhibition*, Warrendale, 2006.

[31] Racelogic, "VBOX 3i 100Hz Data Logger," Racelogic, [Online]. Available: https://www.vboxautomotive.co.uk/index.php/ en/products/data-loggers/vbox-3i. [Accessed June 2018].

[32] Racelogic, "VBOX 3i Dual Antenna | 100Hz Vehicle Dynamics Measurement," Racelogic, [Online]. Available: https://www.vboxautomotive.co.uk/index.php/ en/products/data-loggers/vbox-3i-dual-antenna. [Accessed July 2018].

[33] Racelogic UK, "IMU04 Exploded 3," Racelogic UK, [Online]. Available: http://www.racelogic.co.uk/index.php/us/image-library /vbox-automotive/imu04-exploded-3-155. [Accessed July 2018].

[34] Michigan Scientific Corporation, "Model LW12.8-50 Wheel Load Transducer," Michigan Scientific Corporation, 13 March 2018. [Online]. Available: http://www.michsci.com/products/transducers/wheel-force-transducers/lw12_8/. [Accessed July 2018].

[35] Society of Autmotive Engineers, "Tire Performance Terminology; J2047_201303," SAE International, Warrendale, PA, 2013.

[36] Texys International, "IRN8-WS4 8-Channel wireless infrared temperature sensor," Texys International, Varannes-Vauzelles, France, 2018.

[37] Texys International, "IRN-RC," Texys International, July 2018. [Online]. Available: https://www.texense.com/product/irn-rc/. [Accessed July 2018].

[38] National Instruments, "Controller Area Network (CAN) Overview," National Instruments, 1 August 2014. [Online]. Available: http://www.ni.com/white-paper/2732/en/. [Accessed July 2018].

[39] Racelogic UK, "Racelogic CAN bus," Raclogic UK, 18 January 2018. [Online]. Available: https://racelogic.support/01VBOX_Automotive/ 01VBOX_data_loggers /VBOX_3i_Range/VBOX_3i_User_Manual_(All_Variants)/08_-_VB3i_CAN. [Accessed July 2018].

[40] E. Tingwall, "The Physics of Engine Notes, Or: Why a Toyota V-6 and Porsche Flat-Six Sound So Different," Car and Driver, January 2015. [Online]. Available: https://www.caranddriver.com/features/this-is-why- various-engine- types-sound-so-different-feature. [Accessed July 2018].

[41] H. Tienhaara, "Guidelines to engine dynamics and vibration," Wärtsilä Corporation, 2004.

[42] EPI Inc., "Basics of Vibration," EPI Inc, 25 July 2015. [Online]. Available: http://www.epi-eng.com/mechanical_engineering_basics/vibration_intro.htm. [Accessed July 2018].

[43] Mathworks Inc., "Align Signals Using Cross-Correlation," Mathworks Inc., 2018. [Online]. Available: https://www.mathworks.com/help/signal/ug/ align-signals-using-cross-correlation.html. [Accessed April 2018].

[44] Tire Rack, "ZEON RS3-G1," Tire Rack, [Online]. Available: https://www.tirerack.com/tires/tires.jsp?tireMake= Cooper& tireModel=Zeon+RS3-G1. [Accessed July 2018].

[45] Tire Rack, "CS5 ULTRA TOURING," Tire Rack, [Online]. Available: https://www.tirerack.com/tires/tires.jsp?tireMake= Cooper&tireModel=CS5+Ultra+Touring. [Accessed July 2018].

[46] Mathworks Inc., "butter," [Online]. Available: https://www.mathworks.com/help/signal/ref/butter.html. [Accessed July 2018].

[47] Mathworks Inc, "filtfilt," Mathworks Inc., [Online]. Available: https://www.mathworks.com/help/signal/ref/filtfilt.html. [Accessed July 2018].

[48] OptimumG, "OptimumTire - Tire Analysis Software," OptimumG, Denver, CO.

[49] F. Braghin, F. Cheli and E. Sabbioni, "Environmental effects on Pacejka's scaling factors," *Vehicle System Dynamics,* vol. 44, no. 7, pp. 547-568, 2006.

[50] T. Chai and R. R. Draxler, "Root mean square error (RMSE) or mean absolute error MAE)? - Arguments against avoiding RMSE in the literature," *Geoscientific Model Development,* vol. 7, no. 3, pp. 1247-1250, 2014.

[51] J. A. Cornell and R. D. Berger, "Factors that Influence the Value of the Coefficient of Determination in Simple Linear and Nonlinear Regression Models," *Phytopathology,* vol. 77, no. 1, pp. 63-70, 1986.

[52] Continental Tire, "What is a contact patch? Your car's footprint," Continental Tire the Americas LLC, 2017. [Online]. Available: http://www.continentaltire.com/news/what-contact-patch-your-car%E2%80%99s-footprint. [Accessed October 2017].

[53] B. Ulrich, "What to expect in 2017," January 2017. [Online]. Available: http://www.moderntiredealer.com/uploads/stats/mtd-51st-facts-1.pdf. [Accessed 1 November 2017].

[54] Tire Rack, "Tire Tech: Contact Patch," Tire Rack, 2017. [Online]. Available: https://www.tirerack.com/tires/tiretech/techpage.jsp?techid=10. [Accessed October 2017].

[55] U.S. Department of Transportation, "U.S. Driving Tops 3.1 Trillion Miles in 2015, New Federal Data Show," U.S. Department of Transportation, 22 February 2016. [Online]. Available: https://www.fhwa.dot.gov/pressroom/fhwa1607.cfm. [Accessed October 2017].

[56] E. Wren, "Stopping Distances," Drive and Stay Alive, August 2004. [Online]. Available: http://www.driveandstayalive.com/stopping-distances/. [Accessed October 2017].

[57] SAE International, "Laboratory Testing Machines for Measuring the Steady State Force and Moment Properties of Passenger Car Tires," SAE International, Warrendale, 2012.

[58] X. Xia and J. N. Willis, "The Effects of Tire Cornering Stiffness on Vehicle Linear Handling Performance; 950313," *SAE International Journal of Passenger Cars*, vol. 104, no. 6, p. 12, 1995.

Appendix A: Fast Fourier Transforms of Lateral Acceleration, Lateral Force measured by Wheel Force Transducer and Normal Force measured by Wheel Force Transducer

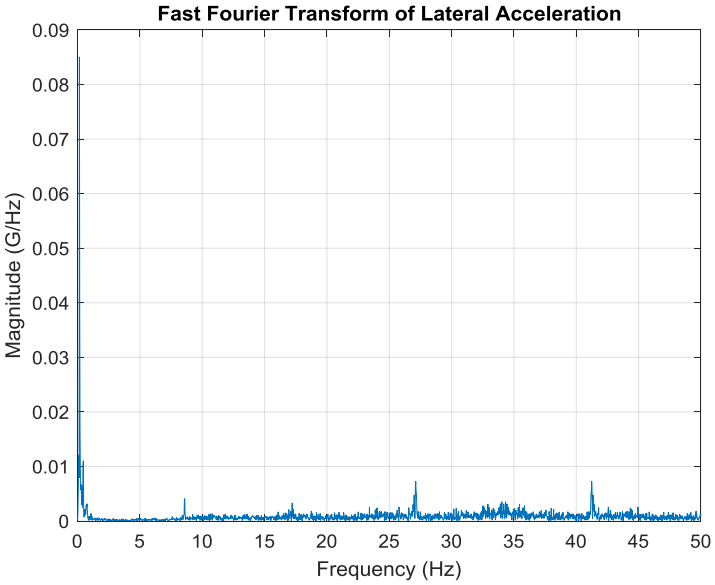

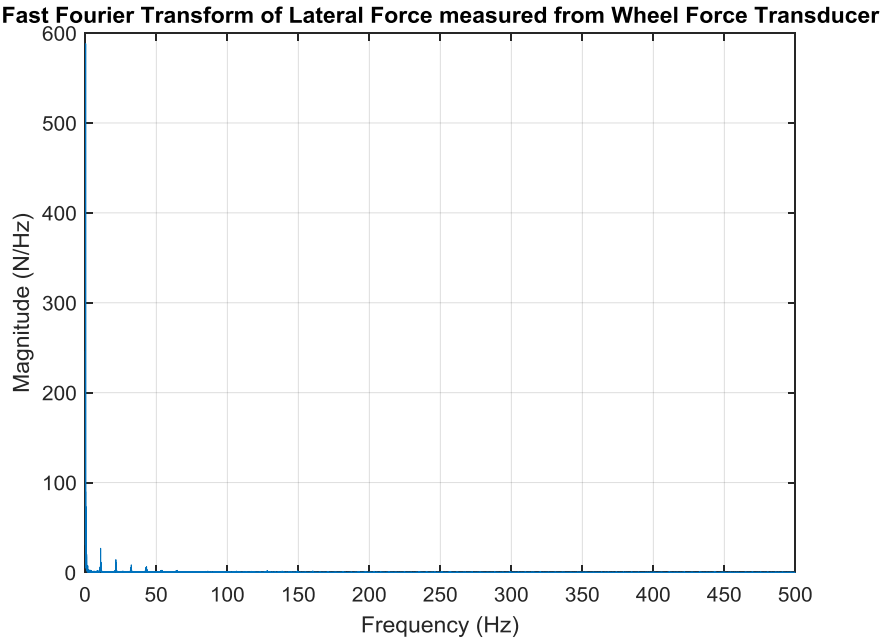
Fast Fourier Transform of Lateral Force measured from Wheel Force Transducer
Magnitude (N/Hz)
Frequency (Hz)
0
100
200
300
400
500
600
0
50
100
150
200
250
300
350
400
450
500

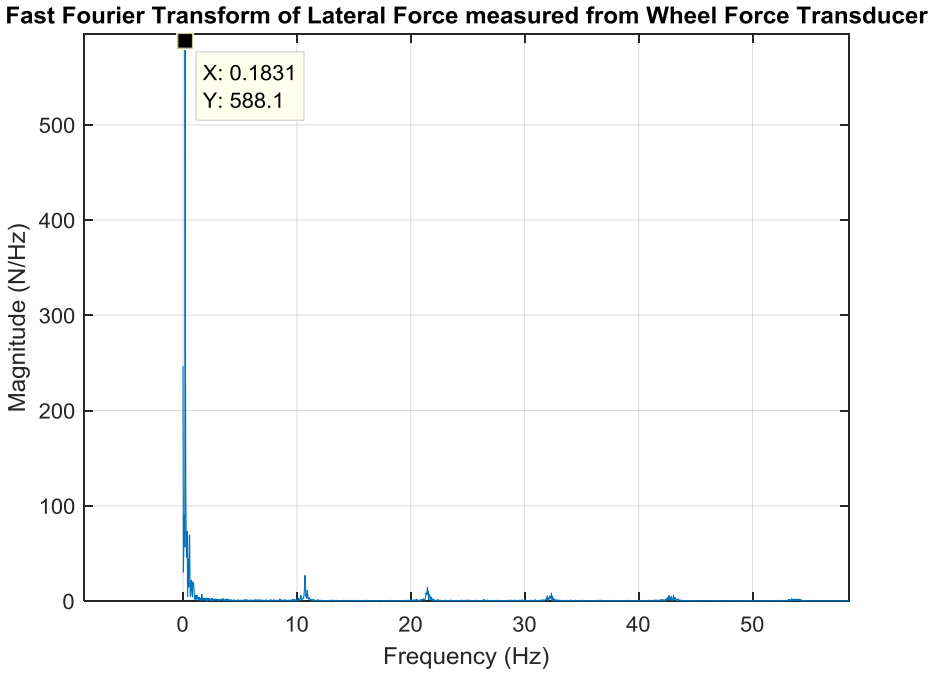
Fast Fourier Transform of Lateral Force measured from Wheel Force Transducer
X: 0.1831
Y: 588.1
Magnitude (N/Hz)
Frequency (Hz)
0
100
200
300
400
500
0
10
20
30
40
50

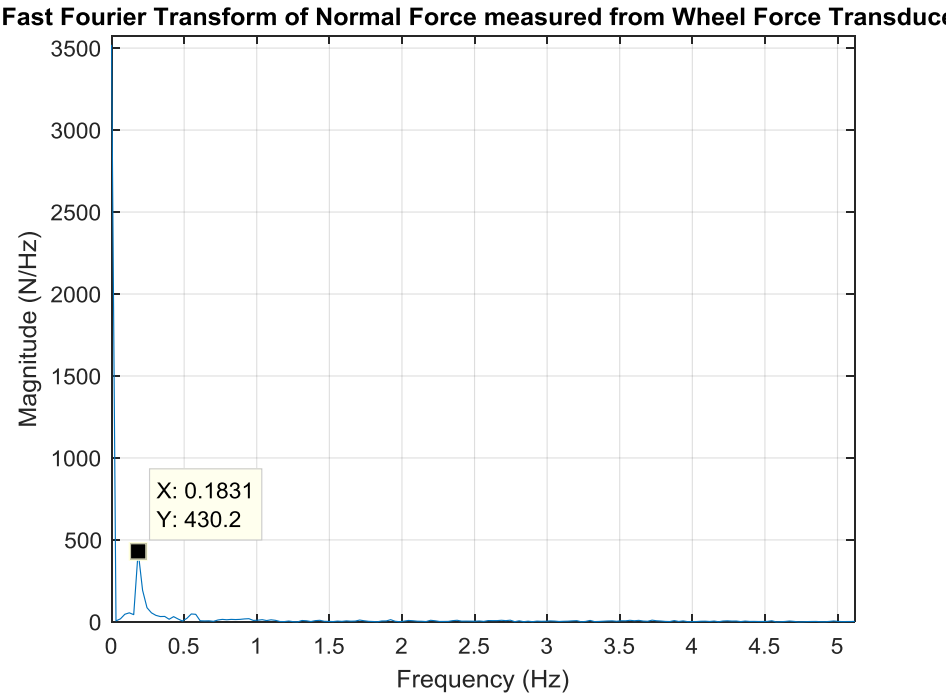
Fast Fourier Transform of Normal Force measured from Wheel Force Transduc
Magnitude (N/Hz)
Frequency (Hz)
X: 0.1831
Y: 430.2
0
500
1000
1500
2000
2500
3000
3500
0
0.5
1
1.5
2
2.5
3
3.5
4
4.5
5

Appendix B: Transition between command normal load and command inclination angle for sLAT02 and sLAT12

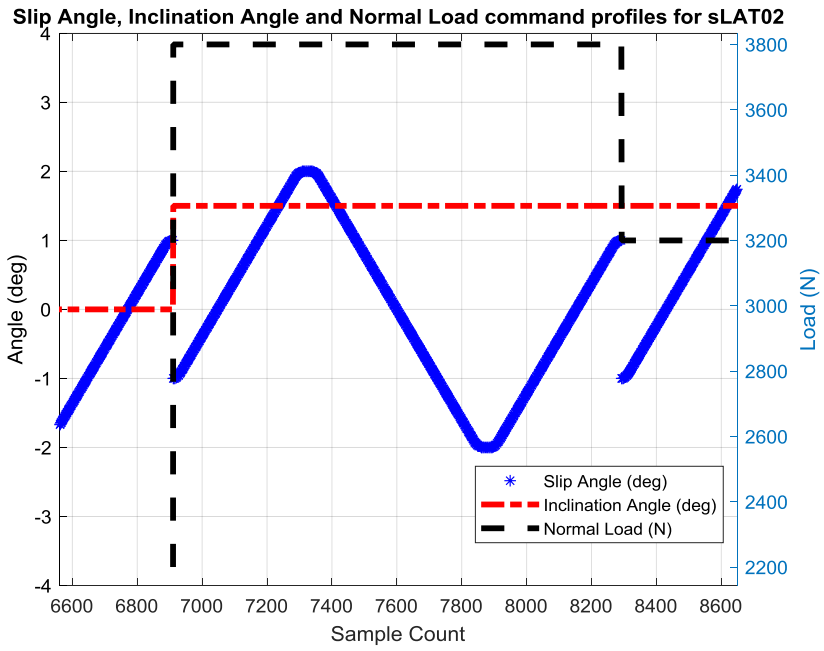

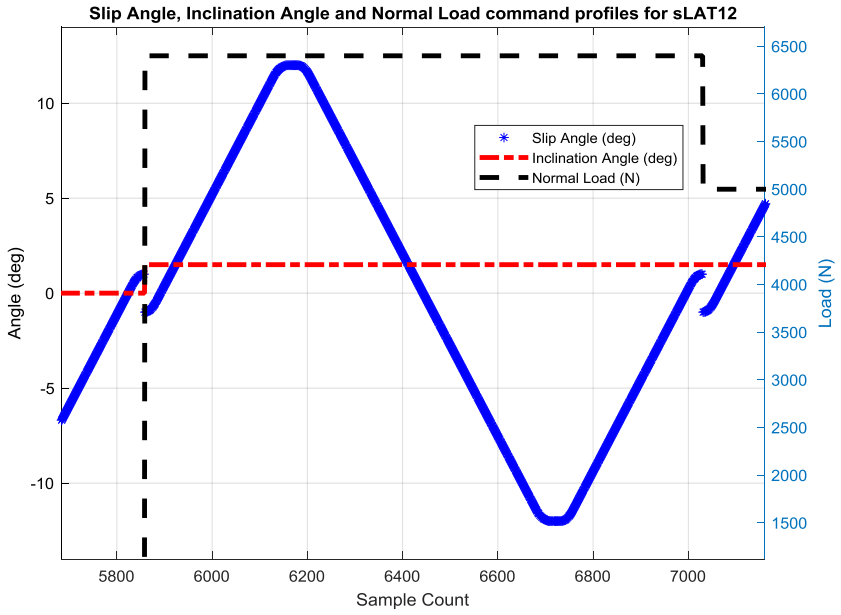
Slip Angle, Inclination Angle and Normal Load command profiles for sLAT12
Slip Angle (deg)
Inclination Angle (deg)
Normal Load (N)
Angle (deg)
Load (N)
Sample Count
10
5
0
-5
-10
6500
6000
5500
5000
4500
4000
3500
3000
2500
2000
1500
5800
6000
6200
6400
6600
6800
7000

## Appendix C: Total Error, Root Mean Square Error and $R^2$ Calculation

a. Total Error

The total error for the Magic Formula 6.1 tire models are calculated within the OptimumTire © software. The equation used is formula [48] –

$$E = \frac{\sum |Model - Data|}{\sum |Data|}$$

Where,

Model = represents the value predicted by the Magic Formula 6.1 tire model for a given value of normal load, inclination angle, slip angle

Data = represents the value of the actual raw data at a given value of normal load, inclination angle and slip angle

b. Root Mean Square Error (RMSE)

The root mean square error is calculated [50] as –

$$RMSE = \sqrt{\frac{1}{n}\sum_{j=1}^{n}\left(y_j - \hat{y}_j\right)^2}$$

Where
n = number of samples
$y_j$ = Data at $j^{th}$ point
$\hat{y}_J$ = Model predicted value at $j^{th}$ point

c. $R^2$ – Coefficient of determination [51]

$$R^2 = 1 - \frac{\sum_{j=1}^{n}\left(y_j - \hat{y}_j\right)^2}{\sum_{j=1}^{n}\left(y_j - \bar{y}\right)^2}$$

Where
n = number of samples
$y_j$ = Data at $j^{th}$ point
$\hat{y}_J$ = Model predicted value at $j^{th}$ point
$\bar{y}$ = Mean value of the data

Appendix D: Comparison between Magic Formula 6.1 Tire Model fit and Linear fit between -1 and +1 deg slip angle for sLAT02 and sLAT12

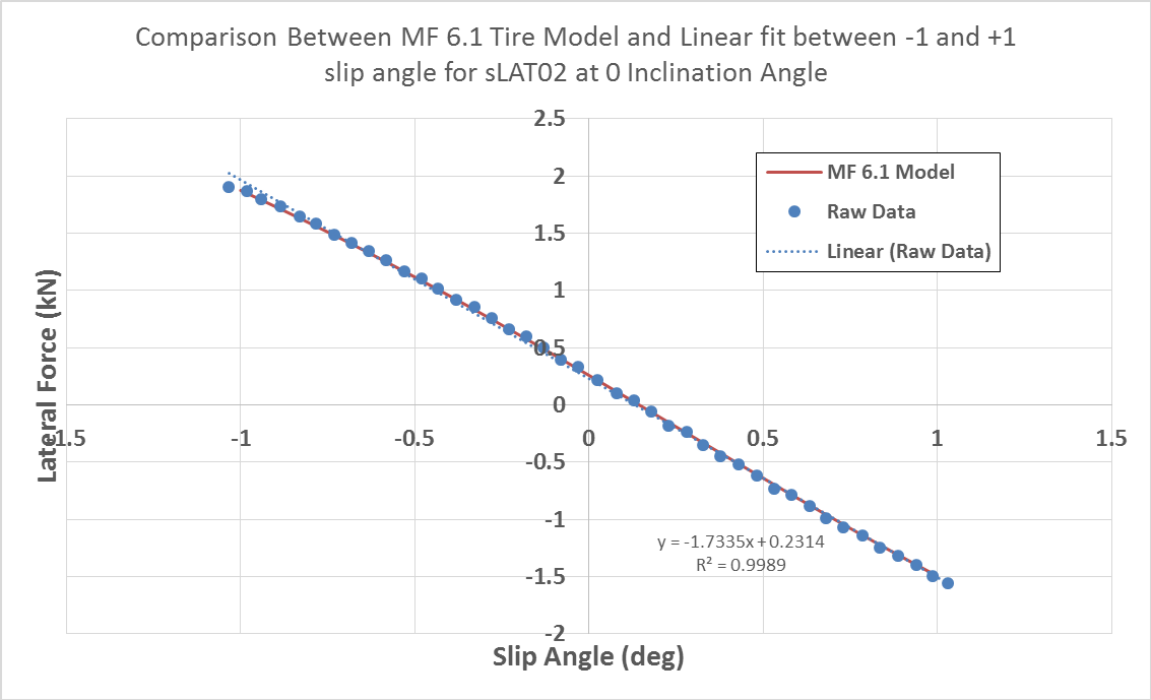


Note that the number of points between -1 and 1 for sLAT02 are larger than sLAT12 due to the fact the slip angle in sLAT02 is swept at 2 deg/s whereas the slip angle is swept at 12 deg/s while keeping the logging frequency constant at 250Hz for both maneuvers.

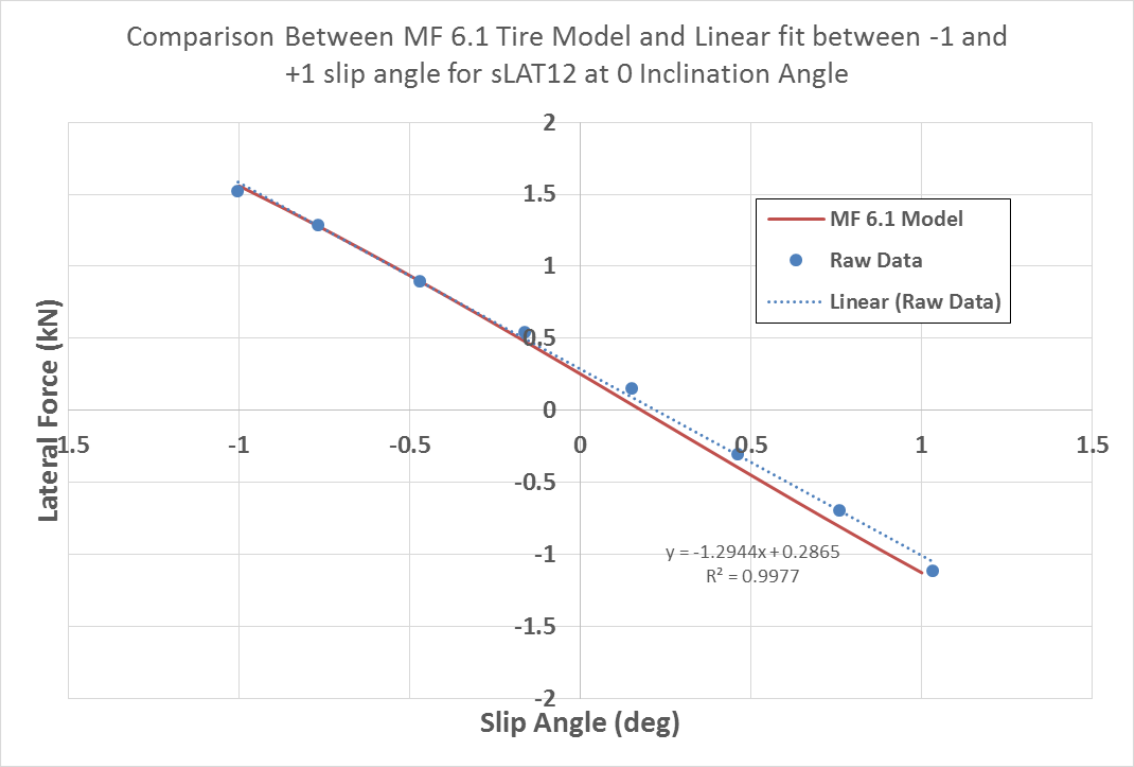
Comparison Between MF 6.1 Tire Model and Linear fit between -1 and +1 slip angle for sLAT12 at 0 Inclination Angle
Lateral Force (kN)
Slip Angle (deg)
MF 6.1 Model
Raw Data
Linear (Raw Data)
y = -1.2944x + 0.2865
R² = 0.9977
2
1.5
1
0.5
0
-0.5
-1
-1.5
-2
-1.5
-1
-0.5
0
0.5
1
1.5